

# Methane Emissions from the Dutch Wadden Sea



## **Master Thesis by Katherine Mesdag**

Date: July 3<sup>rd</sup> 2020

Student number: 6608434

MSc programme: Climate Physics

Supervisor: Thomas Röckmann

Second Supervisor: Maria Elena Popa

Course code: NS-MO552M

*Research vessel Navicula at sunset.  
Picture taken during the July (summer) cruise to the Wadden Sea by Helge Niemann.*

## Acknowledgements

I would like to start by thanking my supervisor Prof. Dr. T. Röckmann for guiding me during my entire research project and always finding time to help me. I would also like to thank Prof. Dr. H. Niemann and T. de Groot MSc for helping me during the cruises and showing me around at the NIOZ. I would like to thank Ing. C. van der Veen and M. Menoud MSc for helping me understand the methane isotope analysis system and providing me with a desk to work at. I want to thank C. Jacques MSc for taking me under her wing during the summer cruise and I would like to thank G. Cover and R. Meinen for joining me on the cruises for technical support. I would also like to thank dr. M.E. Popa for taking time to read and grade my report. I would like to end by thanking my family and friends, and my boyfriend in particular, for supporting me during this master thesis research project.

## Abstract

Methane is an important greenhouse gas, with a greenhouse warming potential that is 34 times higher than for CO<sub>2</sub> over a 100 year horizon. Anoxic sediments, containing a lot of (degrading) organic matter, are sources of methane. However, the majority of the methane released from the sea floor is oxidized to CO<sub>2</sub> in the water column and does not reach the atmosphere. In the Wadden Sea a lot of organic matter is present and the waters are shallow, potentially allowing a lot of methane produced at the sea floor to be emitted into the atmosphere. Methane concentrations in and above the Dutch Wadden Sea and methane emissions from the Dutch Wadden Sea have never been measured before.

To quantify the methane emissions from the Dutch Wadden Sea, methane concentrations in the water, the sediment and the atmosphere, methane oxidation rates in the water, isotopic signatures of methane in the air and water, and methane emissions were measured together with meteorological information and water properties. These variables were measured at an 48 hour station where the research vessel, the *Navicula*, anchored during summer (July 2019) and autumn (November 2019).

Average methane emission rates determined with a bucket technique were  $6.5 \pm 6.3$  nmol/s ( $23 \pm 22$  nmol/m<sup>2</sup>/s) in summer and  $2.0 \pm 1.0$  nmol/s ( $7.1 \pm 3.5$  nmol/m<sup>2</sup>/s) in autumn. Based on methane isotopic signatures in air samples, taken from the bucket, and in water samples, it can be concluded that the emissions measured originate from biogenic processes in the Wadden Sea. Emissions calculated with the bucket techniques are larger than the calculated sea-air flux based on dissolved and atmospheric concentrations, but both show the similar temporal changes, indicating that the bucket emissions are representative for what happens in the atmosphere, but the response is magnified. Measured methane emissions are higher at higher dissolved methane concentrations. Based on the sea-air flux, it can be concluded that higher salinity, water and air temperature, wind speed, roughness length and lower methane concentrations in the atmosphere also cause higher methane emissions from the Dutch Wadden Sea.

Dissolved methane concentrations in autumn peak just after low and high tide. For dissolved methane concentrations of about 20 nmol/L and higher, methane oxidation rates increase with concentration. The higher oxidation rates result in isotope enrichment of the dissolved methane in these samples, and the observed fractionation constant is consistent with microbial oxidation as the main removal process. Dissolved methane concentrations and methane oxidation rates in summer are, respectively, about four and eight times higher than in autumn.

Patterns in atmospheric methane mixing ratios and isotopic signatures in air samples cannot be explained by the temporal cycles of the variables measured during this research project. They are likely caused by passing synoptic-scale plumes with enhanced methane mixing ratios, but this could not be proven in this report.

Future expeditions to the Dutch Wadden Sea, during which the same variables are measured, could reduce uncertainties still present after this research project, for example on emission rates and their variation over a year. In addition, measuring the isotopic signatures of atmospheric air samples could help identifying the origin of the methane elevations in the atmosphere.

## Table of Contents

1. Introduction .....	1
1.1 Importance of methane .....	1
1.2 Methane emissions from oceans .....	1
1.3 Zooming in to continental shelves.....	2
1.4 Wadden Sea .....	2
1.5 Previous Research on Methane in the Wadden Sea.....	5
1.6 Questions dealt with in this report .....	6
2. Methods .....	6
2.1 Cruise .....	6
2.1.1 Route.....	7
2.1.2 Methane mixing ratio measurement .....	7
2.1.3 Sonic and LGR fast GHG analyser .....	9
2.1.4 Bucket measurement.....	10
2.1.5 Air samples.....	10
2.1.6 CTD .....	10
2.1.7 Water samples .....	11
2.1.8 Box core .....	12
2.2 Analysis by and at the NIOZ .....	12
2.2.1 Methane Concentrations in the Water.....	12
2.2.2 Methane Oxidation Rates .....	13
2.2.3 Methane Concentrations in the Sediment.....	14
2.3 Measuring isotopes.....	14
2.3.1 Methane analysis system.....	15
2.3.2 Air samples.....	16
2.3.3 Water samples .....	19
2.4 Data analysis .....	22
2.4.1 CTD .....	22
2.4.2 Methane mixing ratios .....	22
2.4.3 Sonic.....	24
2.4.4 Emissions.....	25
3. Results .....	27
3.1 Tides .....	27
3.2 CTD .....	28
3.3 Methane Concentrations in the Water.....	30

3.4 Methane Oxidation Rates .....	31
3.5 Methane Concentrations in the Sediment .....	33
3.6 $\delta^{13}\text{C-CH}_4$ and $\delta\text{D-CH}_4$ air samples .....	34
3.7 $\delta\text{D-CH}_4$ water samples .....	35
3.8 Methane mixing ratios .....	37
3.8.1 Buckets .....	38
3.8.2 Background .....	40
3.9 Sonic .....	45
3.10 Emissions .....	47
4 Conclusion .....	49
5 Discussion .....	51
5.1 Measurement errors .....	51
5.2 Uncertainties .....	53
References .....	I
Appendix 1 .....	VI
Appendix 2 .....	VII
Appendix 3 .....	XV
Appendix 4 .....	XVI

# 1. Introduction

In this report measurements of methane emissions from the Wadden Sea during summer and autumn 2019 are discussed. This section explains what makes methane important and why it is interesting to study emissions from the Wadden Sea in particular.

## 1.1 Importance of methane

Methane (CH<sub>4</sub>) is an important greenhouse gas (GHG) which absorbs infrared radiation at a higher efficiency per molecule than carbon dioxide (CO<sub>2</sub>) (Myhre et al., 2013). CH<sub>4</sub> has a relatively long lifetime of about 9 years in the troposphere (Dentener et al., 2003; Prather et al., 2012). When biosphere feedbacks are taken into account, CH<sub>4</sub> is 34-times more potent as a GHG than CO<sub>2</sub> over a 100-year horizon, and after CO<sub>2</sub>, CH<sub>4</sub> is the highest contributor to the anthropogenic radiative forcing of the atmosphere (Myhre et al., 2013). Global atmospheric methane concentrations have increased with variable rates over time. The total global atmospheric methane concentration has increased by a factor of 2.5 since 1750 (Ciais et al., 2013). This increasing methane concentration is responsible for about 20% of the additional atmospheric radiative forcing since 1750 (Myhre et al., 2013). All of the points above make it very interesting to study methane sources and sinks, and show that it is important to account for CH<sub>4</sub> when making predictions about future climate change.

## 1.2 Methane emissions from oceans

Methane emissions can be grouped in three categories based on their formation process: biogenic, thermogenic and pyrogenic (Kirschke et al., 2013). Biogenic sources contain methane-generating microbes (methanogens) and are anaerobic environments like natural wetlands, rice paddies, digestive systems of ruminants and termites, organic waste deposits, but also anoxic marine sediments (Cicerone and Oremland, 1988). Thermogenic CH<sub>4</sub> is formed over geological timescales (millions of years) by the breakdown of buried organic matter due to high heat and pressure deep in the Earth's crust (Saunio et al., 2016). It seeps from the subsurface into the atmosphere naturally, for example in marine seeps, and can also be released through the exploitation, distribution, and use of fossil fuels. Pyrogenic methane is produced during incomplete combustion of biomass and soil carbon (Kirschke et al., 2013). From oceans only biogenic and thermogenic methane is released, so pyrogenic CH<sub>4</sub> will not be discussed further in this report.

The primary sink for atmospheric methane is oxidation by hydroxyl radicals (OH) (Cicerone and Oremland, 1988; Kirschke et al., 2013; Dean et al., 2018), which accounts for about 90 percent of the global methane sink (Kirschke et al., 2013). In the ocean, there is another important sink within the water column that removes a large fraction of the CH<sub>4</sub> before the methane produced in sediments or in the anoxic layers of deeper waters reaches the atmosphere: microbial oxidation. Methane is emitted from the ocean to the atmosphere either by diffusive gas transfer or by ebullition (bubbling) across the sea-air interface (Reeburgh, 2007). If methane gas manages to reach the surface within gas bubbles it can bypass microbial oxidation, because microbes can only access dissolved methane (James et al., 2016). When the distance from the sea floor to the surface is larger the chance of methane gas reaching the surface within a gas bubble gets smaller, which is why ebullitive emissions are only significant in regions that are very shallow and where the rates of methane bubbling through the seafloor are high (Hornafius et al., 1999). In other regions dissolution of methane from rising bubbles produces supersaturated waters that drive a diffusive flux to the atmosphere (McGinnis et al, 2006; Weber et al, 2019). This diffusive flux is, contradictory to ebullition, limited by rapid microbial oxidation of dissolved oxygen (Cicerone and Oremland, 1988; James et al, 2016; Leonte et al., 2017).

In the 2000s natural wetland emissions, emissions from agriculture and waste emissions dominate methane emissions, followed by anthropogenic fossil fuel emissions, other natural emissions and emissions from biomass and biofuel burning (Saunois et al., 2016; Kirschke et al., 2013). The global methane emissions from the ocean were estimated to be about 18 Tg of CH<sub>4</sub> per year (1 Tg of CH<sub>4</sub> per year = 10<sup>12</sup> g CH<sub>4</sub> yr<sup>-1</sup>) for the period 2000-2009 by Kirschke et al. (2013), which is only a small fraction of the total global methane emission. This estimate had a huge uncertainty and was reported to be somewhere between 2-40 Tg yr<sup>-1</sup> (visible as pink bar with black error bar in figure 1). Later Saunois et al. (2016) further reduced this uncertainty and estimated the global methane emissions from the ocean to be about 14 Tg yr<sup>-1</sup> for the period 2003-2012 (5-25 Tg yr<sup>-1</sup>, which is about 1-13% of all natural emissions (Saunois et al., 2016; Weber et al., 2019)). Weber et al. (2019) estimated global methane emissions from oceans to be between 6 and 12 Tg yr<sup>-1</sup>, reducing the uncertainty further. A large uncertainty remains, however, providing every new study about CH<sub>4</sub> emissions from the ocean with the opportunity to reduce this uncertainty.

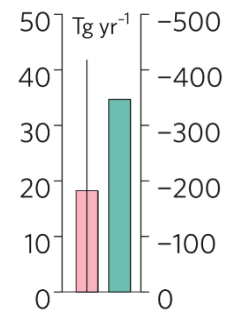


**Figure 1:** Global ocean emissions (pink) and chemical loss of methane over the ocean (turquoise) for 2000-2009 as depicted in a larger figure in Kirschke et al. (2013).

### 1.3 Zooming in to continental shelves

Methane emissions from coastal regions dominate the global oceanic methane flux (Saunois et al., 2016; Weber et al., 2019). Upward seepage of CH<sub>4</sub> of biogenic and thermogenic origin from the deep subsurface through the seafloor is especially common on continental margins (Etiope et al., 2008; Judd, 2003). Biogenic methane is especially abundant in coastal areas, because not too long ago some of our present coastal areas, like the southern North Sea, were still exposed to air due to the lower sea levels during glacial periods (Plets et al., 2007). These newly submerged peaty sediments tend to be rich in organic matter and are, therefore, sources of biogenic methane. Also thermogenic methane is plentiful on continental shelves, because these drowned areas of continental land masses are often underlain by deep sedimentary basins (Judd, 2003).

Besides, 33% of the total continental shelf area consists of shallow coastal areas with well-mixed waters (Borges et al., 2016), and methanotrophy (microbial methane oxidation) cannot keep pace with supply when the water column is fully mixed (Hamdan and Wickland, 2016).

The enhanced source of methane from the seafloor on continental shelves, the shallowness and the well-mixed conditions all lead to emissions from continental shelves of about 13 Tg CH<sub>4</sub> yr<sup>-1</sup> (Bange et al., 1994).

### 1.4 Wadden Sea

This study is about methane emissions from the Dutch Wadden Sea. To understand the emissions it is important to get an idea of the conditions within the Wadden Sea. There are quite a few aspects that make the Wadden Sea a special place. These aspects, and a situation sketch of the Wadden Sea, are described below.

In 2009 and 2014 the Wadden Sea has been placed on the UNESCO's World Heritage List (a list of the natural and cultural wonders of the planet (Enemark et al., 2018)), for its outstanding universal value as an area of natural beauty (Egberts et al., 2018). The Wadden Sea consists of the largest continuous tidal flat area of the temperate world (Reise et al., 2010; Rösner, 2018) and with a coastal stretch of about 500 km and a total area of sand and mud flats of about 4,700 km<sup>2</sup>, it comprises about 60% of the intertidal area at the north-eastern Atlantic shores (Reise et al., 2010). This belt of tidal flats is exposed to the air and then covered by water twice a day in the rhythm of

the tides and it is dissected by more than 30 branching tidal inlets and five major estuaries (Reise et al., 2010). The tidal flats are partly sheltered by a sandy barrier against the waves and wind from the rough North Sea (Reise et al., 2010; Gräwe et al., 2016) and partly for that reason the mudflats sustain abundant marine life (Rösner, 2018). The whole Wadden Sea ecosystem is very young and dynamic (Rösner, 2018) and functions as a gigantic biological filter between land and sea (Reise et al., 2010). All of these features make the Wadden Sea potentially a significant source of methane.

The Wadden Sea is mostly shallow enough to wade across (Reise et al., 2010), but in the tidal inlets it can be up to 40 meters deep (Duran-Matute et al., 2016). The average depths in the Dutch part of the Wadden Sea are depicted in figure 2.

Some authors include marine areas where the water depth during low tide does not exceed 6 m in their definition of wetlands (an area of land covered or saturated with fresh, brackish, or salt water permanently or temporarily) (Navid, 1989; Dean et al., 2018), which means large parts of the Wadden Sea can be considered as wetland areas. Others define wetlands, with respect to CH<sub>4</sub> production, as ecosystems with inundated or saturated soils where anaerobic conditions lead to methane production, excluding estuaries and other brackish and salt water systems (Saunio et al., 2016; Kirschke et al., 2013). In this report the Wadden Sea is considered primarily to be a coastal area and not a wetland.

The sediment transport in the Wadden Sea is linked to the nutrient transport (due to the high organic matter content of suspended matter), and also to the water volume transport (Gräwe et al., 2016). The high organic matter content in the Wadden Sea also facilitates methane production by methanogens, which happens during the decomposition of organic matter (Kamaleson et al., 2019; Niu et al., 2018). In the Wadden Sea the influence of the North Sea dominates over river influence (Reise et al., 2010). Tides are the main generators of sediment transport (Schroor, 2018; Gräwe et al., 2016), resulting in a decrease in soil texture (from sand to clay) landward instead of seaward (Schroor, 2018; van Straaten, 1954). Tides propagate along the coast of North Holland and along the Wadden Sea toward Denmark (Gräwe et al., 2016) and span from 1.5 to 4 m (Reise et al., 2010). Twice a day the tides move an average volume of 15 km<sup>3</sup> of sea water through the tidal channels and inlets into the tidal basins where roughly the same volume remains at low tide, thus resulting in swelling of up to some 30 km<sup>3</sup> at high tide (Reise et al., 2010). This substantial amount of water has the potential to significantly influence methane dynamics. The actual volumes of water entering and leaving on any particular day are however affected by wind as well as the spring-neap cycle (Gräwe et al., 2016). Between barrier islands and elevated sands the tidal flow is compressed and scours deep tidal inlets with a mean flow rate of about 1 m s<sup>-1</sup>. In the back-barrier area, flood waters of adjacent tidal inlets meet at tidal divides (watersheds) where currents tend to calm down (Reise et al., 2010). Tidal flats often remain submerged over several days due to prevailing westerly winds, whereas continuous emergence over several tidal cycles due to southerly or easterly winds is extremely rare (Weisse and Plüb, 2006), because the dominant wind direction opposes the tidally driven volume transport (Duran-Matute et al., 2016). Methane can be oxidised in the water column, but also in aerobic sediments, by methanotrophic bacteria (Kamaleson et al., 2019; Niu et al., 2018). Aerobic sediments may be formed when sediments are exposed to the atmosphere for a notable amount of time.

Salinity in the Wadden Sea ranges mostly between 20 and 30 psu, which is less than in the open ocean (34 psu), but more than in estuaries (0-20 psu) (Reise et al., 2010). At these salinities both methanogens and methanotrophs are present. The salinity gradient is almost always directed offshore (saltier water in the North Sea), which causes the density gradients to generally be directed

offshore as well (Gräwe et al., 2016).

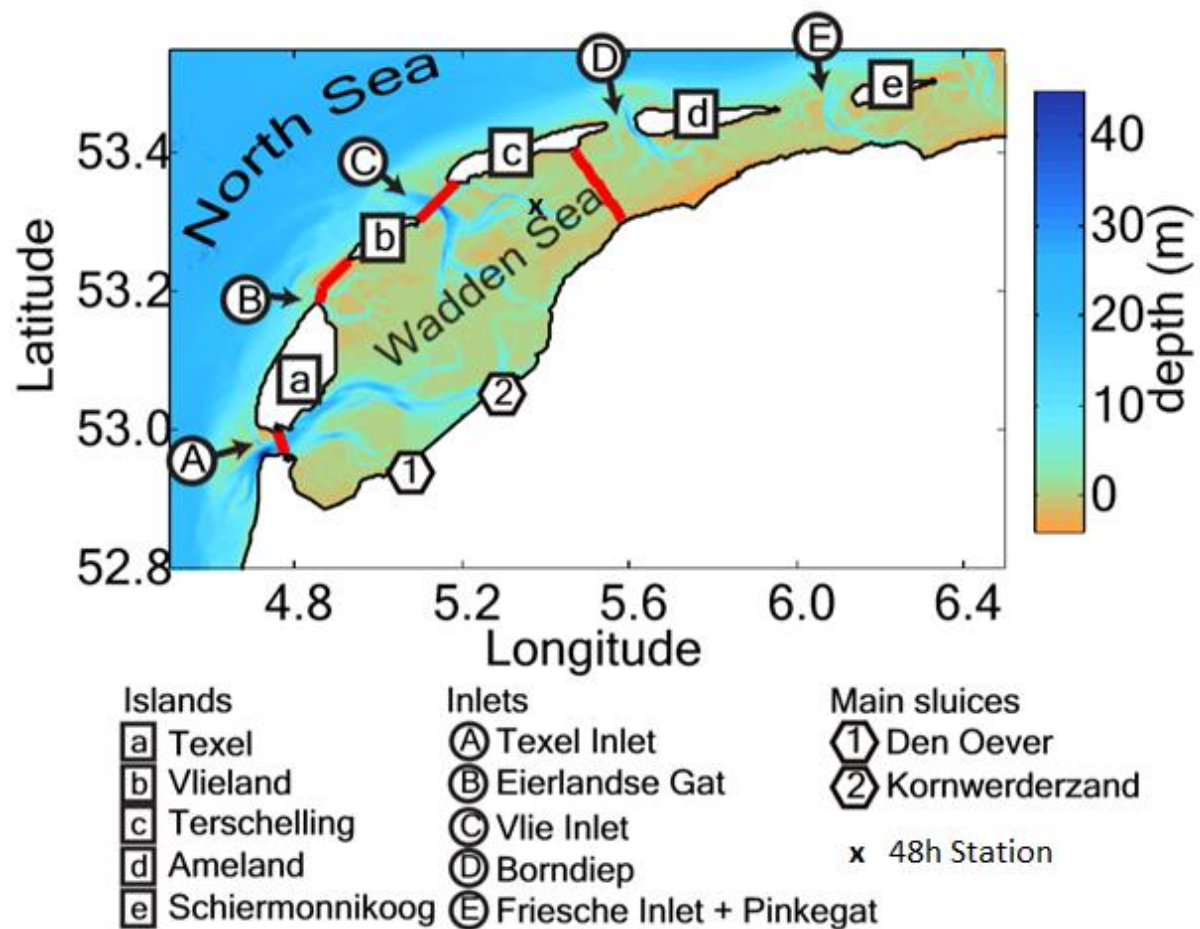


**Figure 2:** Map of the Dutch Wadden Sea with the names of the islands, inlets and the two main sluices as depicted in Duran-Matute et al. (2016). The red lines indicate the boundaries of the western Dutch Wadden Sea. The location of the 48 hour station has been added to indicate where the measurements discussed in this report were done.

The Wadden Sea is heavily used for human activities, such as fishing and recreational activities. Also its borders are defined by man-made structures, like dikes (Renes, 2018). This means that sedimentation in the Wadden Sea is no longer an entirely natural process, but that sedimentation patterns are affected by human activities (Enemark et al., 2018). However, the natural forces in the Wadden Sea are so strong that the area could not be transformed into a cultural landscape before the protection of nature became an important asset for our society about 40 years ago (Rösner, 2018).

The Wadden Sea extends from southern Denmark in the north to North Holland (the Netherlands) in the southwest (Gräwe et al., 2016; Egberts et al., 2018). Based on tidal ranges, coastal orientation and river influence, the Wadden Sea can be divided into a Southern, a Central and a Northern part (Reise et al., 2010). In this report methane concentrations measured in the western Dutch Wadden Sea (see figure 2), which is part of the Southern Wadden Sea, are described. Within the Southern Wadden Sea twelve major barrier islands are located 5 to 15 km off the mainland. These barrier islands shelter the tidal area against waves generated by northwesterly and northerly winds. Sediment imported from the sea does not fully compensate for sea-level rise and islands migrate landwards (Reise et al., 2010).

The western Dutch Wadden Sea specifically is also known as the Marsdiep-Vlie basin. It covers an area of about 1500 km<sup>2</sup> and holds an average volume of about 4.75·10<sup>9</sup> m<sup>3</sup> of water. It is a meso-tidal region with a tidal range slightly larger than 2 m (Duran-Matute et al., 2016).

## 1.5 Previous Research on Methane in the Wadden Sea

In autumn 2002 a time-series station, that measures nutrient and methane concentrations in the water continuously, was installed in the German part of the Wadden Sea (Reuter et al., 2009; Grunwald et al., 2007). Grunwald et al. (2007 and 2009) used the data collected at this station and found a tidal dependence of the methane concentration with maxima (of up to 100 nmol/L) at low tide, which indicates that the Wadden Sea is a source for methane. They conclude that pore water draining from tidal flats seems to be the main source for dissolved CH<sub>4</sub> in the Wadden Sea system at their location between the islands Langeoog and Spiekeroog, which is one of the most eastern locations within the German Wadden Sea. They also conclude that the CH<sub>4</sub> level seems to be irregularly disturbed by wind forcing, due to elevated degassing and prevention of advective flow when tidal flats remain covered by water.

Bange (2006) gathered data published in other papers to conclude that waters in the southern North Sea, bordering the Wadden Sea, were highly saturated with methane, even up to 2000%. Based on these saturation values, and values for other European coastal waters, Bange computed an emission rate of methane for the entire European coastal zone of 0.35-0.75 Tg C yr<sup>-1</sup>.

Røy et al. (2008) studied pore water flow, mainly in the German Wadden Sea, but also on the Engelsmanplaat, which is located on the eastern side of the Dutch Wadden Sea, just outside our area of study. Apart from pore water flow, they also measured the δ<sup>13</sup>C of CH<sub>4</sub> released from the seeps. They measured values of about -68.6‰, indicating a biological origin of the methane. The <sup>14</sup>C signature of the methane they found was elevated by anthropogenic radiocarbon, which indicated that the CH<sub>4</sub> was formed less than 50 years ago.

Finally, Wu et al. (2015) investigated the methanogenesis in sediments in an intertidal flat in the German Wadden Sea. They found the highest rates of methane production in the surface sediments of always submerged tidal flats, probably due to the input of fresh organic matter from the water column. However, they assume that this is not the largest source of CH<sub>4</sub>, because methanogenesis rates are low in the presence of sulphate. They conclude that a more likely source of methane are deeper sulphate-free layers.

Based on the literature search performed as part of this master thesis it can be concluded that the methane concentrations in the atmosphere above the Dutch Wadden Sea and the methane concentrations in the water of the Dutch Wadden Sea have not been measured before. This study can provide more inside in the dynamics influencing methane concentrations in this part of the world.

## 1.6 Questions dealt with in this report

In this report the following questions will be answered:

1. Are methane emissions from the Wadden Sea measurable in the atmosphere?
2. Is there a temporal cycle in the dissolved methane concentrations, oxidation rates and isotopic signatures within the water column and can this (or another) temporal cycle also be seen in the methane mixing ratios and isotopic signatures in the air above the Wadden Sea?
3. What causes enhanced or decreased methane emissions?

This was done by measuring CH<sub>4</sub> mixing ratios in the atmosphere at three levels and taking air and water samples during a cruise of a week to the Wadden Sea in the summer (July) of 2019 and a second cruise in the autumn (November) of 2019. The air and water samples were later analysed for methane concentrations and CH<sub>4</sub> isotopic signatures ( $\delta^{13}\text{C-CH}_4$  and  $\delta\text{D-CH}_4$ ) in the lab. CH<sub>4</sub> isotopic composition is strongly linked to source-sink processes (Röckmann et al., 2016), just like the methane oxidation rates within the water column, which are also determined. The following sub-sections will describe how results were obtained in detail.

## 2. Methods

### 2.1 Cruise

Conclusions drawn in this report are based on measurements done and information gathered during two cruises to the Wadden Sea on the *Navicula* (one of the research vessels of the NIOZ, shown in figure 3). Both cruises lasted a week and during both cruises one station was visited where the boat stayed for 48 hours. The first cruise took place from the 22<sup>nd</sup> until the 26<sup>th</sup> of July, which will be referred to as either the *summer cruise* or the *July cruise*. The second cruise took place from the 11<sup>th</sup> until the 15<sup>th</sup> of November and will be referred to as either the *autumn cruise* or the *November cruise*.



**Figure 3:** Research vessel *Navicula* on a tidal bank. Source: [nioz.nl](http://nioz.nl).

### 2.1.1 Route

During both cruises the first day was spent sailing to the 48 hour station, the following two days were spent anchored at the 48 hour station and the last two days were dedicated to sailing transects for plastic fishing, visiting a reference station in the North Sea and returning to the harbour on Texel. In this report the focus lies on the data gathered at the 48 hour station, depicted in figure 2.

### 2.1.2 Methane mixing ratio measurement

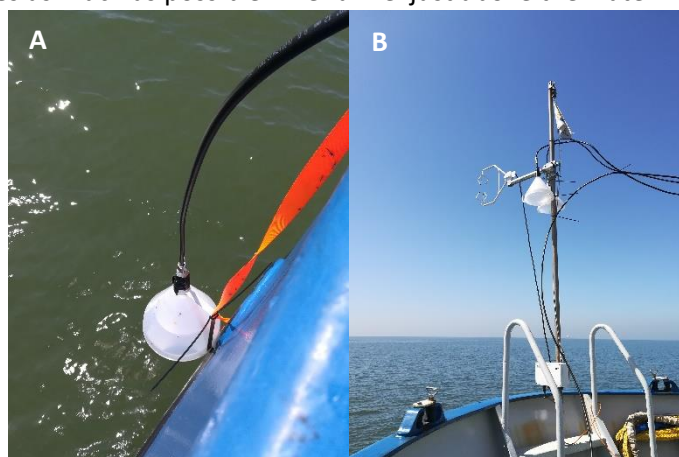
A cavity ringdown spectrometer (CRDS) from Picarro (model G2301) was installed onboard of the *Navicula* to measure methane concentrations continuously. This G2301 instrument is able to make simultaneous fast measurements of CO<sub>2</sub>, CH<sub>4</sub> and H<sub>2</sub>O mole fractions in ppm (Peltola et al., 2014). These mole fractions are measured by introducing a gas sample into an optical cavity and determining the optical absorbance of the sample. The G2301 has a high sensitivity because the light that is introduced travels a very long effective path inside the cavity (Crosson, 2008).

Figure 5 depicts the G2301 setup. In continuous operation mode the air was supplied through three different inlets. One inlet was situated at the very front of the boat in a small mast at the level of the sonic (discussed in section 2.1.3). This 'Level Sonic' inlet was positioned about 4 m above the water. The second inlet was positioned in the highest mast, at a height of about 9 m above the water. During the autumn cruise the inlet line from the mast was not connected properly and air was sucked in from the bottom of the mast, about 5.5 m above the water. This was only discovered near the end of the 48 hour station, so for the entire time before the discovery the G2301 received air from the bottom of the mast. The bottom of the mast is unfortunately close to the smoking area and where the air outlet from the kitchen and the rest of the boat is located, so some contamination of the measurements was expected. The third inlet was positioned just above the water outside the boat at about 1.5 m above the water. The heights of the inlets relative to the water level can also be seen in table 1. The inlets consist of funnels with tubes attached to them to direct the air to the G2301. The funnels were installed to increase the surface area from which air was sampled and they were designed to keep water out of the lines as much as possible. The funnel just above the water

was taken inside the boat when sailing, to keep water from getting in. Figure 4 shows the funnels of the inlets just above the water and at the level of the sonic.

In autumn, the air admitted to the G2301 alternated between the different inlets every two minutes, by controlling three valves on an inlet manifold via software on the G2301. This means that air from one inlet was sampled and analysed for two minutes before switching to the next inlet, analysing that air from that inlet for two minutes, etc. In summer the air from the inlet just above the water and from the high mast was sampled for one minute and the air from the inlet at the level of the sonic was sampled and analysed for five minutes. Note that this setup means that methane mole fractions at different heights above the water were never measured simultaneously.

Because the inlet lines towards the G2301 are very long, a high flow pump (Edwards XDS35i Dry Scroll Pump), indicated as Pump A in figure 5, was installed to suck the air into the lines. The pump ensures that there is turbulent (and not laminar) flow and minimizes the mixing of air in the tubes.



**Figure 4A:** Funnel at the start of the inlet just above the water. **2B:** Sonic and two funnels at the start of the fast GHG analyser and G2301 inlet at the level of the sonic in the front mast.

**Table 1:** Heights of G2301 inlets relative to the water level.

Inlet	Height [m above water]
Just above water	1.5
Level Sonic	4
Level Mast	9 or 5.5 (autumn)

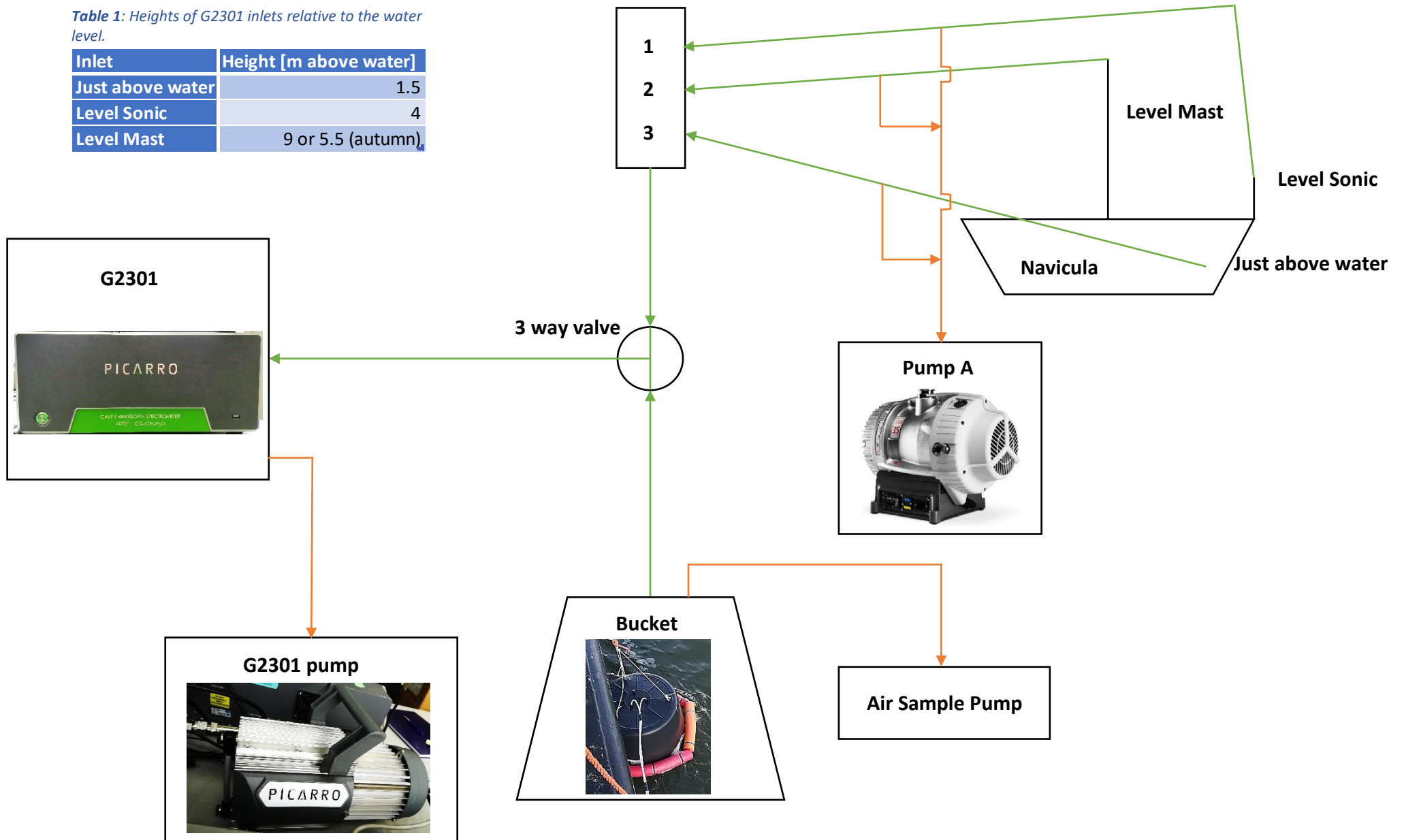


**Figure 5:** Setup of the G2301. Green lines depict airflows flowing into the G2301. Orange lines depict airflows flowing away from the G2301.

All air from the inlets that were not sampled by the G2301 at that moment got sucked into the exit lines and exited the system via the pump. Part of the air from the inlet from which air was being sampled got sucked into the G2301 by the G2301 pump (Vacuubrand MD1) and the rest was still exiting the system via Pump A. During the autumn cruise Pump A broke down and was replaced by Pump B (Varian Tri Scroll Vacuum Pump). Pump B was originally used as pump for the LGR fast GHG analyser (discussed in section 2.1.3).

The G2301 could also sample air from the bucket (discussed in section 2.1.4) by manually turning a 3-way valve. The sampling frequency of the G2301 was about 1 Hz.

### 2.1.3 Sonic and LGR fast GHG analyser

At the front mast a Campbell Scientific CSAT3 sonic anemometer was installed to measure both the wind speed components (x,y and z) relative to the boat and the air temperature. In combination with methane mole fractions at that level relations between wind speed and methane mole fractions may be deduced. Because the G2301 only measured at the level of the sonic every four minutes in autumn (and every two minutes in summer), a LGR (Los Gatos Research) Fast Greenhouse Gas Analyzer Model 907-0010 was installed to measure the methane mole fraction at the level of the sonic continuously. The setup of the fast GHG analyser is depicted in figure 6.

During the summer cruise the fast GHG analyser was switched off shortly after departure, because its measurements were unreliable. The mirror inside the fast GHG analyser, used to elongate the effective path inside the cavity, was dirty and could only be cleaned after return to the onshore lab in Utrecht. During the autumn cruise, the high flow Pump B was needed to replace Pump A for the continuous methane mixing ratio measurements and the fast GHG analyser had to run on its internal pump. This setup resulted in too slow gas exchange times in the measurement cell to carry out flux measurements and therefore the fast GHG analyser data are not further analysed in this report. The wind speed components and the air temperature, measured with the sonic, were still used for other purposes described in section 2.4.3.

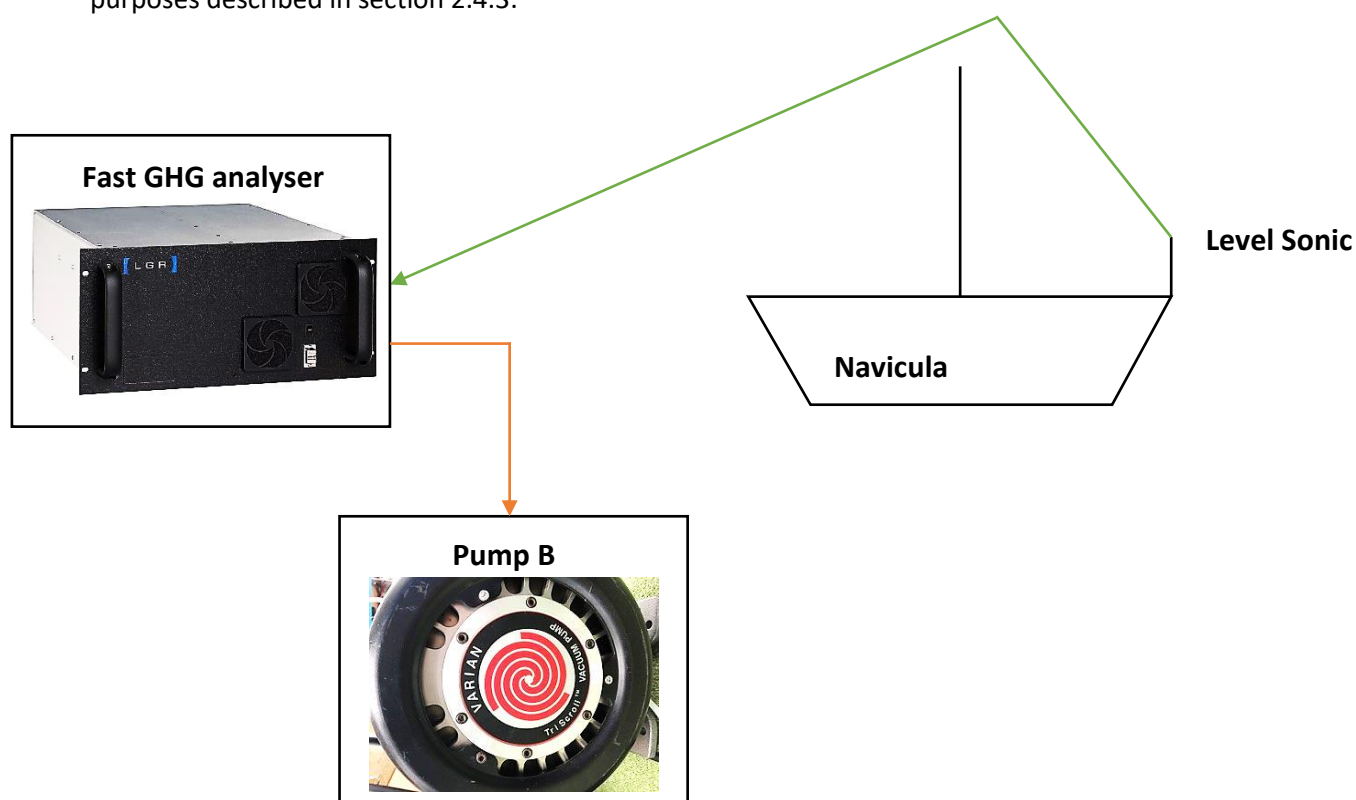


**Figure 6:** Setup of the fast GHG analyser. The green line depicts the airflow flowing into the fast GHG analyser and the orange line depicts the airflow flowing away from the fast GHG analyser.

### 2.1.4 Bucket measurement

About every three hours a bucket measurement was attempted to determine the rate of methane emission to the atmosphere. During a bucket measurement a large bucket with a volume of about 65 litres was placed on the water upside down, as depicted in figure 5. The valve to the G2301 was switched immediately after placing the bucket on the water, so the G2301 records the methane mole fractions inside the bucket. As long as the bucket remained in contact with the water surface no atmospheric air could enter and methane emitted from the water should build up in the bucket. In practice waves and currents made it difficult to keep the bucket closed off from the atmosphere for longer periods of time. Another difficulty was that water and salt should not enter the G2301 at any time, because this would severely damage the system. When the bucket sank, the line started sucking in water or water splashes into the line and the valve had to be switched immediately to prevent water from reaching the G2301. Sucking in water was especially an issue during the autumn cruise. To prevent the bucket from sinking and at the same time keep it low enough in the water so it does not open at every wave, floaters and weights were attached to the bucket.

### 2.1.5 Air samples

At the beginning of a bucket measurement and after every 10 minutes (for as long as the bucket measurement lasted) air samples were taken. To take an air sample a Multi-Layer Foil Gas Sampling Bag (5 and 12 L, depicted in figure 7) was attached to a customised Air Sample Pump (KNF NMP 830 KNDC Bag Sample Pump) in autumn and to a hand pump in summer. During the autumn cruise a stone got stuck in the pump, making the filling of the bags extremely slow and taking samples impossible at some point. Despite these difficulties plenty of bags were filled correctly.

The bags that were filled correctly were taken to the onshore lab at the IMAU to be analysed for  $\delta^{13}\text{C-CH}_4$  and  $\delta\text{D-CH}_4$ .

Apart from the samples taken during the bucket measurements, also two background samples were taken during the autumn cruise. The background samples were taken by hanging the bucket over board, but still about one meter above the water surface, and sampling the air from the bucket. The background samples were not analysed separately.



**Figure 7:** Multi-Layer Foil Gas Sampling Bag. Source: <https://www.restek.com/catalog/view/11097>.

### 2.1.6 CTD

At the 48 hour station a Conductivity-Temperature-Depth (CTD) measurement was done every hour. The CTD device (Sea Bird SBE 911plus CTD, depicted in figure 8) was lowered into the water with a crane and as it was lowered it measured the conductivity and temperature at each depth. This information was used to create depth profiles of density, temperature and salinity.



**Figure 8:** Sea Bird SBE 911plus CTD. Source: <https://www.seabird.com/profiling/sbe-911plus-ctd/family?productCategoryId=54627473769#>.

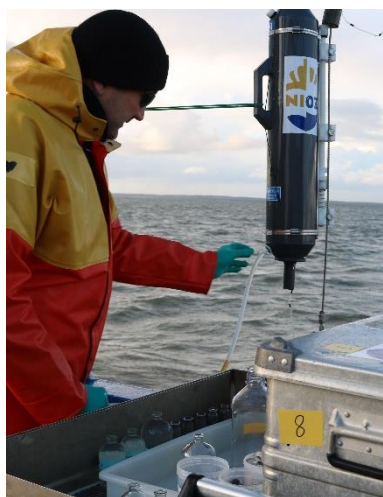


**Figure 9:** Helge Niemann taking water samples from the Niskin bottle. Picture taken by Julia Engelmann.

### 2.1.7 Water samples

Right after every CTD a Niskin bottle (depicted in figure 9) was lowered into the water to take water samples. Water samples were taken at approximately 1 and 3 meters depth. Once the Niskin bottle reached the required depth a weight was dropped along the line attached to the Niskin bottle, causing the bottle to close. The bottle, containing water from the desired depth, was then brought back to the surface, where smaller bottles were filled with the water from the Niskin bottle using a rubber tube. The bottles were allowed to overflow in order to flush the bottles and reduce the amount of air bubbles. Different bottles were filled for different purposes. The bottles used are shortly described below.

#### 2.1.7.1 Samples for isotope measurements

Two glass bottles of about 125 ml were filled bubble-free for each depth (for each CTD in autumn and about every three CTDs in summer). The glass bottles were sealed with grey butyl stoppers and crimpers and poisoned with 60  $\mu$ l mercury chloride ( $\text{HgCl}_2$ ) to avoid any methane oxidation (or production) after water collection. The bottles were stored until  $\delta^{13}\text{C}-\text{CH}_4$  and  $\delta\text{D}-\text{CH}_4$  were determined in the onshore lab at the IMAU. In summer some small, 60 ml bottles, were used at the end of the 48 hour station, because there were no more 125 ml bottles left. Also, during summer different stoppers were used than during autumn. The type of stoppers used in summer and autumn are depicted in figure 10. The type of stoppers used in summer made it very hard not to allow air to enter the bottle when sealing it. This caused almost all summer samples to contain small air bubbles, while hardly any air bubbles were present in the autumn water samples.

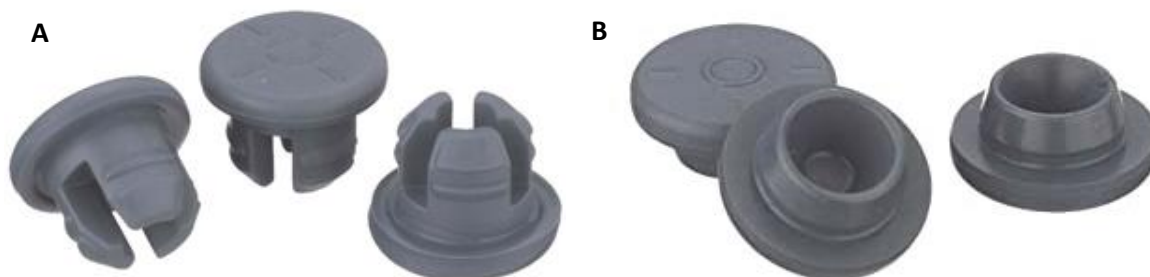


**Figure 10A:** Stoppers type with three legs used during the summer cruise. Source: <https://wheaton.com/20-mm-stopper-3-leg-ultra-pure.html>. **10B:** Stoppers type used during the autumn cruise. Source: <https://www.amazon.com/Wheaton-W224100-405-Straight-Stopper-Bromobutyl/dp/B003FSTUPU>.

#### 2.1.7.2 Samples for methane concentrations

For each CTD one glass bottle of about 250 ml was filled with water from the Niskin bottle at each depth for determination of the methane concentration in the water. After the bottles were sealed, headspace was created by injecting 5 mL of nitrogen ( $\text{N}_2$ ) and allowing water to exit the bottle to avoid overpressure, using a second syringe. Also 5 ml of concentrated salt solution (25% NaOH) was added, again allowing water to escape to avoid overpressure. This salt solution is added to force all methane (and other dissolved gasses) from the water into the headspace, because water containing more dissolved salts can contain less dissolved gas. The bottles were stored on their sides, to avoid gas escaping through tiny holes possible present in the (reused) stoppers, until methane concentrations were determined at the NIOZ.

### 2.1.7.3 Samples for methane oxidation rates

For every CTD at every height three small (15 ml) bottles were filled to determine the methane oxidation rate in the water. These bottles were, just like the others, sealed with butyl stoppers and crimpers. At the end of the cruise all of the small bottles were incubated with radioactive tritium ( $^3\text{H}$ ). This tritium is introduced as radioactive methane ( $\text{C}^3\text{H}_4$ ), which is turned into radioactive water ( $^3\text{H}_2\text{O}$ ) by methane oxidizing bacteria. Onshore at the NIOZ the samples were further prepared and ultimately the amount of radioactive molecules was determined.

### 2.1.8 Box core

After the last CTD at the 48 hour station a short sediment core was taken. The box corer, depicted in figure 11, is dropped to the bottom, closed, and slowly taken back up to the surface. In this way a sample of the bottom sediments is taken, without compromising the vertical structure of the sediment. A plastic cylinder with a diameter of about 10 cm with holes in the sides was inserted into the box core sediments and a cylinder of sediment was extracted. The holes are about one cm apart to allow sediment samples of about 5 ml to be taken from the cylinder at every depth. These sediment samples were stored in 60 ml glass vials, together with 30 ml of saturated salt solution. The vials were sealed with butyl stoppers and crimpers and stored on their sides until methane concentrations are determined at the NIOZ. During the summer cruise two box cores were taken on either side of the ship. During the autumn cruise only one box core was taken.



*Figure 11: Box corer on board of the Navicula. Picture taken by Julia Engelmann.*

## 2.2 Analysis by and at the NIOZ

Right after returning from the autumn cruise I spent two weeks at the NIOZ. During these two weeks I measured methane concentrations and methane oxidation rates in the water samples. Also the methane concentrations in the sediment were determined. All samples measured during the time at the NIOZ were autumn samples. Summer samples had already been measured at the NIOZ.

### 2.2.1 Methane Concentrations in the Water

The methane concentrations in the water were determined using a Focus Gas Chromatograph (GC) with Flame-Ionization Detector (FID) from Thermo Fisher Scientific. From a water sample, in the 250 ml glass bottle, 200  $\mu\text{l}$  of the headspace gas was extracted using a 250  $\mu\text{l}$  glass syringe. After injection into the GC, the gas sample was mixed with hydrogen, which carried the sample through a long, thin (capillary) column. In the column different compounds were separated based on the degree to which they interact with the internal coating of the column. In the FID the different gas compounds were combusted as they exited the column. This produced carbon ions that induced a current in the nearby electrodes, which was directly proportional to the carbon mass (JoVE, 2020). The peaks measured by the GC were integrated. The peak area integration by the GC program was not very accurate for small peaks, so for most peaks the peak area was re-integrated manually by adjusting integration parameters. All samples were measured at least three times. When the peak area varied greatly (standard deviation more than five percent of the average) another injection was done.

Measured peak areas could vary between measurement days. To detect and correct for these daily variations a reference gas, containing 101 ppm methane (for the autumn samples), was measured at

the start of each measurement day.

To convert areas to methane concentrations a calibration curve was created. The methane concentration in the reference gas was known, so by injecting different volumes of the reference gas, peak areas of different (known) volumes of methane could be determined. The volumes were converted to the amount of methane (in nmol) using the ideal gas law. Standard atmospheric pressure and a constant temperature were assumed in this conversion. The temperature in the lab was approximately 21°C.

When the measured peak areas were plotted against the corresponding amounts of methane a line could be drawn through the points. The line is the standard curve and should also intercept the origin (0,0), which was forced by adding a point at (0,0). The slope of the standard was used to convert peak areas of samples in which the methane concentration was unknown, to the amount of methane injected. An example of a standard curve is illustrated in figure 12.

A different reference gas, and therefore a different calibration curve, was used to measure the concentrations in the summer samples.

Multiplying the peak area with the slope of the calibration curve resulted in the amount of methane in the injection. The formula used to convert peak areas to amount of methane in the injection is given below in equation (1).

$$CH_4_{inject} = \frac{CH_4_{cal}}{Peak Area_{cal}} \times Peak Area_{sample} \quad (1)$$

Knowing the volume of the injection (200 µl) the amount of methane in the headspace is derived. The amount of methane in the headspace is the amount of methane that used to be in the water in the flask, which means the amount of methane in a litre of water can be determined using the volume of water in the flask. This conversion from amount of injected methane to methane concentrations in the water is summarized in equation (2).

$$[CH_4] = \frac{CH_4_{inject} \times (V_{head}/V_{inject})}{V_{bottle}} \quad (2)$$

In equation (2) the headspace volume ( $V_{head}$ ) and the injection volume ( $V_{inject}$ ) are both in microliter and the bottle volume ( $V_{bottle}$ ) is in liter.

The resulting methane concentrations are loaded into Python and used for further analysis.

### 2.2.2 Methane Oxidation Rates

As mentioned before, tritium in the form of radioactive methane ( $C^3H_4$ ) was introduced to the water samples on board of the Navicula. This radioactive methane can be turned into radioactive water ( $^3H_2O$ ) by methane oxidizing bacteria. The reaction is given below (Steinle et al., 2015; Mau et al., 2013; Reeburgh, 2007).



After an incubation of about 90 hours, refrigerated at about 2°C and in the dark, the flasks were opened and redistributed over two other plastic flasks. One of these plastic flasks already contained a polymer mixture (Ultima Gold) and was closed with the screw-on cap immediately after adding the water sample. This flask was shaken and set aside and used to determine the total amount of tritium added ( $^3H_2O + C^3H_4$ ). The other flask was put into a special setup, where nitrogen was pumped into

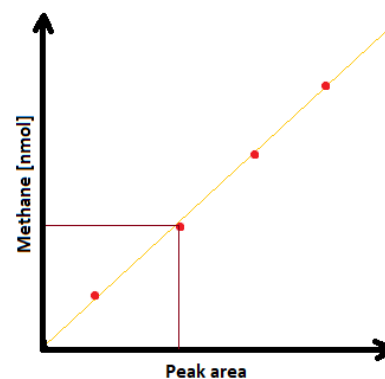


Figure 12: Example of a calibration curve. The red dots are the measurements done with a reference gas and the yellow line is the calibration curve constructed based on these measurements.

the water. This bubbling allowed the methane to escape the bottle, which means that the only radioactivity that remained was accountable to the radioactive water ( $^3\text{H}_2\text{O}$ ). After about 20 minutes of bubbling the same polymer mixture was added to this flask. The flask was sealed with a screw-on cap and shaken. The polymer mixture becomes luminescent when there is radioactivity, because the molecules in the polymer mixture absorb the energy of the emitted radioactive particle and ultimately emit photons following the absorption of the transferred energy. The amount of photon emissions was counted by a TRI-CARB 4810TR Liquid Scintillation Counter (depicted in figure 13). From the count rates the first order rate coefficient for methane oxidation ( $k'$ ) was constructed, using equation (4).

$$k' = \frac{1}{t} \frac{^3\text{H}_2\text{O}}{^3\text{H}_2\text{O} + C^3\text{H}_4} \quad (4)$$

Here  $C^3\text{H}_4$  = total counts -  $^3\text{H}_2\text{O}$  and  $t$  is the incubation period in seconds). To get the methane oxidation (MOX) rates this  $k'$  was multiplied with the methane concentrations in the water (Mau et al, 2013).

$$k' [\text{CH}_4] = \text{MOX} \quad (5)$$

Apart from the regular water samples, also three blanks, three death controls at 1 meter depth and three death controls at 3 meter depth were created. A blank contained Wadden Sea water without addition of tritium. The average count rate in the blanks was subtracted from the count rates of the other samples to correct for radioactivity naturally present in the water. Death controls are water samples that were treated with tritium, but also received an injection of  $\text{HgCl}_2$  solution. This poisons the water and kills the methane oxidizing bacteria. From the count rates and incubation time the  $k'$  values of the death controls were computed. These  $k'$  values should in principle be zero, but they were not, which means either not all methane oxidizing bacteria were killed, which is unlikely, or that some radioactive water is present in the polymer mixture. The  $k'$  values of the death controls were subtracted from the  $k'$  values of the samples. The averages and standard deviations of the three water samples at each depth were computed. The standard deviations are only based on the different  $k'$  values of different samples. The standard deviation in the methane concentrations were not taken into account here.

### 2.2.3 Methane Concentrations in the Sediment

The methane concentrations in the sediment were determined in a similar way as the concentrations in the water. One extra aspect here is that two calibration curves were created for the same reference and they were both used during the conversion from peak areas to methane concentrations. This was done to see if using different calibration curves would significantly influence the outcome, which it did not (see section 3.5).

## 2.3 Measuring isotopes

Isotopic signatures of methane in the air and water samples were determined in the onshore lab at the IMAU. There, a special system is available to determine both  $\delta^{13}\text{C}-\text{CH}_4$  and  $\delta\text{D}-\text{CH}_4$ .



*Figure 13: TRI-CARB 4810TR Liquid Scintillation Counter at NIOZ Texel containing water samples from the autumn cruise.*

### 2.3.1 Methane analysis system

An isotope-ratio mass spectrometer (IRMS) was used to measure the isotopic composition of methane. The input for the IRMS should be pure methane (mixed with helium gas, which was used as carrier gas). Extracting methane from an air sample is not easy and requires an extraction and purification system. The overview of the system is depicted in figure 14.

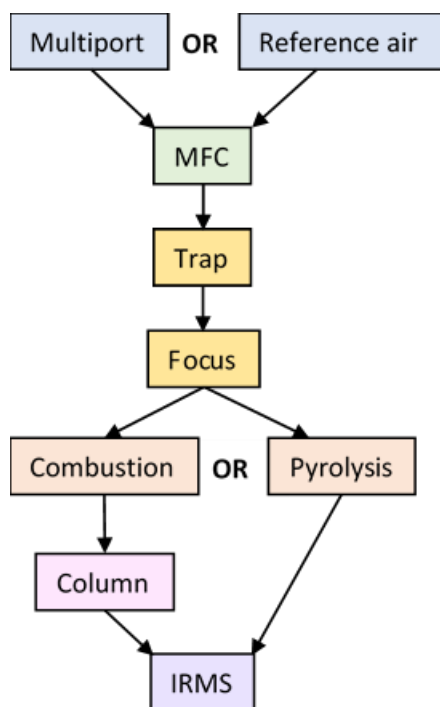


**Figure 14:** Schematic overview of the main steps in the methane analysis system at the IMAU in Utrecht.

The first step in the process is loading some air to measure. This can either be a sample attached to the multiport or reference air. A mass flow controller (MFC) loads a certain amount of the sample gas. At the same time another MFC ensures a constant amount of helium to flow through the system, flushing the system. Helium is the carrier gas in this system and it not only flushes the system, but also carries the sample through it.

After the sample was injected it reached the trap. In the preconcentration trap the 6 cm column (of HayeSep D) through which the gas flows was cooled down to about  $-130^{\circ}\text{C}$ . At these temperatures methane condensed to an absorbent on the column walls, but  $\text{N}_2$  and  $\text{O}_2$  were still in the gas phase and flushed out with helium. When most gases were gone, methane was released by heating the trap to about  $-85^{\circ}\text{C}$ . At this temperature  $\text{CH}_4$  is gaseous, but  $\text{CO}_2$  and  $\text{H}_2\text{O}$  are still frozen and remain in the trap. After the whole methane sample had left the trap, the temperature was increased further and also  $\text{CO}_2$  and  $\text{H}_2\text{O}$  were flushed out

(Brass and Röckmann, 2010). The trap does not perfectly separate  $\text{CH}_4$  from other gases, which is why the focus isolated  $\text{CH}_4$  for a second time, removing the small remaining amounts of other gases. Also, even though the sample was pumped through tiny glass capillaries and had been concentrated in the trap, the methane sample needed to be more concentrated to be measured as a higher, less broad peak. The focus functions the same as the trap and also contains a PoraPLOT Q column, which is used to perform gas chromatographical separation. The temperature inside the focus was set to  $-130$  to  $-150^{\circ}\text{C}$ . After this trapping, the methane was released by heating the focus to about  $50^{\circ}\text{C}$  (Brass and Röckmann, 2010). Injecting pure methane into the IRMS allowed determination of isotopes in the  $\text{CH}_4$  (see below). The IRMS cannot distinguish whether the mass differences were caused by deviations in the mass of the carbon or the hydrogen atoms. To determine  $\delta^{13}\text{C}-\text{CH}_4$  and  $\delta\text{D}-\text{CH}_4$  the carbon and hydrogen atoms had to be separated by conversion to different gases.

(Brass and Röckmann, 2010).

To determine  $\delta^{13}\text{C}-\text{CH}_4$ , methane was combusted to  $\text{CO}_2$  and  $\text{H}_2\text{O}$  at a temperature of about  $1130^{\circ}\text{C}$ . After combustion the sample was led through a final column to separate  $\text{CO}_2$  and  $\text{H}_2\text{O}$ . To determine  $\delta\text{D}-\text{CH}_4$ , methane was pyrolyzed to  $\text{H}_2$ , which happens at an even higher temperature (up to  $1500^{\circ}\text{C}$ ) than combustion. During methane pyrolysis  $\text{H}_2$  was formed and carbon was deposited on the reactor surface.

Finally, the sample was injected into the IRMS. In the IRMS the sample was introduced to an ion source and the molecules were ionized by electron impact and accelerated by an electric field. A magnetic sector separated the different isotopologues based on their mass. The ions were collected in Faraday cups positioned at different locations for the different masses and the ion currents were

evaluated and compared to the ratio in a “running gas” to calculate the isotope ratio (Rice et al., 2001 and Brass and Röckmann, 2010) as illustrated by equation (6).

$$\frac{{}^{13}\text{C}_{\text{sample}}}{{}^{12}\text{C}_{\text{sample}}} = \frac{\text{ion current } {}^{13}\text{C}_{\text{sample}} / \text{ion current } {}^{12}\text{C}_{\text{sample}}}{\text{ion current } {}^{13}\text{C}_{\text{ref}} / \text{ion current } {}^{12}\text{C}_{\text{ref}}} \times \frac{{}^{13}\text{C}_{\text{ref}}}{{}^{12}\text{C}_{\text{ref}}} \quad (6)$$

The measurement of a single sample took about 21 minutes.

### 2.3.2 Air samples

To measure air samples a run script was created that controlled the admission of different gasses to the system, and selected between  $\delta^{13}\text{C}$  and  $\delta\text{D}$  analysis. At the start of each measurement day first three measurements of  $\delta\text{D}-\text{CH}_4$  and three measurements of  $\delta^{13}\text{C}-\text{CH}_4$  of the reference gas were performed to check the stability of the system.

Next the  $\delta\text{D}-\text{CH}_4$  and  $\delta^{13}\text{C}-\text{CH}_4$  of the air sample was measured twice, followed by another measurement set of the reference gas and the measurement of the second air sample. A schematic representation of the run script is depicted in figure 15. The multiport valve allowed multiple sample bags to be attached to the methane analysing system, which means that after attaching several sample bags the system ran fully automated for a couple of hours. The isotopic signatures of each sample were measured twice, so the difference between the two results could serve as an indication of the measurement error.

The IRMS generated four peaks. Three peaks of an internal running gas and one sample peak. An example of the output of the IRMS for a deuterium measurement is depicted in figure 16. The sample measured in this figure is not part of the Wadden Sea samples. In the figure small peaks before and after the sample peak are present. These peaks are probably caused by other gasses than methane still present in the sample. These peaks were not observed for the Wadden Sea data. For  $\delta^{13}\text{C}-\text{CH}_4$  the output looks the same, but instead of  $\text{H}_2$  with and without deuterium  $\text{CO}_2$  with  $^{13}\text{C}$  and  $^{12}\text{C}$  is measured.

In figure 16 it can be seen that the internal running gas peaks are square peaks. This is because the internal running gas is pure  $\text{H}_2$  and this gas is injected into the gas flow right before the IRMS using an open split system, so that it does not diffuse to a near-Gaussian peak. The running gas peaks were used to determine  $\delta\text{D}$  (or  $\delta^{13}\text{C}$ ) of a sample relative to this internal running gas. The size of the sample peaks had to be approximately similar to, and not higher than, the size of the internal running gas peaks, because the isotope ratio depends to some degree on the peak height, which is an analytical issue of IRMS instruments that had to be carefully monitored and corrected for. When methane concentrations in the samples were high, the samples needed to be diluted, by loading less sample or adding nitrogen to the sample. Note that the internal running gas is not the same as the reference gas mentioned before. When measuring the reference gas, it appeared in the output as the same kind of peak as the sample, in between the internal running gas peaks. Also the  $\delta\text{D}$  (or  $\delta^{13}\text{C}$ ) of the reference gas was measured relative to the internal running gas. For all peaks, two lines were shown. One line represents the amount of  $\text{H}_2$  without deuterium (or  $^{12}\text{C}$  in the case of  $\delta^{13}\text{C}-\text{CH}_4$  measurements), and the other represents the amount of  $\text{H}_2$  with deuterium (or  $^{13}\text{C}$ ) measured by the IRMS. The fraction of  $\text{H}_2$  with deuterium over  $\text{H}_2$  without deuterium was

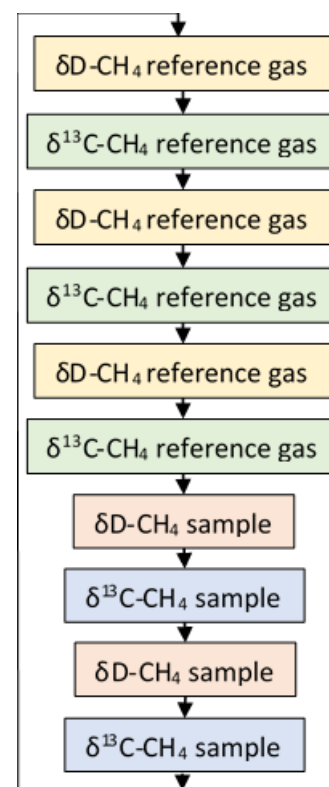


*Figure 15: Schematic representation of the run script for the measurement of air samples.*

used to determine  $\delta D$  (and the fraction  $^{13}C$  over  $^{12}C$  was used to determine  $\delta^{13}C$ ). The mathematical representation of these fractions are given in equation (7) and (8).

$${}^2R = \frac{{}^3H_2}{H_2} \quad (7)$$

$${}^{13}R = \frac{{}^{13}C}{{}^{12}C} \quad (8)$$

The isotope ratios were converted to delta values according to:

$$\delta D_{s,ref} = \frac{{}^2R_s - {}^2R_{ref}}{{}^2R_{ref}} \quad (9)$$

$$\delta^{13}C_{s,ref} = \frac{{}^{13}R_s - {}^{13}R_{ref}}{{}^{13}R_{ref}}. \quad (10)$$

In equations (9) and (10) the isotopic signatures are both relative to the reference gas ( $R_s$  is the fraction  ${}^3H_2$  or  $^{13}C$  in the sample and  $R_{ref}$  is the fraction  ${}^3H_2$  or  $^{13}C$  in the reference gas).

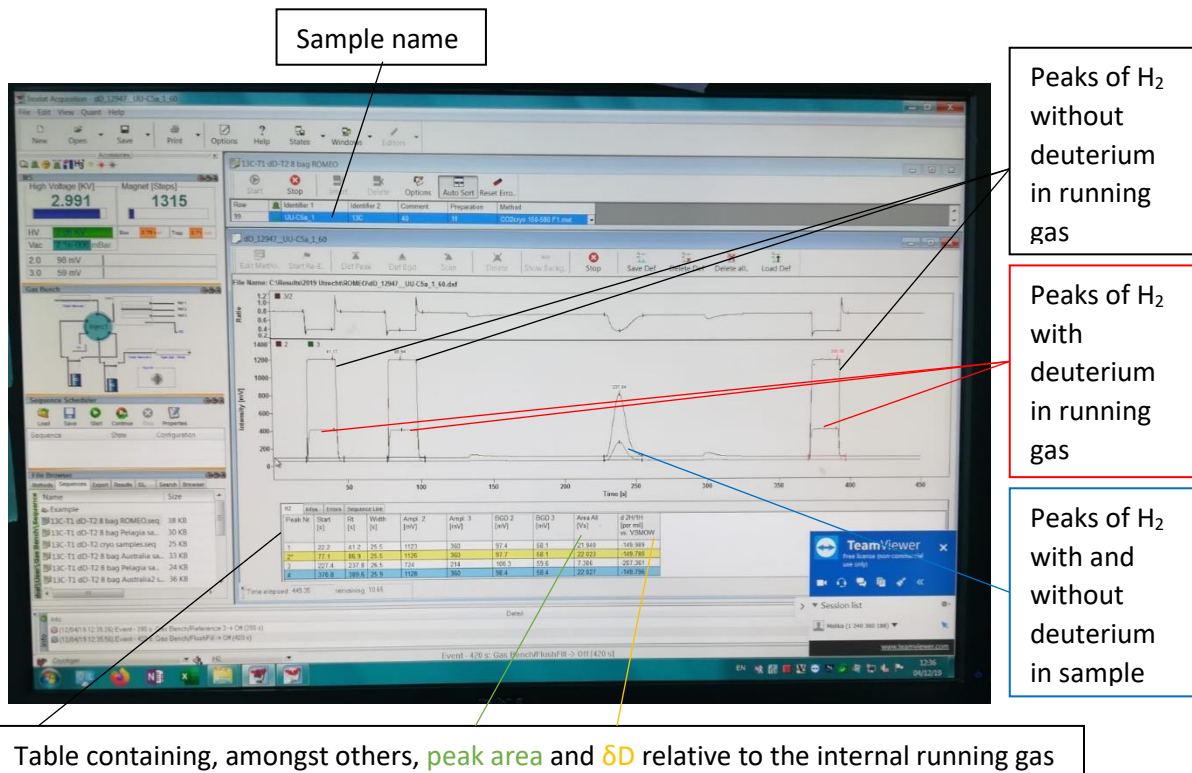


**Figure 16:** Example of the IRMS output. Textboxes have been added to clarify which parts are important to have a look at and what these parts represent.

To be able to compare the isotopic signatures with signatures in literature they were converted to isotopic signatures relative to the international standard. The steps of this conversion are given below. This is shown here only for  $\delta D$ . The steps are, however, the exact same for  $\delta^{13}C$  when you replace  $\delta D$  with  $\delta^{13}C$  and  ${}^2R$  with  ${}^{13}R$ .

The first step in determining the isotopic signatures relative to the international standard, is formulating the expressions like equations (9) and (10).

$$\delta D_{s,int} = \frac{{}^2R_s - {}^2R_{int}}{{}^2R_{int}} \quad (11)$$

Equation (11) can be rewritten to isolate  $R_s$ .

$${}^2R_s = (\delta D_{s,int} + 1)R_{int} \quad (12)$$

$R_{ref}$  can be expressed in the same way as  $R_s$ :

$${}^2R_{ref} = (\delta D_{ref,int} + 1)R_{int}. \quad (13)$$

Filling the expressions for  $R_s$  and  $R_{ref}$  in equation (9) leads to the following formula:

$$\delta D_{s,ref} = \frac{\delta D_{s,int} - \delta D_{ref,int}}{\delta D_{ref,int} + 1}. \quad (14)$$

Rewriting equation (14) finally results in the expression for the isotopic signatures relative to the international standard.

$$\delta D_{s,int} = (\delta D_{ref,int} \times \delta D_{s,ref}) + \delta D_{s,ref} + \delta D_{ref,int} \quad (15)$$

In equation (15)  $\delta D_{s,ref}$  was calculated from equation (9) ( ${}^2R_s$  and  ${}^2R_{ref}$  were both measured by the IRMS) and  $\delta D_{ref,int}$  is known. The international standard for deuterium is Vienna Standard Mean Ocean Water (VSMOW) and  ${}^2R_{VSMOW} = 0.0020052$  (Baertschi, 1976). The international standard for  ${}^{13}\text{C}$  is Vienna Pee Dee Belemnite (VPDB) and  ${}^{13}R_{VPDB} = 0.011180$  (Zhang et al., 1990). The methane concentration of the reference gas and its isotopic signatures relative to the international standards are given in table 2.

**Table 2:** Methane concentration and isotopic signatures of the reference gas relative to international standards.

Reference gas			
$\text{CH}_4$	1907	ppb	
$\delta^{13}\text{C}$	-47.75	‰	VPDB
$\delta\text{D}$	-83.38	‰	VSMOW

After the isotopic signatures of the samples relative to the international standards were determined, the average values and standard deviations were calculated and visualized in Python.

For scientific evaluation it is useful to compare the isotopic signatures to methane concentrations. While the air samples were taken, the methane mixing ratios measured by the G2301 were written down during the autumn cruise. The inverse of these mixing ratios was determined and used to plot the isotopic signatures against, to create Keeling plots (Keeling, 1958). Linear regression was done for the Keeling plots to determine the y-axis intercept, which is a measure for the isotopic signature of the methane source.

For the summer data only  $\delta^{13}\text{C}\text{-CH}_4$  was measured and mixing ratios were determined after completion of the cruise, based on the isotope measurements as described in the section 2.3.3 (equation (16)).

### 2.3.3 Water samples

The input of the methane analysis system is a gaseous sample. For water samples this requires an extraction procedure. The headspace equilibrium technique was used to extract methane from the water samples. This technique involves injecting a headspace gas, waiting until the water sample is in equilibrium with the headspace gas and injecting the headspace gas into the methane analysis system (Wilson et al., 2018; Borges et al., 2016). A schematic overview of the steps taken to extract a gas sample containing methane from a water sample is depicted in figure 17. Because the water samples were poisoned with mercury chloride, it was important to wear gloves during the entire procedure. The first step was injecting pure nitrogen ( $N_2$ ) into the sealed water sample, to create a headspace. Based on the exchange rate of methane between the headspace and the water and the amount of methane present, an optimum headspace volume was

determined. The exchange rate is based on the Bunsen solubility coefficients determined by Yamamoto et al. (1976). This Bunsen solubility coefficient depends on temperature and salinity. An average lab temperature of about 22°C, summer salinity of about 30 PSU and autumn salinity of about 20 PSU were assumed (leading to a Bunsen solubility coefficient of 0.02770 ml  $CH_4$  dissolved in 1 ml  $H_2O$  for the summer cruise and 0.02947 ml  $CH_4$  dissolved in 1 ml  $H_2O$  for the autumn cruise). With a headspace volume of about 30 ml (over 95 ml remaining water), more than 99% of the methane in the water would, in theory, be transferred to the headspace. As depicted in figure 18,

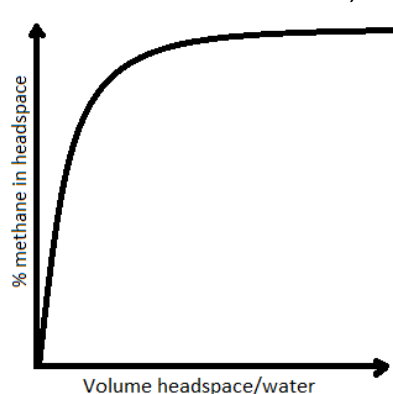


**Figure 18:** Example of the shape of the curve describing the relation between the percentage of  $CH_4$  in the headspace and the ratio of headspace volume over water volume.

the percentage of methane in the headspace is not extremely sensitive to the ratio of headspace over water, as long as this ratio is not below a certain threshold value. With a headspace of 30 ml the ratio was above the threshold value at all times.

To add this headspace, the bottle containing the water sample was hung upside down on a standard with the upper clamp, depicted in figure 19. A syringe, with a three-way valve and a needle, was filled with pure  $N_2$  and emptied into the surroundings three times, to rinse the syringe. It was filled a final time with about 40 ml of  $N_2$  and the three-way valve was closed, so the  $N_2$  inside of the syringe was closed off from the environment. A second syringe, with needle, was rinsed with demineralized water three times. After the water syringe was emptied for the third time, pressure was applied to the plunger and the needle of the syringe was injected into the water sample. After insertion of the needle the plunger was released and the bottom of the syringe was allowed to rest on the lower clamp. The valve of the  $N_2$  syringe was opened and the excess of  $N_2$  was pushed out. When the syringe only contained about 30 ml of  $N_2$ , the syringe was injected into the water bottle, while maintaining a constant pressure on the plunger. Excess  $N_2$  was removed from the syringe just before inserting it into the water bottle to flush the needle. Maintaining constant pressure kept water from entering the syringe. As the  $N_2$  syringe was emptied the water syringe filled with about 30 ml of water. After the  $N_2$  syringe was empty both syringes were extracted and the water was dumped in the toxic wastewater container.

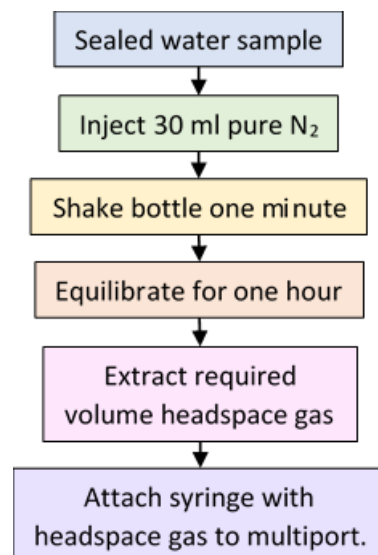


**Figure 17:** Schematic representation of the headspace equilibrium procedure.

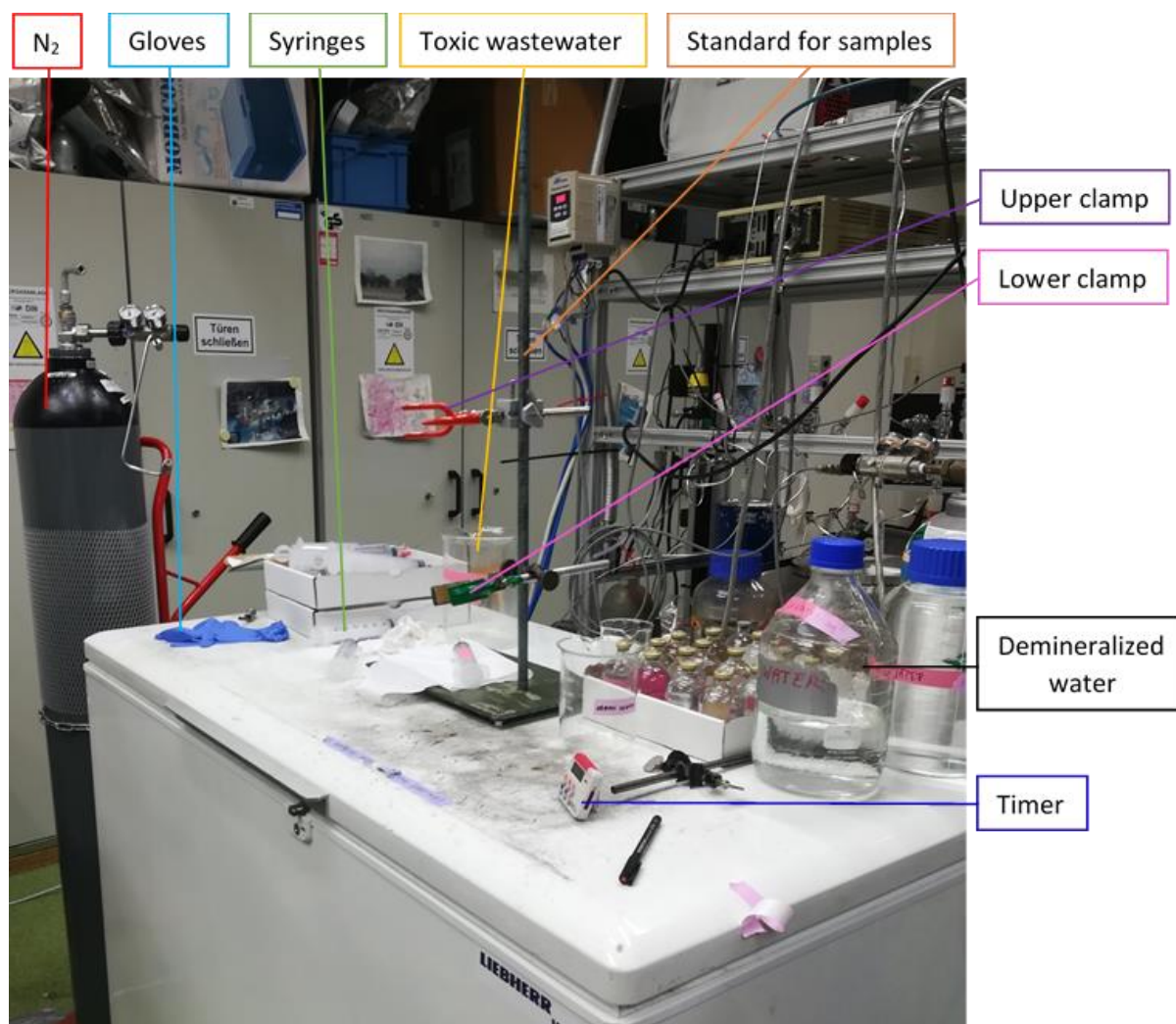


**Figure 19:** Experimental setup for extracting methane containing gas from water samples.

The sample was shaken for one minute to enhance the amount of mixing between the water and the headspace. After this the bottle was left upside down for at least an hour to allow the headspace and the water to equilibrate.

Once the water sample had equilibrated the bottle was placed upright in the lower clamp. Both the water and the N<sub>2</sub> syringe were flushed three times, but this time about 10 ml of N<sub>2</sub> was left in the N<sub>2</sub> syringe and the water syringe was filled with the volume needed for the measurement of the isotopic signature and 10 ml excess demineralized water. The N<sub>2</sub> syringe was emptied and inserted into the sample bottle while keeping pressure on the plunger. The needle of the N<sub>2</sub> syringe had to stay within the headspace volume at all time to avoid water entering the syringe. The 10 ml excess water was removed from the water syringe and this syringe was also inserted when the volume required for the analysis was left in the syringe. The water syringe was injected into the bottle while the N<sub>2</sub> syringe filled with a volume of headspace about equal to the volume of inserted water. When the water syringe was empty both syringes were removed (before removal of the N<sub>2</sub>/sample syringe the three-way valve was closed). For most samples the methane analysis system loaded a little less than 30 ml for one measurement, which means at least 30 ml of sample was needed. The amount of sample loaded could be adjusted according to the CH<sub>4</sub> concentration in the water sample. For samples with a high methane concentration a smaller amount of sample was loaded. Also, when methane concentrations in the water samples were high, samples were diluted in order to get the sample peaks a similar size as the reference peaks (as discussed in section 2.3.2). Samples were diluted by extracting 30 ml, or less for samples with a very high CH<sub>4</sub> concentration, of the sample and



**Figure 20:** Syringe pump. Picture taken by Caroline Jacques.

adding N<sub>2</sub> to the sample syringe.

Finally, the needle was removed and the syringe was attached to one of the ports of the multiport. The syringe was placed in a syringe pump (depicted in figure 20). This pump was turned on one minute before the loading started, to ensure a constant sample flow during loading. Trial and error had indicated that when only the MFC was used to draw in sample gas, also air from the environment was sucked in.

The procedure for measuring isotopic signatures in water samples is far more labour intensive than the measurement of air samples. During the entire duration of the measurement an operator had to be present. This is why water samples were only measured during the day. A typical measurement day is schematically depicted in figure 21. Each day the reference gas was measured, followed by a blank. A blank is air from

a syringe filled with N<sub>2</sub>, which means no peak should show up in the IRMS output. After the blank, another reference was measured, followed by the first sample. The CH<sub>4</sub> concentrations in the summer samples were high enough to measure duplicates. After both duplicates, another reference was measured. When samples were only measured once, a single sample measurement was directly followed by a reference gas measurement.

After about three samples another blank was measured to make sure no contamination of the samples took place. At the end of the measurement day two references were measured and the night program was started. At night different volumes of reference gas were loaded to test the linearity of the system. The system was sound when injections of the same volume resulted in similar peak areas, because peak area is proportional to methane concentration, which is proportional to volume. The isotopic signatures of the reference gas are not supposed to vary greatly either.

Due to limited lab access during the COVID-19 pandemic only δD-CH<sub>4</sub> was determined for the water samples. Apart from δD-CH<sub>4</sub>, also the CH<sub>4</sub> concentrations of the samples were determined. Throughout this report the methane concentrations measured at with the GC at the NIOZ are used, but IMAU CH<sub>4</sub> concentrations were constructed to see how the two compare. Because the methane concentration of the reference gas was known, the injection volumes were recorded and the peak areas of the sample and the reference gas were measured, the methane concentration of the sample could be determined using equation (16).

$$[CH_4]_s = \frac{Area_s/V_s}{Area_{ref}/V_{ref}} [CH_4]_{ref} \quad (16)$$

Isotopic fractionation happens when methane is oxidized, and the Rayleigh fractionation model (equation 17) can be used to characterize methane oxidation processes based on the isotope measurements (Mahieu et al., 2006). The fractionation constant was determined by taking the natural logarithm (ln)

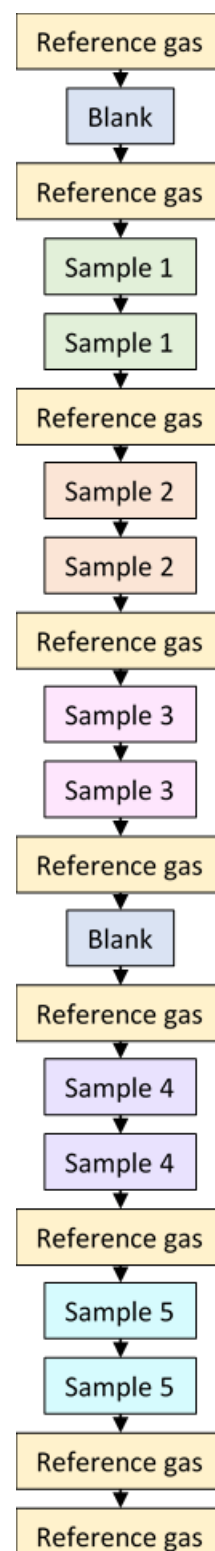


**Figure 21:** Schematic representation of the daily measurement scheme of the water samples.

of the methane concentration over the maximum  $\text{CH}_4$  concentration and plotting the natural logarithm of  $\delta\text{D}-\text{CH}_4 + 1$  against it, and determining the linear regression line and its statistical parameters.

$$\ln(\delta\text{D} + 1) = \varepsilon \ln\left(\frac{\text{CH}_4}{\text{CH}_{4\max}}\right) \quad (17)$$

The NIOZ and IMAU methane concentrations were also plotted against each other.

## 2.4 Data analysis

Most of the data analysis and visualization was performed mostly in Python and partly in Excel. There are three data sources that required quite some processing to reach final results. The data processing steps are described below.

### 2.4.1 CTD

To visualize the CTD data, contour plots of temperature, depth and salinity were created. Contour plots were preferred, because they show how the variables change both in time and with depth.

The steps taken to analyse the CTD data are depicted in figure 22.

The first step was loading the CTD cast data and the times the CTD measurements were done. The time was converted to seconds from the time the first CTD was taken. This was done for all variables in this report in order to plot them against time in hours since the first CTD. A list with depths for which the temperature, depth and salinity was desired was constructed. This list starts with the shallowest depth all CTD measurements had in common. So when two CTD measurements recorded from a depth of half a meter and further down and a third CTD measurement recorded from a depth of one meter, the list of depths started at one meter depth. Similarly, the list ended with the deepest level recorded by all CTD measurements. After every 0.05 meter a depth was inserted in the list.

The CTD variables were interpolated over the depths in the list to create lists of equal size.

Interpolation was possible, because the CTD recorded variables at a lot of depths. The interpolated variables for each CTD were combined in a single matrix, which was ultimately plotted against time and depth in a contour plot.

### 2.4.2 Methane mixing ratios

The G2301 instrument recorded  $\text{CH}_4$ ,  $\text{H}_2\text{O}$  and  $\text{CO}_2$  mixing ratios throughout the cruise. The inlets from which the G2301 measured were continuously changing. Based on the data from the program that controlled from which inlet air entered the G2301, the measurements were split into measurements from different inlets. Subsequently the data were filtered so only the data from the 48 hour station were left. These data were plotted against time relative to the first CTD and separated and plotted around individual CTD measurements. Plotting the individual CTD measurement data was done to examine the data further. The next step was splitting the data into bucket and background data based on recorded times of

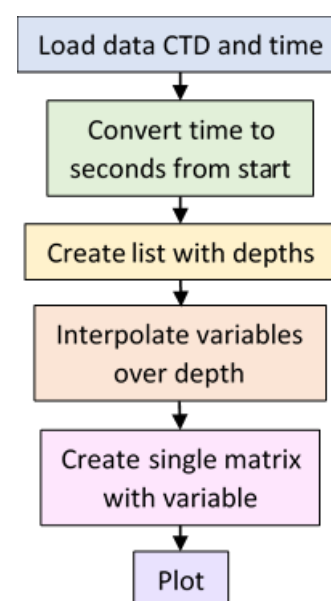


Figure 22: Schematic overview of the data analysis performed on the CTD data.

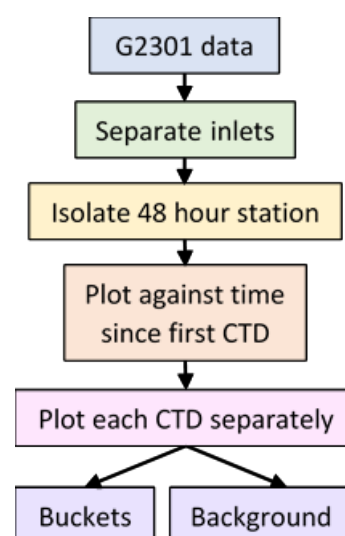
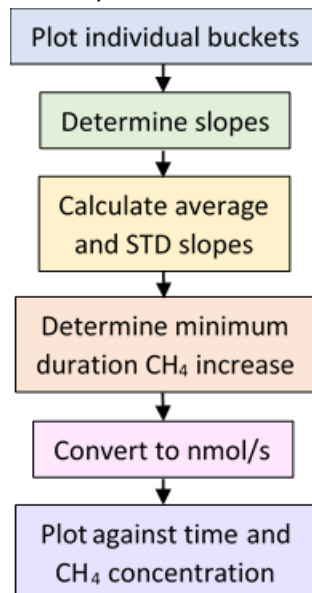


Figure 23: Schematic overview of data analysis of the G2301 data up to the point at which the bucket and background data were split.

bucket measurements. Below the bucket and background data are discussed separately. A schematic overview of the data analysis of the G2301 data up to this point is depicted in figure 23.

#### 2.4.2.1 Bucket data

All bucket data were saved in separate files. Subsequently each bucket measurement was plotted and slopes were determined. Slopes were determined for all methane mixing ratios from the start of



a methane increase until the methane mixing ratio dropped again. For some buckets the moments the bucket opens were determined and slopes in between the openings were determined. Other buckets did not open as much, but during the measurement the rate at which the methane mixing ratio inside the bucket increased changed. For different rates of methane increase, different slopes were determined. An example of slopes determined for autumn and summer buckets can be found in appendix 1. The slopes were calculated by subtracting the first methane mixing ratio, determined to belong to the slope, from the last mixing ratio, and dividing this by the difference in time. For each bucket measurement the slopes were averaged and the standard deviations were determined. Methane increases that lasted only a few seconds can have very different slopes than methane increases that last longer. Based on the duration of the CH<sub>4</sub> increase, obvious outliers, causing a large standard deviation (STD), were removed from the data.

**Figure 24:** Schematic overview of the steps taken to analyse the bucket data.

Thereafter, the rates of methane increase were converted from ppm/s to nmol/s. This was done using the ideal gas law and by assuming atmospheric pressure and an average temperature of about 6°C in autumn, and 28°C in summer. The average slopes per bucket were plotted against time. Error bars, based on the standard deviations were also added.

Finally, the methane concentrations that were measured around the same time as the bucket measurements were performed, were plotted against the emissions determined with the buckets. The overview of the analysis of the bucket data is given in figure 24.

#### 2.4.2.2 Background data

The first thing that was done to the G2301 data after the bucket data were removed, was plotting methane mixing ratios, CO<sub>2</sub> mixing ratios and water fractions. For the summer data the noise levels were calculated, by subtracting averages over 10 measurements from the actual measured values. The residuals at each CTD were constructed by averaging all residuals 12 minutes before and 12 minutes after each CTD. The air temperatures measured by the sonic were plotted to compare with the temporal variations in the methane mixing ratio.

The next step was to average the background data for each inlet. This means that in winter for each inlet the methane mixing ratios were averaged over two minutes, or about 40 measurements. The first 15 values were neglected to ensure no methane left in the lines from the previous measurement was accounted to the wrong inlet. In summer the air from the inlet just above the water and the inlet in the high mast was measured for one minute, or about 20 measurement. The CH<sub>4</sub> mixing ratios for these inlets were averaged over one minute and only the first 7 values were neglected. Air from the inlet at the level of the sonic was measured for five minutes and was

averaged over the entire five minutes, neglecting the first 15 values. Also, the first and last 20 measurements from the inlet at the level of the sonic were averaged, neglecting the first 7 values to construct variables based on the same amount of measurements as for the inlets they were compared with in another step. The time coupled to these averages was determined by adding half the difference between the time the first and the last measurements were taken to the time the first measurement was done. Standard deviations were also constructed. The Python functions used to determine the averages, standard deviations and new times for the autumn and the summer cruise can be found in appendix 2.

Averages with a high standard deviation were removed from the dataset, because further investigation pointed out that those averages were representations of high temporary peaks in methane. For the autumn data all averages with standard deviations higher than, or equal to, 0.005 ppm were removed. For the summer data all averages with standard deviations higher than, or equal to, 0.03 ppm were removed. Finally, differences between the averages of different inlets were determined and plotted against time. The average methane mixing ratio for both summer and autumn were also computed. The steps taken to analyse the background G2301 data are depicted in figure 25.

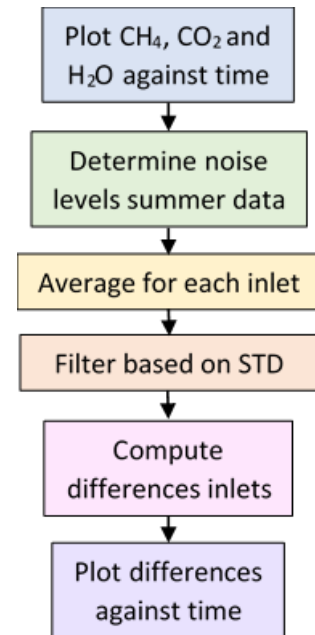


Figure 25: Schematic representation of the data analysis done for the background G2301 data.

### 2.4.3 Sonic

From the sonic data the wind direction and wind speed were determined according to the steps depicted in figure 26.

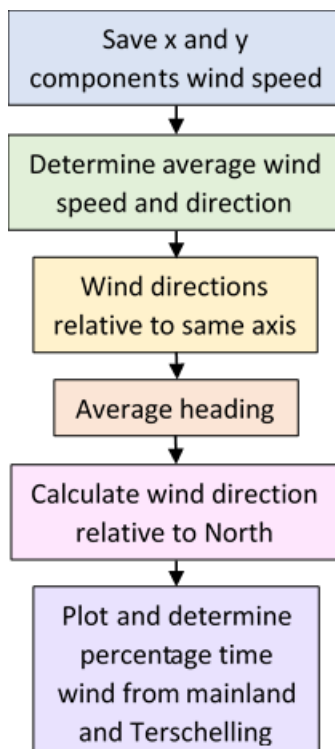


Figure 26: Schematic representation of the steps taken to analyse the sonic data.

The first step was loading the sonic data and saving the x and y component of the wind speed.

These components were averaged over half an hour. With these components the average wind speed and direction were determined using the cosine and the tangent, as depicted in figure 27.

Based on this figure the following formula was constructed:

$$\tan(\alpha) = \frac{U_y}{U_x} \quad (18)$$

Which means the wind direction,  $\alpha$ , can be expressed as:

$$\alpha = \tan^{-1}\left(\frac{U_y}{U_x}\right) \quad (19)$$

In the same way the wind speed,  $U$ , can be expressed as:

$$U = \frac{U_x}{\cos(\alpha)} \quad (20)$$

The wind direction retrieved using this method depends on the sign of the x and y components of the windspeed, as illustrated in figure 28. To convert the wind directions to wind direction

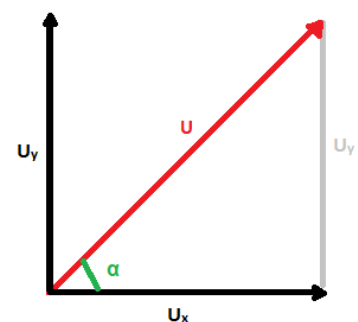
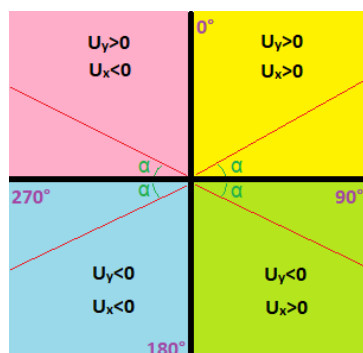


Figure 27: Definition of wind speed (red) and direction (green) based on the x and y components of wind speed.

relative to the same axis, the wind directions belonging to the yellow



**Figure 28:** Definitions of wind directions for different signs of the  $x$  and  $y$  component of the wind speed.

square were subtracted from  $90^\circ$ ,  $90^\circ$  was added to the values belonging to the green square, the wind directions in the blue square were subtracted from  $270^\circ$ , and  $270^\circ$  was added to the wind directions in the pink square.

These steps led to wind speed and direction relative to the boat. Using the heading of the boat, recorded by the ship's navigation system, the wind direction was expressed in degrees relative to the North. During the summer cruise the heading was recorded every 20 minutes, while in autumn it was recorded 30 seconds. To create a similar variable as the wind direction the heading was averaged over 30 minutes. The half an hour of values before the time the average was determined for are averaged, because this is also how the wind direction and speed were averaged.

Once the average heading was determined it was subtracted from the wind direction. If that resulted in a negative wind direction,  $360^\circ$  were added. The standard deviation in the heading was taken as the error in direction. For summer the error was not taken into account, because the averaged heading consisted either of a single value or two values.

Finally, the wind direction and speed were plotted against time and the percentage of time the wind blew from shore and from Terschelling was determined. The wind blew from the mainland when the wind direction was between  $270$  and  $360^\circ$ . It blew from Terschelling when the wind direction was between  $105$  and  $225^\circ$ . The wind speed and direction were also plotted in the same plot as the background  $\text{CH}_4$  mixing ratios.

#### 2.4.4 Emissions

Finally, many data were combined to determine the flux of methane from the water to the atmosphere (sea-air flux). In the end these fluxes were compared with the emissions determined with the bucket to see how they agree.

The sea-air flux was determined using the method described by Holmes et al. (2000). They define the flux of methane from the water to the atmosphere as follows:

$$F = K_L(C_{meas} - C_{eq}). \quad (21)$$

Here,  $K_L$  is the gas transfer coefficient,  $C_{meas}$  is the methane concentration in the surface mixed layer, and  $C_{eq}$  is the air-equilibrated gas concentration.

The equilibrium methane concentration was also determined to decide on the volume of the headspace to create in the water samples. As described in section 2.3.3, this concentration was determined using the Bunsen solubility coefficient defined by Yamamoto et al. (1976), but this time the CTD data was used to find the salinities and temperatures of the water. The temperatures and salinities measured from the water surface up to a depth of 1 meter were averaged to obtain an average temperature and salinity for each CTD. Maximum and minimum values of temperature and salinity in the top 1 meter were also determined to see if taking the maximum or minimum values would influence the value of the Bunsen solubility coefficient. To convert this coefficient to nmol/L, the molar volume of methane was determined using the ideal gas law. For this the average air temperature measured by the Sonic was used and atmospheric pressure (1000 hPa) was assumed. The methane mixing ratios determined from the background G2301 data were averaged to get a single average and standard deviation for each CTD. These were multiplied with the Bunsen solubility coefficient to get the equilibrium  $\text{CH}_4$  concentration and a standard deviation based on the atmospheric  $\text{CH}_4$  mixing ratios.

The methane concentration in the surface mixed layer was the  $\text{CH}_4$  concentration measured at about

1 meter depth at the NIOZ. Also the standard deviation of this concentration was taken into account. The gas transfer coefficient depends on the friction velocity ( $U^*$ ), like in equations (22) and (23), which were defined by Barber et al. (1988).

$$\text{for } U^* \leq 15 \text{ cm/s} \quad K_L = 2.0 \text{ cm/h} \quad (22)$$

$$\text{for } 15 < U^* < 65 \text{ cm/s} \quad K_L = 1.0U^* - 12.1 \text{ cm/h} \quad (23)$$

The friction velocity was determined by assuming a logarithmic wind profile. When the lowest level is the level at which the wind speed is zero, the expression given by Tennekes (1972) applies. This expression is given below as equation (24). Equation (25) is the rewritten version to create an expression for the friction velocity.

$$\frac{U}{U^*} = \frac{1}{\kappa} \ln \left( \frac{z}{z_0} \right) \quad (24)$$

$$U^* = \frac{U \times \kappa}{\ln \left( \frac{z}{z_0} \right)} \quad (25)$$

The wind speed,  $U$ , was determined using the data from the sonic and the same values were used again here. The von Kàrmàn constant,  $\kappa$ , is a constant with a value of 0.4. The height,  $z$ , is the height at which the wind speed is measured. In this case this is the height at which the sonic was installed, which was at about 4 meters above the water. The aerodynamic roughness length,  $z_0$ , is estimated to be between about 0.1 and 0.01 mm over smooth water bodies (Sheng et al., 2003). Here it was decided to take a value of 0.2 mm for the roughness length in summer. During the summer cruise the water was extremely flat, only occasionally disturbed by some ripples. A value of 1.5 mm was taken for the roughness length in autumn. During the autumn cruise the sea was not smooth at all and occasionally large waves rocked the ship. Larger values for the roughness length gave values higher than 65 cm/s for the friction velocity. With frictions velocities higher than 65 cm/s gas transfer coefficients could not be determined based on equations (22) and (23).

After the friction velocity and the gas transfer coefficient were determined, the sea-air flux was determined using equation (18). This resulted in a sea-air flux in nmol per m<sup>2</sup> per day for each CTD. The bucket emissions were in nmol/s and were converted to nmol/m<sup>2</sup>/s by dividing the bucket emissions by the area of the bucket, which is about 0.3 m<sup>2</sup>. This was done to compare the bucket emissions to the sea-air flux.

### 3. Results

Below, the results of the analysis described in section 2 are depicted. Relations between different results are drawn to answer the research questions. Possible explanations for the visible relations are also given. In figures summer results are indicated with a yellow sun and autumn results with a grey cloud.

#### 3.1 Tides

The tidal cycles are depicted in figure 29. This figure provides an overview of the moments in time that certain measurements were done and the corresponding relative water height in the tidal cycle. The tidal cycle is one of the elements that varies periodically in time and has the potential to influence methane emissions from the Wadden Sea.

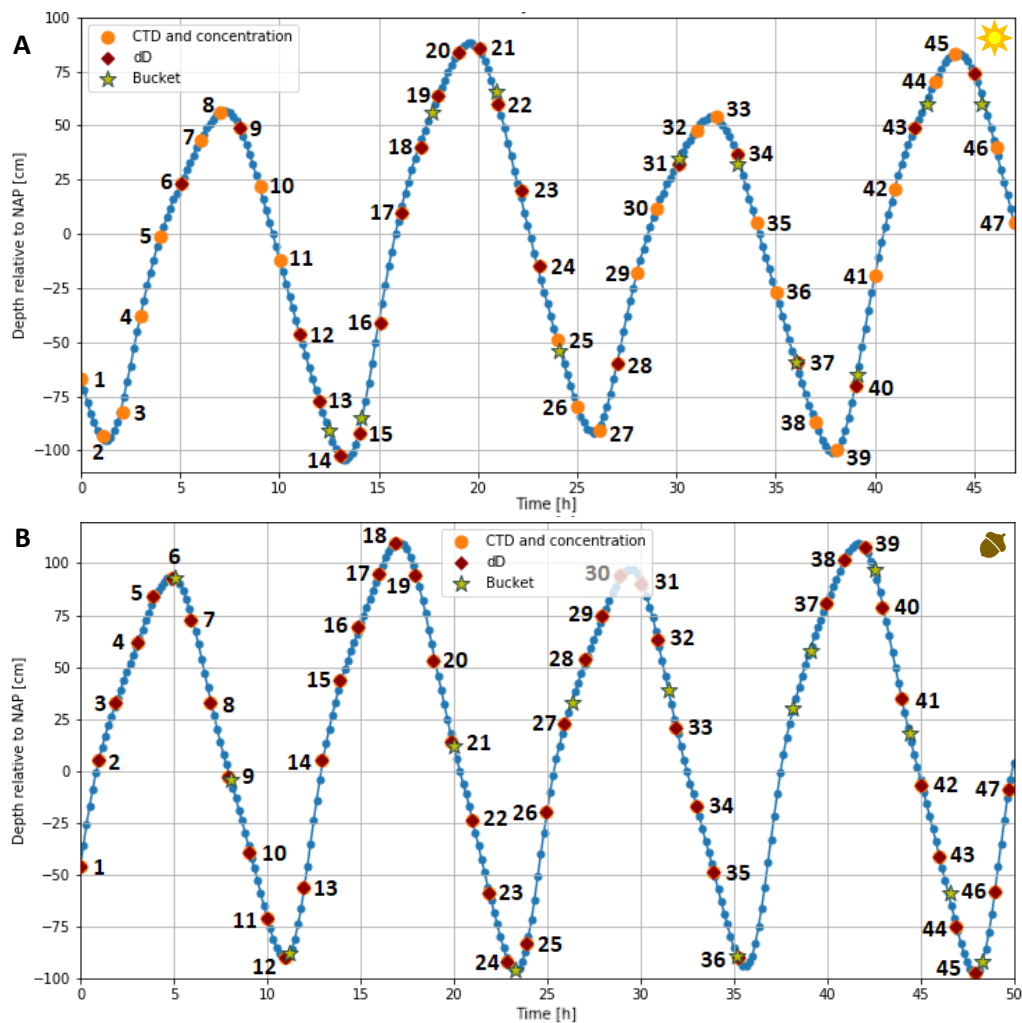


**Figure 29A:** Tidal cycle during the summer cruise plotted against time. **29B:** Tidal cycle during the autumn cruise plotted against time. In both figures the moments in time when CTD measurements were taken, when water samples were taken to measure the concentration and  $\delta D$ , and when bucket measurements were done, are indicated.

### 3.2 CTD

The contourplots of water temperature, density and salinity against depth and time for the summer cruise can be seen in figure 30A, B and C.

The tidal cycle is also added (figure 30D) as an indication of the conditions during the measurements.

High density and high salinity prevail from just before the high water peak until just before the low water trough. This is an indication of North Sea water being drawn into the Wadden Sea at high tide, which is exactly what is to be expected. The temperature in summer is quite homogeneously high, but the highest temperatures do occur during low tide. This temperature pattern might at least be partly explained by the smaller amount of cool North Sea water being drawn in at low tide.

In figure 31 the same variables are depicted for the autumn cruise. The white part in the graphs is the moment in time when the CTD stopped working.

In autumn the density,

salinity and temperature are higher just before the high water peak until just before the low water trough, again indicating North Sea water being drawn into the Wadden Sea at high tide.

From figure 30A and 31A it can also be seen that water temperature is higher in summer.

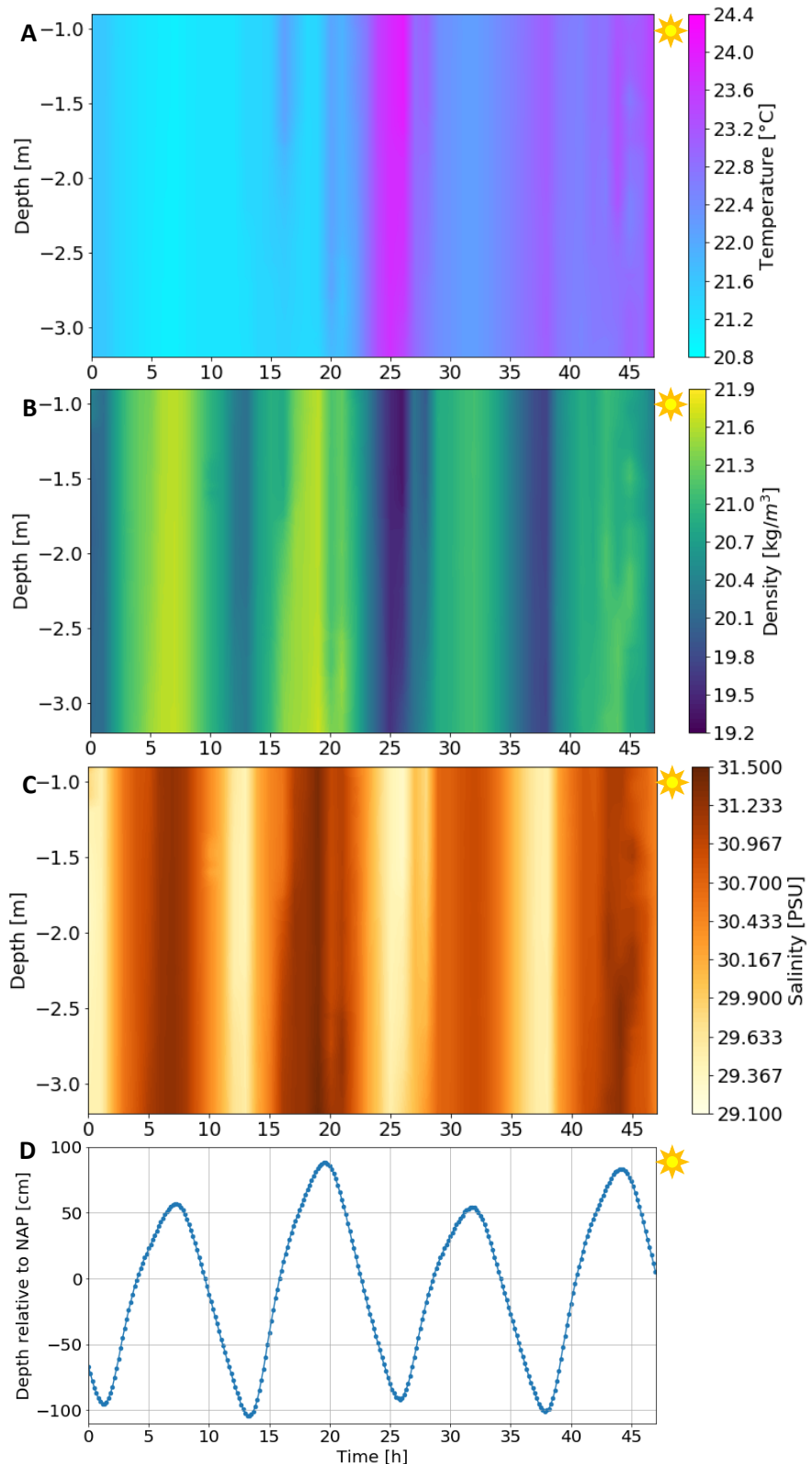


**Figure 30A:** Temperature against depth and time. **30B:** Density against time and depth. **30C:** Salinity against depth and time. **30D:** Tidal cycle against time. All figures show conditions during the summer cruise.

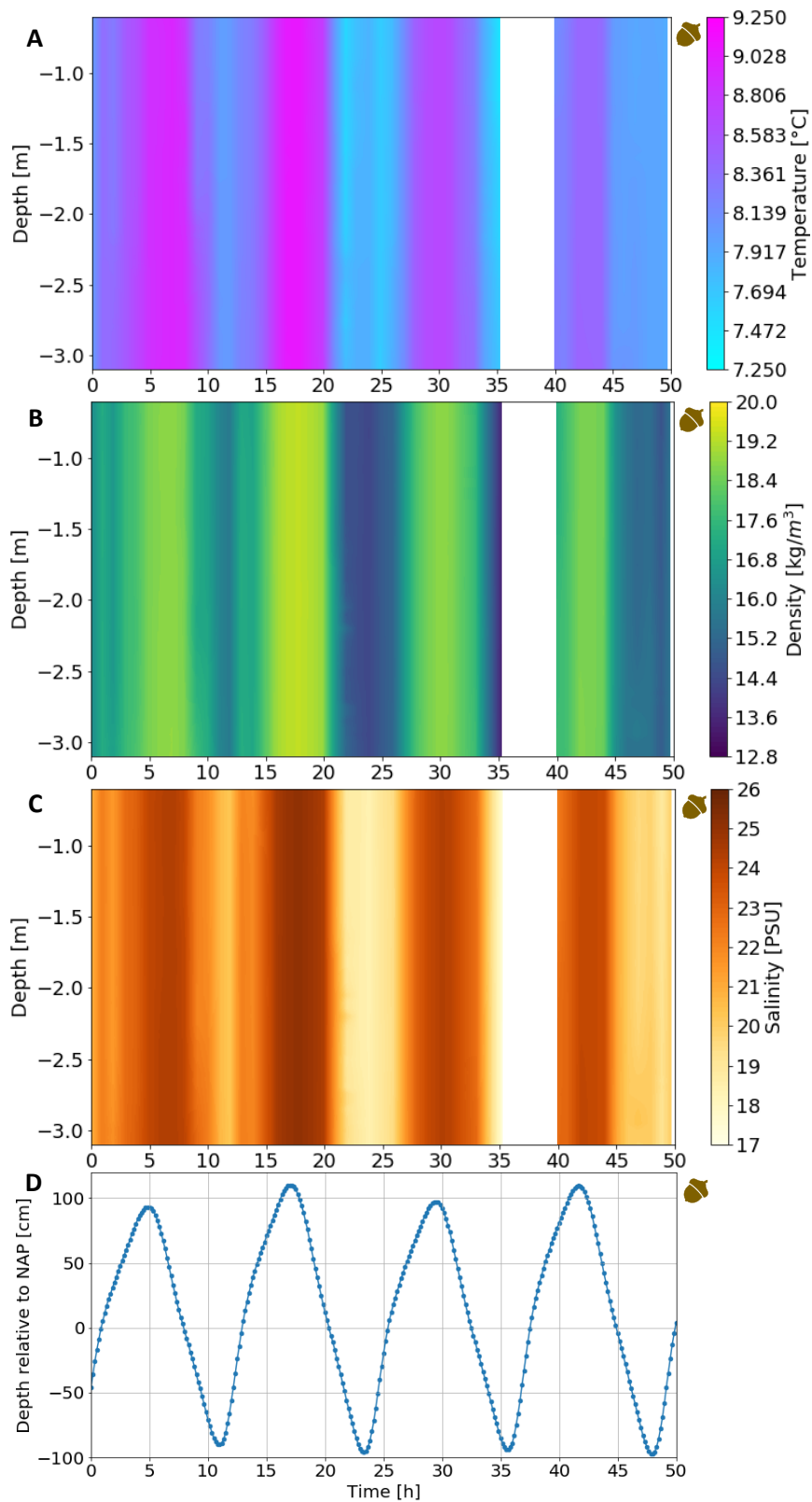


**Figure 31A:** Temperature against depth and time. **31B:** Density against time and depth. **31C:** Salinity against depth and time. **31D:** Tidal cycle against time. All figures show conditions during the autumn cruise. The white gap indicates the time that the CTD stopped working for a couple of hours.

### 3.3 Methane Concentrations in the Water

Figure 32 shows the methane concentrations in the water and the tidal cycles during both the summer and the autumn cruise. During the summer cruise there is no clear relation between the tides and the  $\text{CH}_4$  concentrations. The high  $\text{CH}_4$  concentration peak at about 40 hours occurs at changing tides, when water from the North Sea is flowing in. This is not a point in time when it is expected that methane builds up. The methane concentrations in autumn do peak at a moment when it can be expected that methane builds up. The peaks at about 1 hour, 12 hours, and 24 hours after the first CTD all correspond to a period just after low tide, when the water is relatively stagnant and methane can build up. Also the peaks at about 18, 30, and 43 hours after the first CTD correspond to a period of relatively stagnant water, just after high tide. This does not agree with the tidal dependence of the methane concentration with maxima at low tide that Grunwald et al. (2007 and 2009) found in the German part of the Wadden Sea.

Furthermore, both the general downward trend in autumn and the upward trend in summer correspond to trends in water temperature, with higher  $\text{CH}_4$  concentrations at higher temperatures. This is a likely relation, because methane production is higher at higher temperatures.

Both for summer and autumn the  $\text{CH}_4$  concentrations in the water at 1 and 3 meter depth are quite similar. This can also be seen in table 3, which contains the averages, standard deviation, maximum and minimum values of the  $\text{CH}_4$  concentrations at 1 and 3 meters depth for the entire duration of

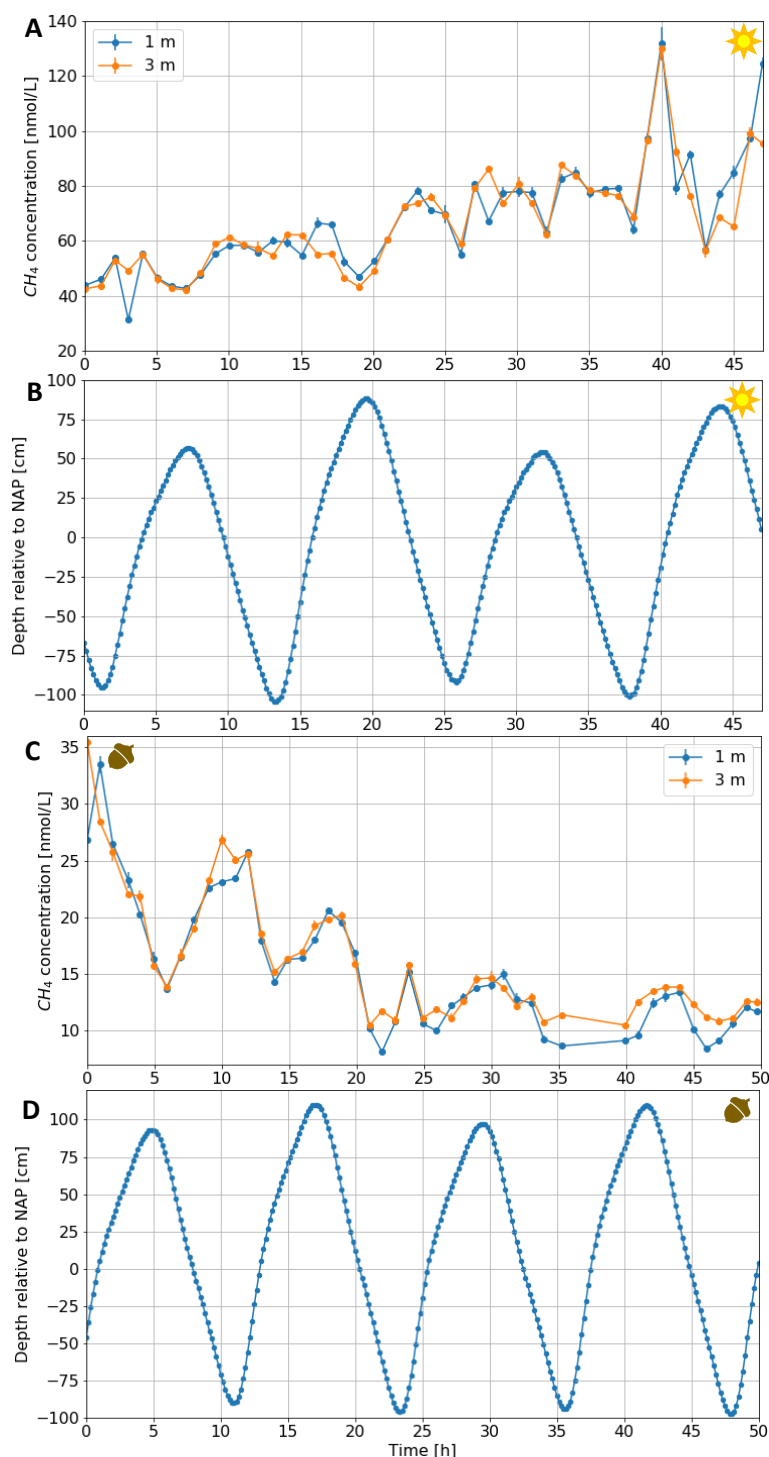


**Figure 32A:** Methane concentration at 1 and 3 meter depth, measured in water samples taken during the summer cruise, against time. **32B:** Tidal cycle summer against time. **32C:** Methane concentration at 1 and 3 meter depth, measured in water samples taken during the autumn cruise, against time. **32D:** Tidal cycle autumn against time.

the 48 hour station. The difference between the average methane concentrations at 3 and 1 meter depth can be found in table 4.

In theory the methane is produced at the seafloor and oxidized as it travels up through the water column. On average the CH<sub>4</sub> concentration at 1 meter depth in summer is about one nmol/L higher than at 3 meter depth. For the autumn cruise the CH<sub>4</sub> concentration at 1 meter depth is on average about 0.75 nmol/L higher than at 3 meter depth, which agrees with the theory. However, the error in both summer and autumn is larger than the average, making these results not significant.

Finally, the CH<sub>4</sub> concentrations are on average about 50 nmol/L higher in summer than in autumn. This could possibly be explained by the higher water temperatures in summer.

**Table 4:** Averages, standard deviation, maximum and minimum values of the average CH<sub>4</sub> concentrations at 1 and 3 meters depth for the entire duration of the 48 hour station during the summer and autumn cruise.

		Average	STD	Maximum	Minimum
Summer	1 m	67.80	19.82	131.69	31.26
	3 m	66.77	18.14	129.82	42.14
Autumn	1 m	15.47	5.83	33.46	8.13
	3 m	16.22	5.72	35.47	10.46

**Table 3:** Difference between the average methane concentrations at 3 and 1 meter depth for the summer and autumn cruise.

Difference 3-1 m	Average	STD	Maximum	Minimum
Summer	-1.03	7.92	-29.24	0.05
Autumn	0.75	1.87	8.61	0.06

### 3.4 Methane Oxidation Rates

The methane oxidation rates at 1 and 3 meters depth plotted against time and CH<sub>4</sub> concentration for the summer cruise can be found in figure 33. From these figures it can be seen that the standard deviation of the oxidation rates is very high in summer. Also, no clear temporal cycle can be

detected. When the oxidation rates are plotted against methane concentration (Figure 33B), it can be seen that the oxidation rates increase as the methane concentration increases. This is clearest for the highest values. The highest oxidation rates are found at the highest methane concentrations, both corresponding to the samples taken about 40 hours after the first CTD. This implies that at higher methane concentrations the CH<sub>4</sub> oxidation increases, but not enough to cause a significant decrease of CH<sub>4</sub> concentrations in the water. Even though methane oxidation is higher at higher temperatures, it is unlikely that this increase in oxidation rate is caused by

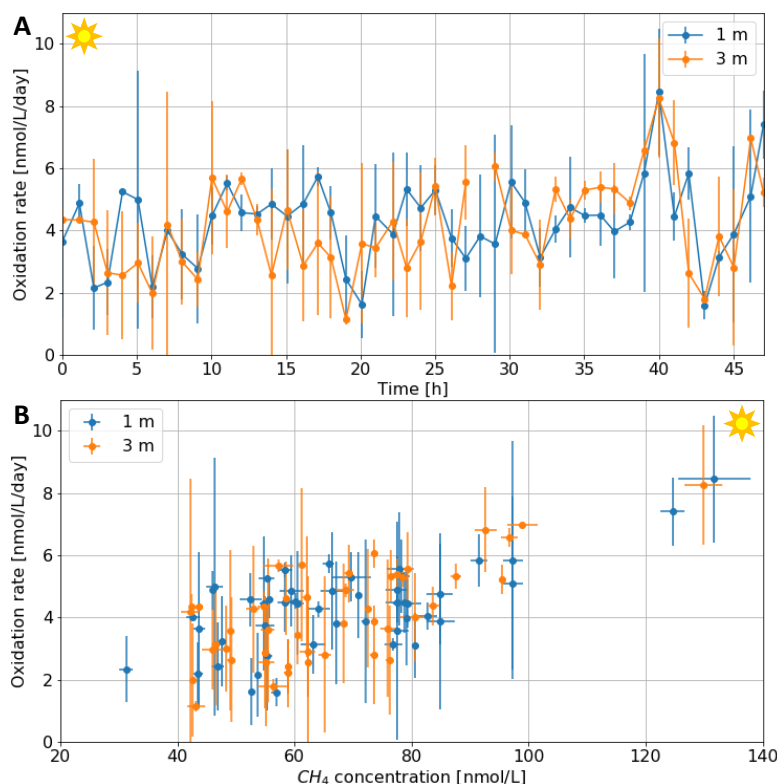


**Figure 33A:** Oxidation rates at 1 and 3 meter depth measured in summer plotted against time. **33B:** Summer oxidation rate at 1 and 3 meter depth against summer CH<sub>4</sub> concentrations at 1 and 3 meter depth.

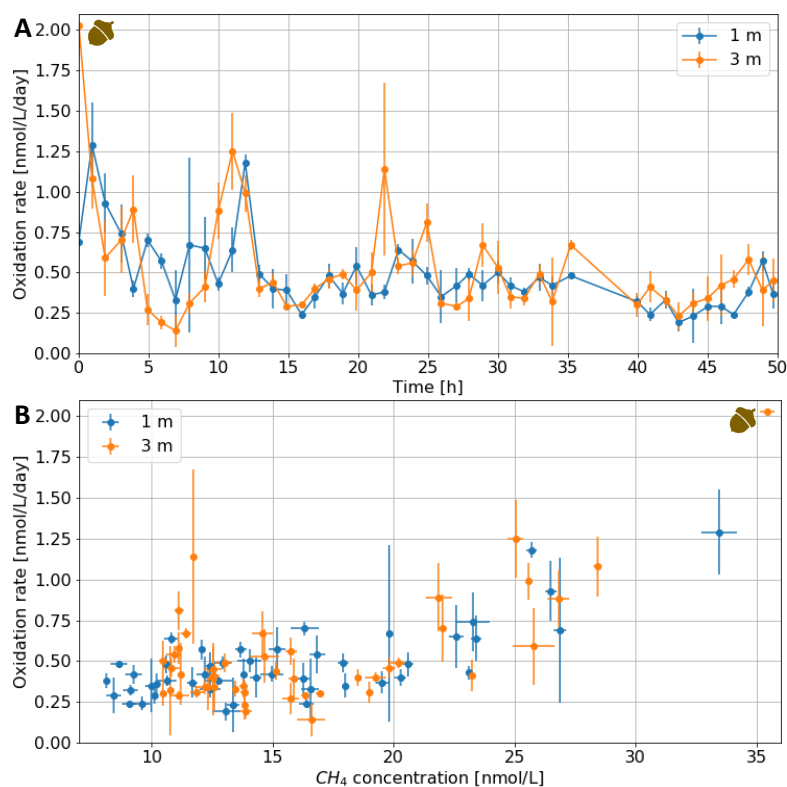


**Figure 34A:** Oxidation rates at 1 and 3 meter depth measured in autumn plotted against time. **34B:** Autumn oxidation rate at 1 and 3 meter depth against autumn  $\text{CH}_4$  concentrations at 1 and 3 meter depth.

higher water temperatures, because methane oxidising bacteria need time to adjust to water temperatures. That methanotrophs require several days to fully adjust to temperature changes was proved by He et al. (2012) for methanotrophs in Arctic lake sediments.

Figure 34 shows the same plots as figure 33, but this time for autumn. In November the standard deviation and the average oxidation rates are lower than in July. In July the average oxidation rate at 1 and 3 meter depth is about  $4.2 \pm 1.5$  nmol/L/day. In November the average oxidation rate at 1 and 3 meter is much smaller. It is about  $0.5 \pm 0.3$  nmol/L/day (see table 5).

The higher oxidation rates in summer could be related to higher methane concentrations or higher water temperatures in summer. Because water temperatures in summer are high for weeks this does give the methane oxidising bacteria enough time to adjust to the water temperatures. In autumn the peaks in oxidation rate around 1 hour, 12 hours and 23 hours after the first CTD, match the  $\text{CH}_4$  concentration peaks just after low tide. Figure 34B suggests a simultaneous increase of methane concentration and oxidation rate at methane concentrations higher than about 20 nmol/L. Up to a  $\text{CH}_4$  concentration of about 20 nmol/L the methane oxidation rate does not significantly increase with methane concentration, indicating that the oxidation rate starts adjusting to the methane supply at a threshold of about 20 nmol/L.

**Table 5:** Average methane oxidation rates and standard deviations in summer and autumn in  $\text{nmol L}^{-1} \text{day}^{-1}$ .

	Average	STD
Summer	1m	4.3
	3m	4.0
	All	4.2
Autumn	1m	0.5
	3m	0.5
	All	0.5

### 3.5 Methane Concentrations in the Sediment

In figure 35 the methane concentrations in the sediment at different depths are plotted. Figure 35A and B represent sediments collected during box cores taken in July and figure 35C represents sediments collected in a box core taken in November. In all of these cores the methane concentrations vary differently over depth, and the magnitude of the CH<sub>4</sub> concentrations also changes significantly. The box cores in summer were taken immediately after each other, but are extremely different. The autumn box core profile does seem to correspond with the theory of CH<sub>4</sub> production in deeper, oxygen and sulphate poor sediments and methane reduction in shallower, oxygen rich sediments (Kamaleson et al., 2019). In these box cores oxygen and sulphate were not measured. However, all conclusions based on these data should be treated with care, due to the large variability between measurements. Constructing the same depth profiles using the calibration curve composed by Tim de Groot leads to the same profiles. The differences in the CH<sub>4</sub> concentrations computed with different calibration curves is very small (negligible). What is meant by calibration curves is described in section 2.2.1.

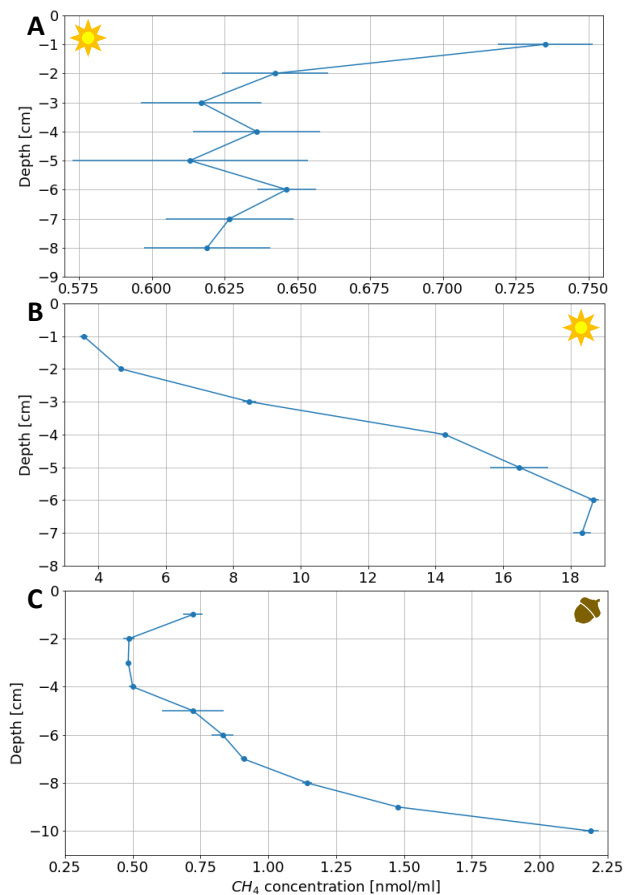


**Figure 35A&B:** Methane concentrations at several depths in the sediment in summer. **35C:** CH<sub>4</sub> concentrations at several depths in the sediment in autumn.

### 3.6 $\delta^{13}\text{C-CH}_4$ and $\delta\text{D-CH}_4$ air samples

Figure 36A and 36B show the summer  $\delta^{13}\text{C-CH}_4$  and the autumn  $\delta^{13}\text{C-CH}_4$  and  $\delta\text{D-CH}_4$  values plotted against time. The patterns in isotopic composition do not seem to be related to the tides, water temperatures or methane concentrations in the water. Figure 36C shows the Keeling plots of  $\delta^{13}\text{C-CH}_4$ .

Methane formed by different processes has different isotopic signatures. For example, methane from biological processes is usually strongly depleted in both  $^{13}\text{C}$  and deuterium ( $\delta^{13}\text{C} \approx -60\text{‰}$  and  $\delta\text{D} \approx -300\text{‰}$ ),  $\text{CH}_4$  from thermogenic processes is more enriched in both heavy isotopes ( $\delta^{13}\text{C} \approx -40\text{‰}$  and  $\delta\text{D} \approx -150\text{‰}$ ) and methane from biomass burning is more enriched in  $^{13}\text{C}$  ( $\delta^{13}\text{C} \approx -25\text{‰}$  and  $\delta\text{D} \approx -230\text{‰}$ ) (Brass and Röckmann, 2010). Note that the values stated here are typical values, but also values in the same range can be accounted to the same sources. The y-intercepts of the summer Keeling plots are  $-52.1 \pm 0.5\text{‰}$  and  $-57.1 \pm 0.9\text{‰}$  (see table 6), which indicates that the source of this methane is probably biogenic.

Methane from the Wadden

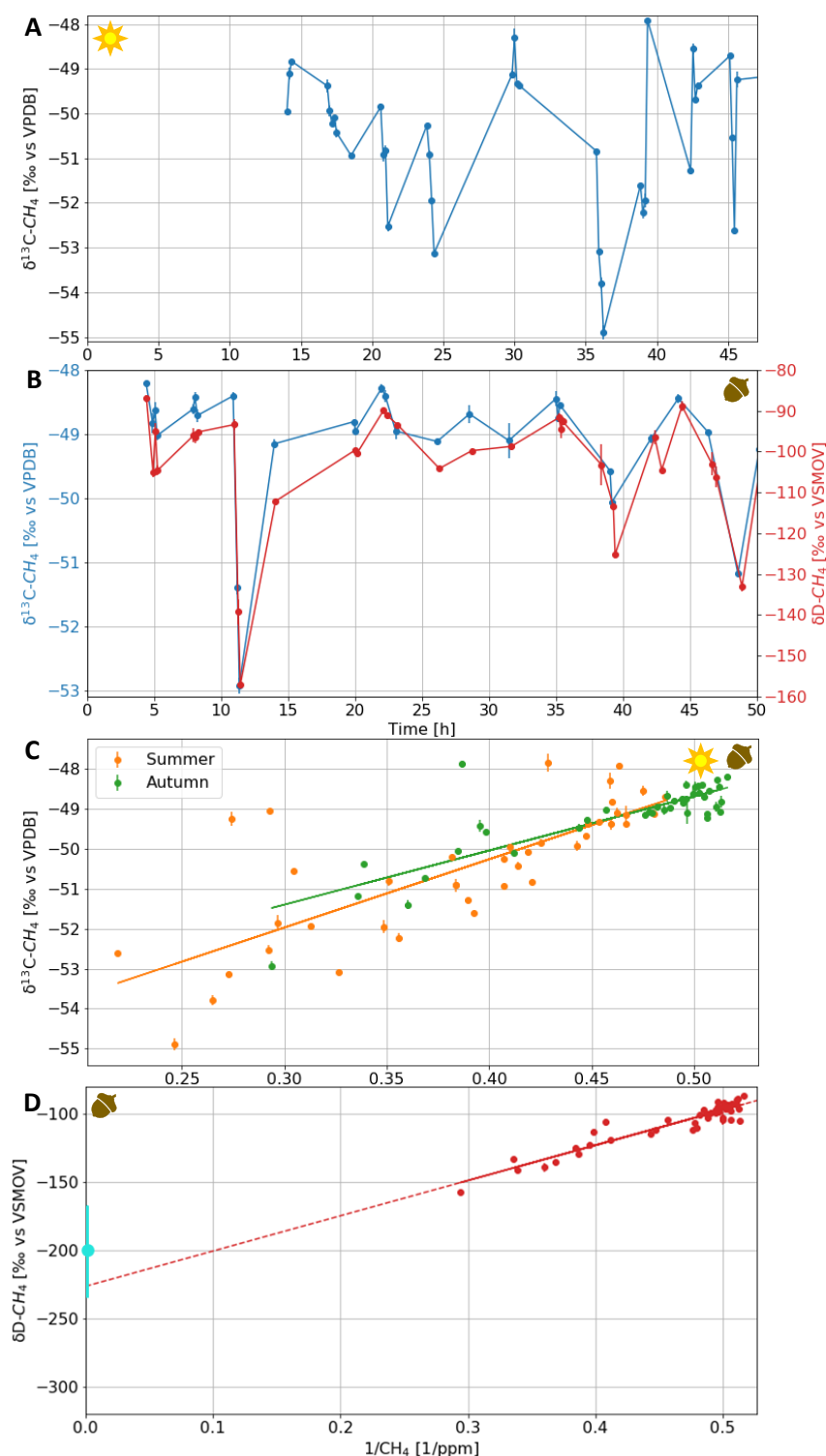


**Figure 36A:**  $\delta^{13}\text{C-CH}_4$  measured in air samples taken during the summer cruise, plotted against time. **36B:**  $\delta^{13}\text{C-CH}_4$  and  $\delta\text{D-CH}_4$  measured in air samples taken during the autumn cruise, plotted against time. **36C:** Keeling plots of  $\delta^{13}\text{C-CH}_4$  against inverse  $\text{CH}_4$  concentration for summer based on concentrations determined using G2301 data (blue), for summer based on concentrations determined using the isotope measurements (orange), and for autumn. The lines are lines of linear regression. **36D:** Keeling plot of the  $\delta\text{D-CH}_4$  values measured in air samples taken during the autumn cruise. The line is the line of linear regression. The light blue dot is the average autumn deuterium isotopic signature found in the water samples. Error bars are also depicted for the average deuterium signature found in the water samples.

**Table 6:** Statistical parameters of the linear regression lines determined for the Keeling plots depicted in figure 35.

	R <sup>2</sup>	Intercept	Error intercept	Slope	Error slope
$\delta^{13}\text{C}$ Summer Picarro	0.24	-52.1	0.5	5.8	1.7
$\delta^{13}\text{C}$ Summer isotope	0.60	-57.1	0.9	17.1	2.2
$\delta^{13}\text{C}$ Autumn	0.70	-55.5	0.7	13.5	1.4
$\delta\text{D}$ Autumn	0.89	-226	6	258.4	13.8

Sea is expected to be biogenic (formed during organic matter degradation).

For autumn the  $^{13}\text{C}$  signature of the methane source is about  $-55.5 \pm 0.7\text{‰}$  and the deuterium signature of the methane source is about  $-226 \pm 6\text{‰}$  (see figure 36D). These values indicate that the

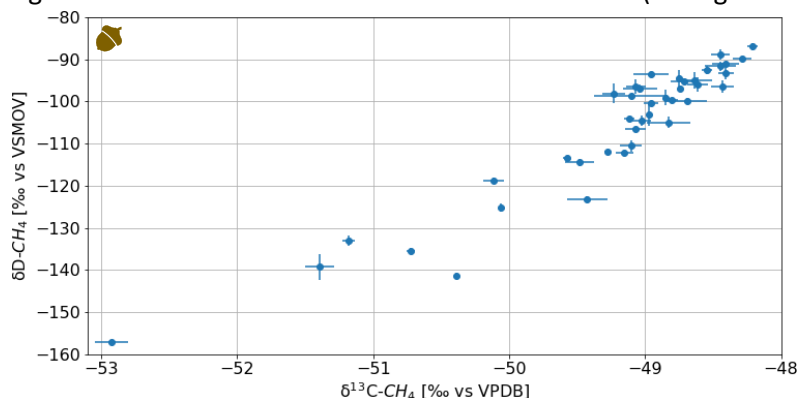


**Figure 37:**  $\delta\text{D}-\text{CH}_4$  plotted against  $\delta^{13}\text{C}-\text{CH}_4$ , both measured in air samples taken during the autumn cruise.

methane source in autumn is probably also biogenic. Finally, from figure 37 it can be concluded that, in autumn, when methane gets enriched in  $^{13}\text{C}$ , it also gets enriched in deuterium. This is what would be expected, because here methane oxidation by methanotrophs cause relative enrichment of both isotopes.

### 3.7 $\delta\text{D}-\text{CH}_4$ water samples

Figure 38A and B depict the temporal cycle of the deuterium signature of dissolved methane at 1 and 3 meters depth for summer and autumn. The duplicate values in summer are quite similar, which means the deuterium signatures measured from water samples with the methane analysis system are reliable. Some depleted autumn signatures seem to correspond to periods at which the methane concentrations in the water peak, but no relation between the tides or  $\text{CH}_4$  concentrations can be detected in summer. Figure 38C and D, show the Rayleigh fractionation plots of the deuterium signatures, and table 7 shows the statistical parameters belonging to the Rayleigh fractionation plots. The summer results show no statistically significant dependence of  $\delta\text{D}$  on concentration.

The autumn results show a correlation for the samples with lower  $\text{CH}_4$  concentration. The boundary

**Table 7:** Statistical parameters of the linear regression lines drawn in figure 38C and D. The slope is the Rayleigh fractionation factor.

		R <sup>2</sup>	Intercept	Error intercept	Slope	Error slope
Summer	1m	0.01	-0.25	0.01	-0.01	0.02
	3m	0.03	-0.24	0.01	0.01	0.02
Autumn	1m	0.68	-0.30	0.01	-0.10	0.01
	3m	0.63	-0.29	0.01	-0.08	0.01
	1m low	0.74	-0.32	0.01	-0.11	0.01
	3m low	0.64	-0.34	0.02	-0.13	0.02
	1m high	0.00	-0.27	0.03	0.00	0.07
	3m high	0.02	-0.26	0.01	-0.01	0.02

between high and low concentrations is drawn visually at a value of  $\ln(\text{CH}_4 / \text{CH}_{4,\text{max}}) = -0.6$ , which corresponds to a methane concentration of about 20 nmol/L. At this concentration also a difference in trend in the measured methane oxidation rates was found. The changes in isotopic data thus seem to agree with the changes in measured oxidation rates. The regression lines through all autumn results, or through the samples with low concentrations, both have slopes of about -0.10. This means the autumn fractionation factor is about -0.10. This fractionation factor falls within the range determined for methane-oxidizing bacteria (Sessions et al., 2002). For autumn samples with concentrations higher than 20 nmol/L and for summer samples, for which most samples had methane concentrations higher than 20 nmol/L, no significant fractionation is observed. This suggests that methane oxidation does not significantly affect the methane isotopic composition of the entire methane pool when a lot of methane is supplied. The average  $\delta\text{D}-\text{CH}_4$  of the Wadden Sea water at 1 meter depth in autumn is about  $-200\text{‰} \pm 33\text{‰}$ , which is close to the source deuterium value of the air samples in autumn ( $-226\text{‰} \pm 6\text{‰}$ ). The source deuterium signature of the air samples also falls nicely between the most and the least depleted deuterium isotopic signatures measured in the water samples, as can be seen in figure 36D. This proves that the methane measured in the bucket is indeed coming from the Wadden Sea water. The methane concentrations determined at the NIOZ, with the GC, and those determined at IMAU,

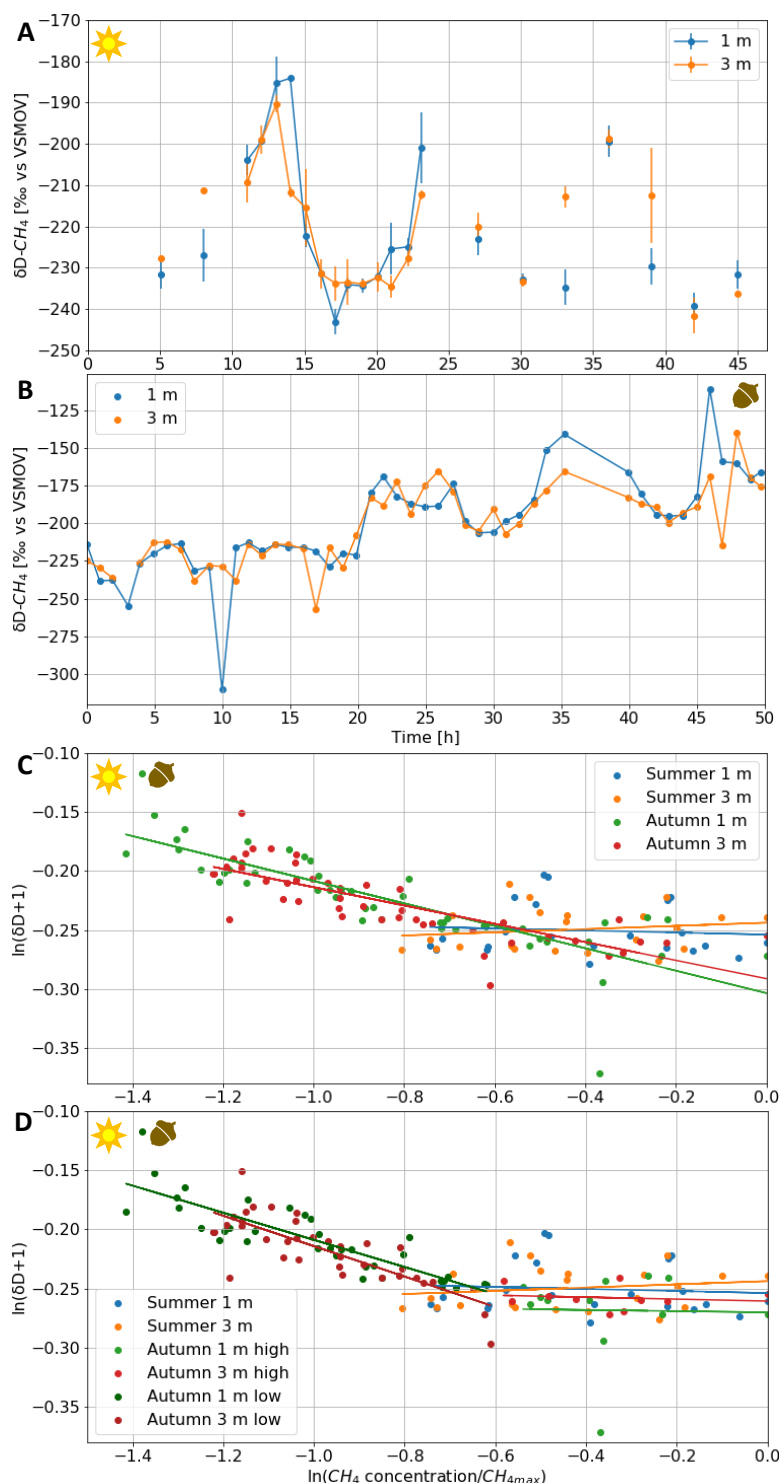


**Figure 38A:**  $\delta\text{D}-\text{CH}_4$  measured in the water samples taken at 1 (blue) and 3 (orange) meter depth during the summer cruise, plotted against time. **37B:**  $\delta\text{D}-\text{CH}_4$  measured in the water samples taken at 1 (blue) and 3 (orange) meter depth during the autumn cruise, plotted against time. **37C:** Rayleigh fractionation plot of the summer deuterium signatures, at 1 (blue) and 3 (orange) meter depth, and the autumn deuterium signatures, at 1 (green) and 3 (red) meter depth. **37D:** Rayleigh fractionation plot with autumn values split in values below and above a  $\ln(\text{CH}_4 \text{ concentration}/\text{CH}_{4,\text{max}})$  value of -0.6.

using the isotope measurement, are plotted against each other. This plot can be seen in figure 39. Apart from one outlier, at an IMAU methane concentration of about 13.5 ppm, the relation looks quite linear. This indicates that methane concentration measurements based on the isotope measurement are reliable.

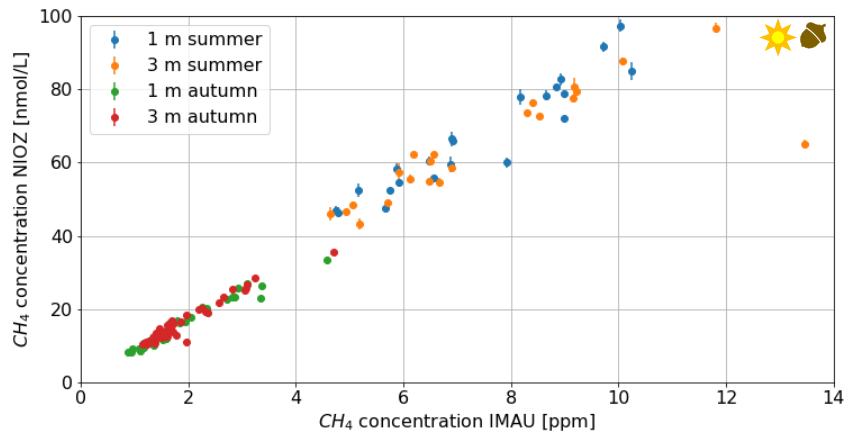


**Figure 39:** Methane concentrations measured at the NIOZ, with the GC, plotted against the methane concentrations measured at IMAU with the methane analysis system.

### 3.8 Methane mixing ratios

In figure 40A and B the methane mixing ratios measured by the G2301 in summer and autumn are plotted. Here the buckets and background measurements were not separated yet. The large spikes visible are the bucket measurements. Just like the CH<sub>4</sub> concentrations in the water, the measured methane mixing ratios are higher in summer than in autumn, both for the bucket peaks and the average methane mixing ratios.

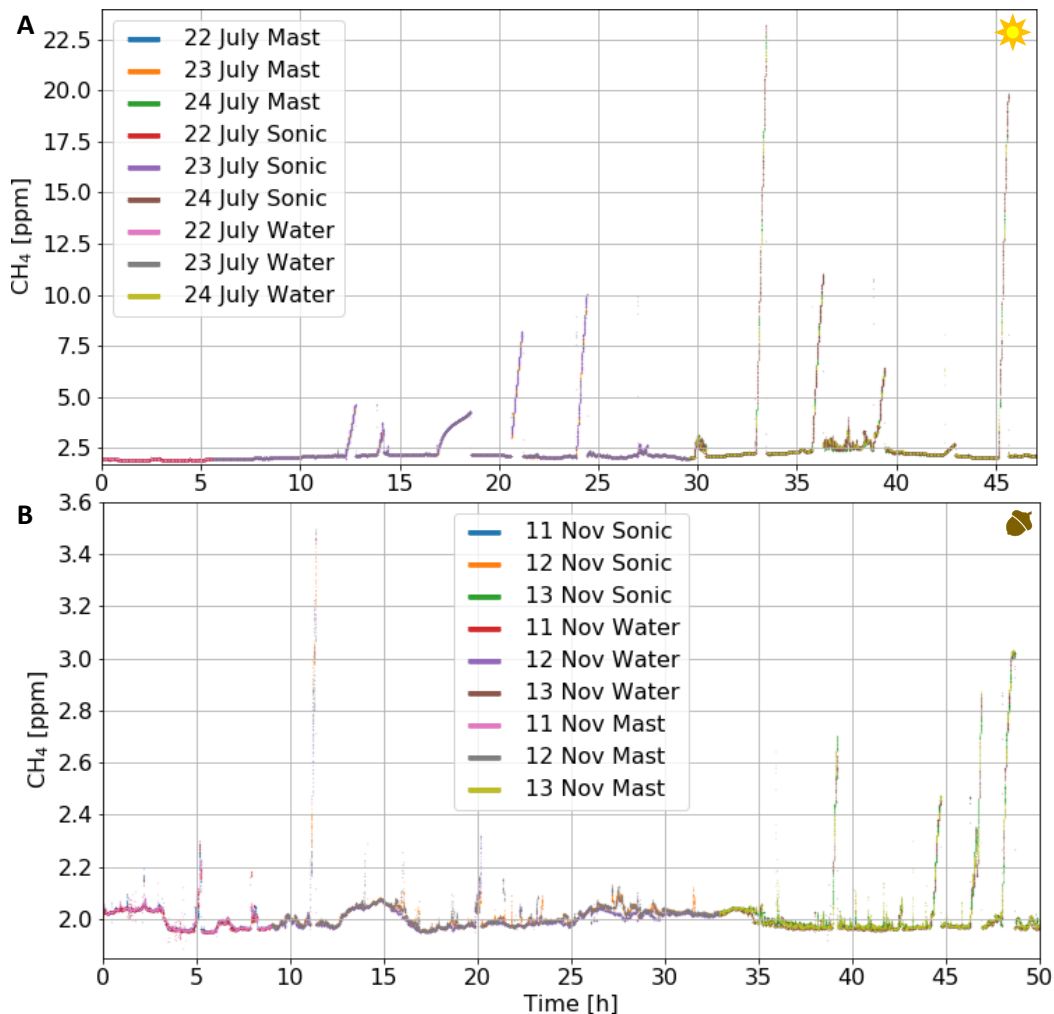


**Figure 40A:** Methane mixing ratios measured by the G2301 during the entire 48 hours in summer. **40B:** Methane mixing ratios measured by the G2301 during the entire 48 hours in autumn.

### 3.8.1 Buckets

The rates of methane increase are plotted in figure 41. In summer periods where the methane increase could be followed for at least 45 seconds were evaluated, in autumn this period was 20 seconds. This filtering was necessary to remove periods where the bucket was not stable in the water (see section 2.4.2.1). The averages and standard deviations for the summer cruise are given in table 8 and those for the autumn cruise are given in table 9. In autumn the standard deviations of some rates of methane increase are zero, which means the average rates are based on a single value.

Both for autumn and summer there does not seem to be a clear pattern in the methane emission rates. The summer rates do seem to be almost linearly related to the CH<sub>4</sub> concentrations in the water (as can be seen in figure 41B). This relation indicates that methane emissions from the Wadden Sea are higher when methane concentrations in the Wadden Sea water are higher, which is the expected behaviour. The exception to this relation is the bucket measurement Low\_up40. For the unusually high methane concentration, or unusually low emissions measured at this concentration, no explanation has been found. In autumn there is also a relation between rates of CH<sub>4</sub> increase and methane concentrations, but it is less clear. The reason for this weaker relationship might be the lower methane concentrations and emissions in autumn.

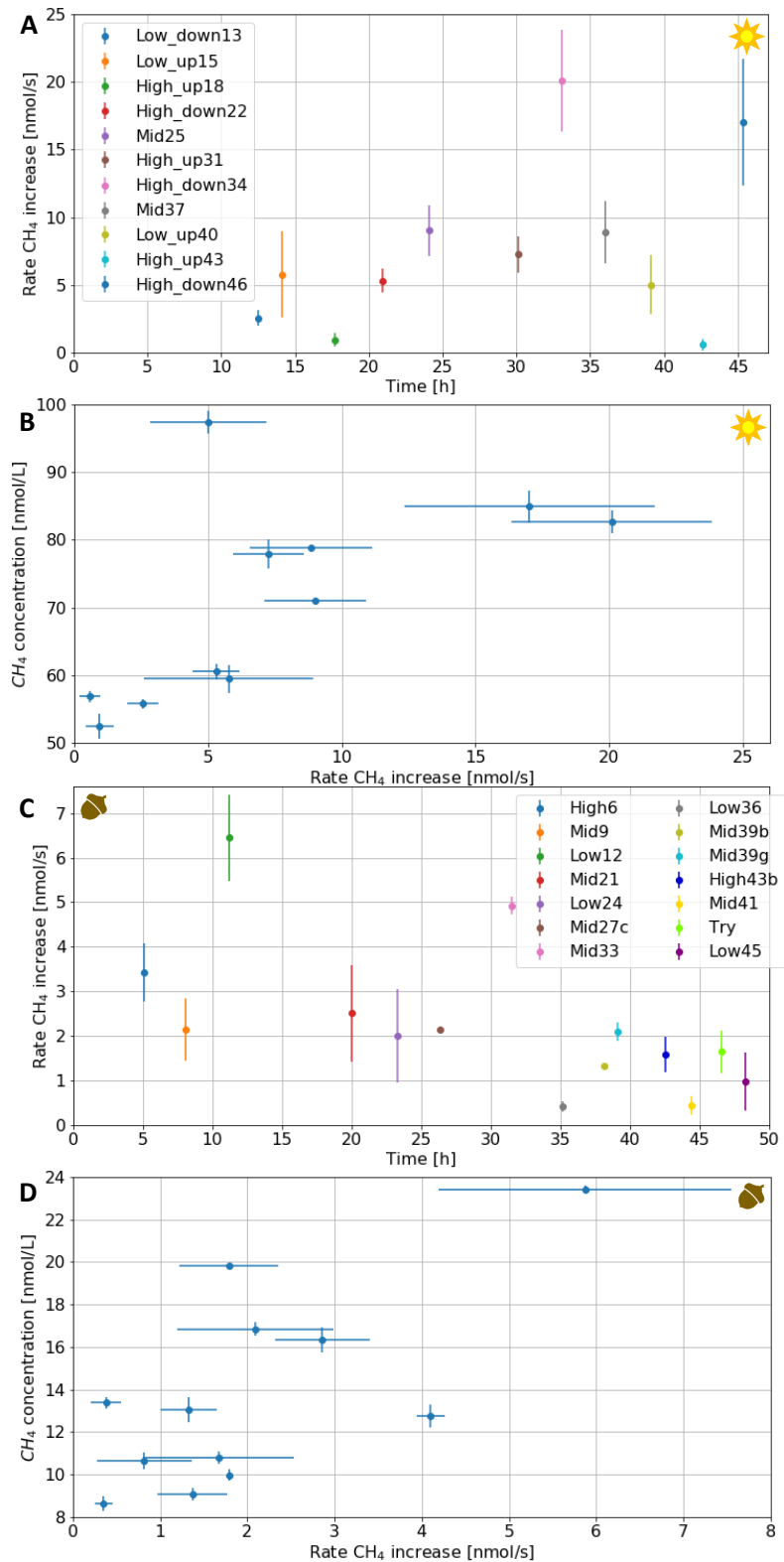


**Figure 41A:** Average rate of methane increase inside the bucket, measured in summer. **41B:** Methane concentration in the water plotted against rate of CH<sub>4</sub> increase measured in summer. **41C:** Average rate of methane increase inside the bucket, measured in autumn. **41D:** Methane concentration in the water plotted against rate of CH<sub>4</sub> increase measured in autumn. In all plots the standard deviations are visualized as error bars.

The average emissions determined with the bucket method in summer are about  $6.5 \pm 6.3$  nmol/s ( $23 \pm 22$  nmol/m<sup>2</sup>/s) and in autumn the average emissions are about  $2.0 \pm 1.0$  nmol/s ( $7.1 \pm 3.5$  nmol/m<sup>2</sup>/s).

**Table 8:** Average, standard deviation, and percentage of average, that the standard deviation accounts for, of the rates of CH<sub>4</sub> increase (in nmol/s) measured with the bucket in summer. The amount and of rates considered in the average and the average duration of the CH<sub>4</sub> increases (in seconds) are also added. 

Bucket	Average slope	STD slope	% STD of Average	Amount	Duration
Low_down13	2.56	0.57	22	3	585
Low_up15	5.77	3.18	55	10	95
High_up18	0.95	0.52	55	9	666
High_down22	5.30	0.87	16	11	170
Mid25	9.01	1.90	21	3	627
High_up31	7.25	1.31	18	13	81
High_down34	20.10	3.75	19	2	982
Mid37	8.86	2.30	26	2	989
Low_up40	5.01	2.18	44	7	220
High_up43	0.58	0.39	67	11	162
High_down46	17.01	4.68	28	4	445
Mid_end	17.94	7.24	40	8	256
High_up_end	0.85	0.24	28	4	462
All_High	5.17	5.54	107	54	302
All_Mid	14.48	7.24	50	13	454
All_Low	5.02	2.82	56	20	212
All_High_up	3.04	3.22	106	37	288
All_High_down	9.80	6.62	68	17	330
All_Low_up	5.46	2.84	52	17	146
All_Low_down	2.56	0.57	22	3	585
All	6.53	6.31	97	87	304

Inspecting table 8 and 9 further, it can be seen that most of the standard deviations in summer are higher than the standard deviations in autumn. This is at least partly due to the fact that the averages for the summer emissions consist of more individual rates than in autumn. Not only the number of rates considered, but also the average duration of the methane increase can influence the accuracy of the measurement. If the standard deviation is low and based on many values, but the duration of methane increase is short, the determined rate might not be representative of the longer term CH<sub>4</sub> emissions. Overall the average duration of the measurements is longer in summer, due to more stable conditions. Unstable conditions make it very hard to prevent the bucket from opening to the atmosphere.

In autumn some buckets near the end of the 48 hour station have been removed to decrease the standard deviation. Both the averages with and without these outliers are present in table 9.

**Table 9:** Average, standard deviation and percentage of average, that the standard deviation accounts for, of the rates of CH<sub>4</sub> increase (in nmol/s) measured with the bucket measurements in autumn. The amount and of rates considered in the average and the average duration of the CH<sub>4</sub> increases (in seconds) are also added.

Bucket	Average slope	STD slope	% STD of Average	Amount	Duration
High6	2.86	0.55	19	17	40
Mid9	1.79	0.57	32	11	33
Low12	5.87	1.68	29	10	83
Mid21	2.09	0.90	43	8	73
Low24	1.67	0.87	52	6	37
Mid27c	1.80	0.00	0	1	47
Mid33	4.10	0.16	4	2	23
Low36	0.35	0.10	28	5	104
Mid39b	1.11	0.00	0	1	45
Mid39g	1.74	0.17	10	3	292
High43b	1.32	0.32	25	6	42
Mid41	0.38	0.17	46	11	167
Try	1.37	0.40	29	4	495
Low45	0.82	0.54	67	9	213
Mid47	0.76	0.22	30	9	202
High end	1.22	0.52	43	8	354
All High	2.14	0.94	44	31	121
All Mid	1.38	0.97	71	50	152
All Low	0.96	0.78	82	30	116
All	1.53	1.03	67	111	134
Mid27c, 33, 39b	2.78	1.35	49	4	35
High without High end	2.46	0.84	34	23	40
Mid without Mid41, Try, 47	2.03	0.89	44	41	75
Low without Low45	1.07	0.92	86	21	75
All without outliers	2.02	1.00	50	60	64

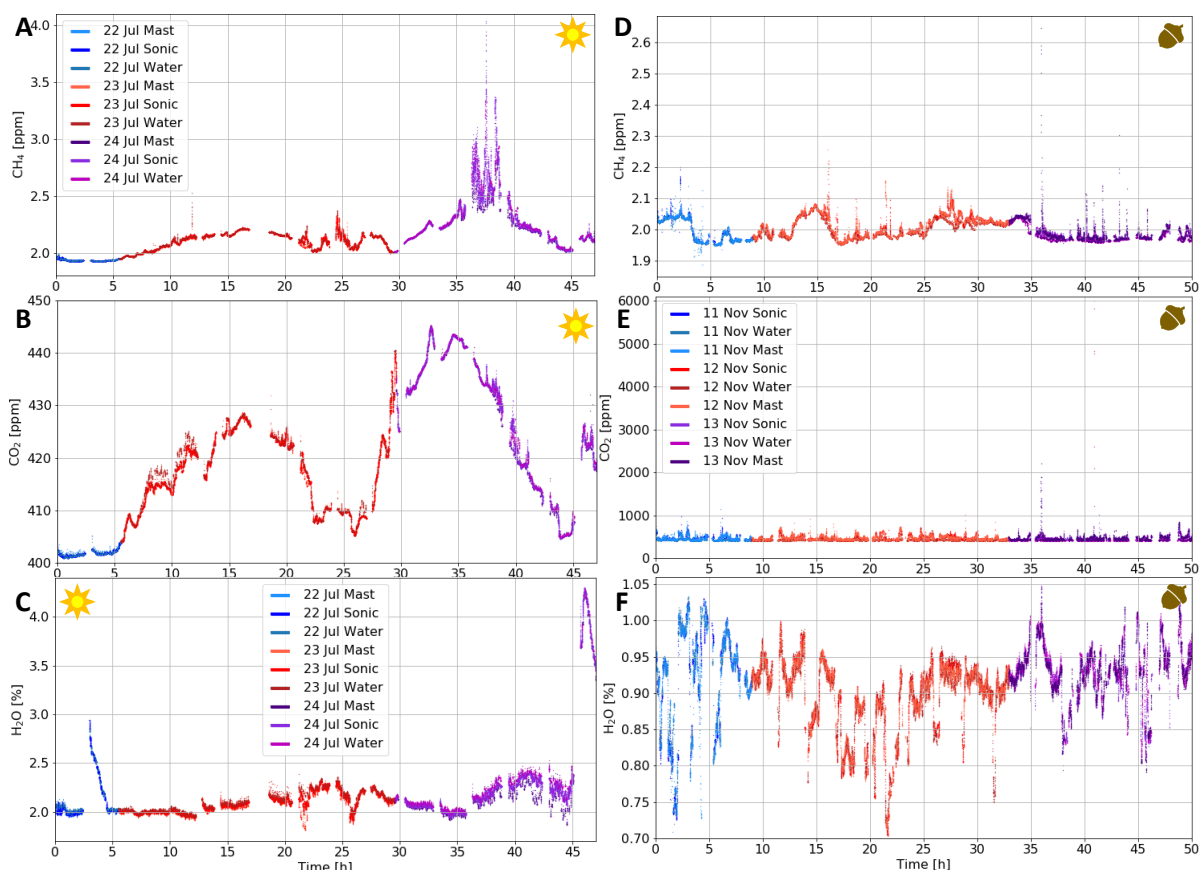
### 3.8.2 Background

Figure 42 depicts the methane, CO<sub>2</sub> and water mixing ratios measured by the G2301 at the 48 hour station during the summer and autumn cruise. The bucket measurements were already removed. For the CH<sub>4</sub> mixing ratio of the summer 48 hour station the period between 35 and 40 hours after the first CTD measurement stands out due to the large variation around the average. The unusually large variation is also visible in the residual plot in figure 43. The average residuals and the standard deviation per CTD of the data displayed in figure 43 can be found in appendix 3. The large variation is not present in the CO<sub>2</sub> and water measurements, indicating that the variation is probably not caused by smoke or exhaust from our own boat or passing boats.

The methane mixing ratios in autumn (figure 42D) show several short peaks, for example, at about 36 hours after the first CTD. These peaks are also present in the CO<sub>2</sub> mixing ratios, which indicates that these peaks probably are caused by contaminated air from our own boat or passing boats. The water mixing ratio shows a normal amount of variation without large peaks, that are present in summer. The large peaks in water mixing ratio in summer indicate that water has entered the lines and reached the G2301, which should have been prevented to allow the G2301 to function optimally.

Both in summer and autumn the variations in methane mixing ratio do not follow the variations in the methane concentration in the water.

In summer two wide peaks in the CO<sub>2</sub> and CH<sub>4</sub> data can be seen. The first peak starts at about 5 hours after the first CTD, which is at about 1:30 AM local time. The maximum of this peak is reached at about 15 hours after the first CTD, which is at about 11:30 AM local time. The second peak starts at about 30 hours after the first CTD, which is at about 2:30 AM local time. In the CO<sub>2</sub> measurements the second peak starts a little earlier at about 0:30 AM local time. The second peak reaches its maximum at about 37 hours after the first CTD (at about 9:30 AM local time) for methane and at about 7:30 AM local time for CO<sub>2</sub>. This indicates methane in the atmosphere peaks at night when air temperatures are lowest (see figure 44A) and wind speed is highest. This is also the time that plants do not perform photosynthesis and actually emit CO<sub>2</sub>, possibly explaining the enhanced CO<sub>2</sub> mixing ratio. Plants also influence the methane production and emission of methane by producing methane through an abiotic photochemical process induced by stress, drawing methane produced by microbes into anoxic soils, and by providing an environment suitable for microbial methanogenesis (Saunois et al., 2016). Methane emissions from plants are temperature dependent, but Keppler et al. (2006) find an increase in methane emissions with increasing temperatures (above 30°C). This is opposite to what is seen here. Also, Nisbet et al. (2009) proved that methane emissions from plants are really small. In autumn there is less temporal variability and the variability does not seem to be related to temperature (see figure 44B). It is most likely that the broad peaks in summer are caused



**Figure 42:** Methane concentration (42A) and carbon dioxide (42B) mixing ratios and percent water (42C) measured by the G2301 during the 48 hour station during the summer cruise. The legend in 42A and C also correspond with the colour coding in 42B as well. The CH<sub>4</sub> concentration (42D) and CO<sub>2</sub> (42E) mixing ratios and percent H<sub>2</sub>O (42F) measured during the 48 hour station during the autumn cruise all share the legend depicted in 42E.

by plumes with higher methane mixing ratios passing the boat.

The average methane mixing ratio for summer ( $2.14 \pm 0.19$  ppm) is a little higher than the average CH<sub>4</sub> mixing ratio in autumn ( $2.06 \pm 0.14$  ppm), as can be seen in table 10. This is opposite to the seasonal cycle of methane above Ireland reported by Derwent et al (2006), who actually show that

the methane mixing ratio in the atmosphere is lowest in July. The seasonal methane cycle reported by Derwent et al (2006) was also reported at other sites all over the world, like in the United States (Shipham et al., 1998). The deviations from the methane seasonal cycles found here are most likely also caused by plumes with higher methane mixing ratios passing the boat in summer. Both summer and autumn average methane mixing ratios are higher than the average atmospheric methane mixing ratio of about 1.8 ppm in 2011 reported in the IPCC report (Hartmann et al., 2013).

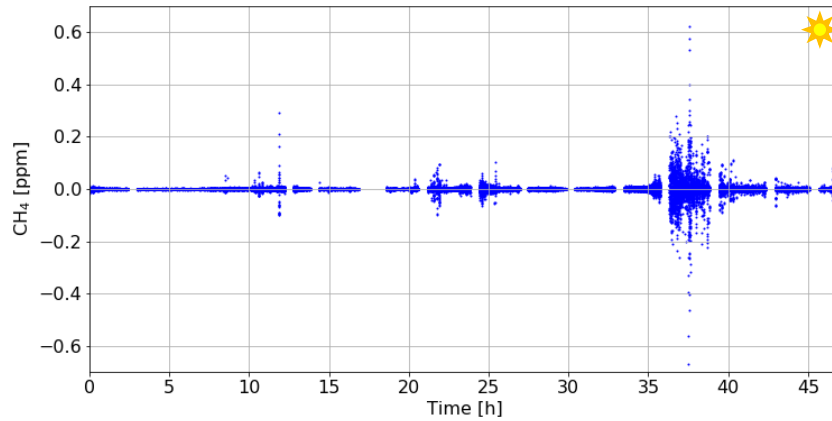


Figure 43: Residuals of the methane mixing ratios measured during the 48 hour station during summer by the G2301 plotted against time since the first CTD.

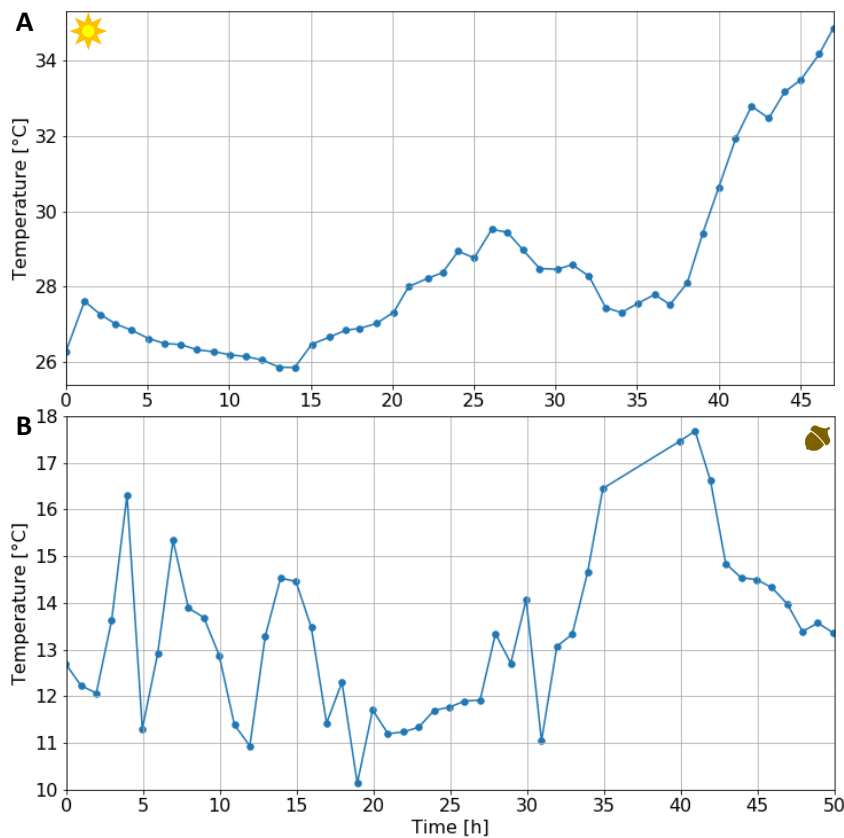
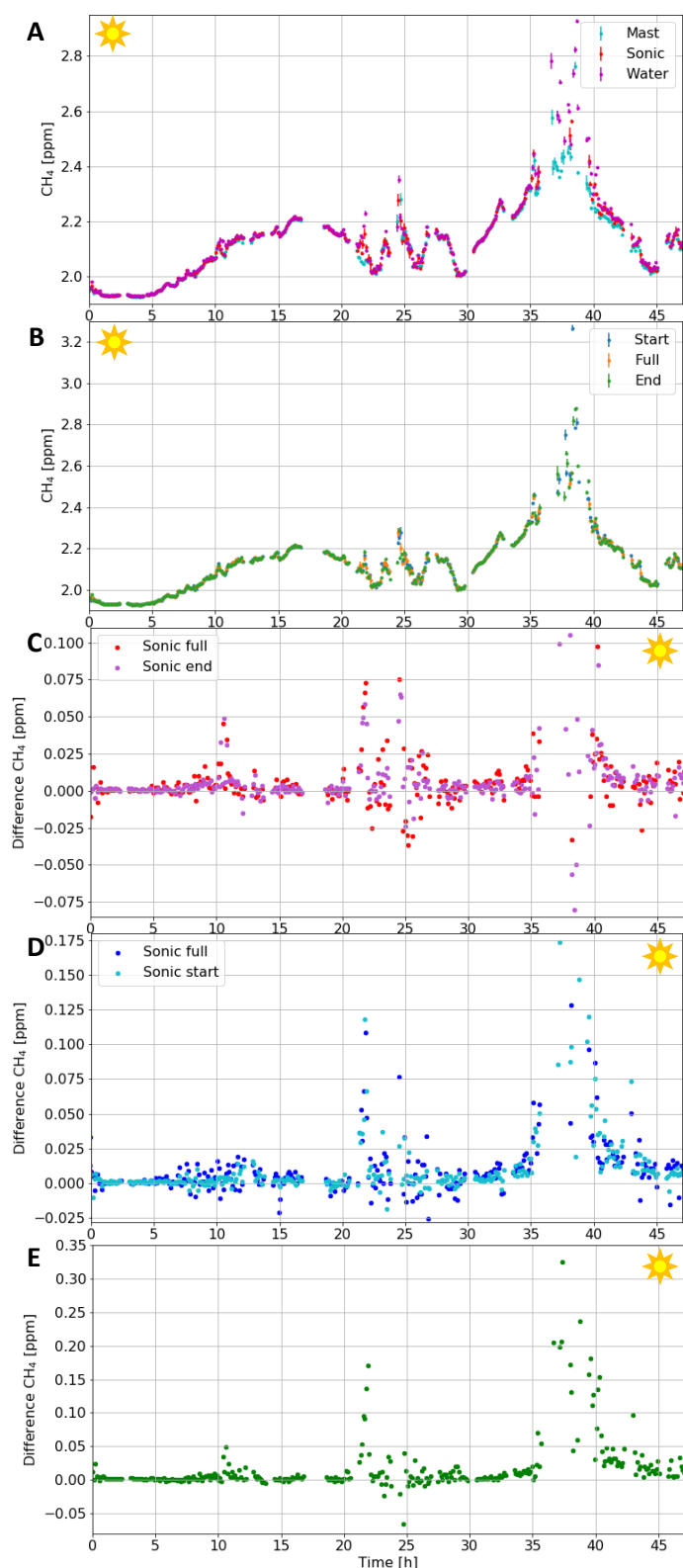


Figure 44A: Air temperature against time in summer. 44B: Air temperature against time in autumn.

Table 10: Average and standard deviation of the background methane mixing ratios in the atmosphere in summer and autumn.

	Average [ppm]	STD [ppm]
Summer	2.14	0.19
Autumn	2.06	0.14



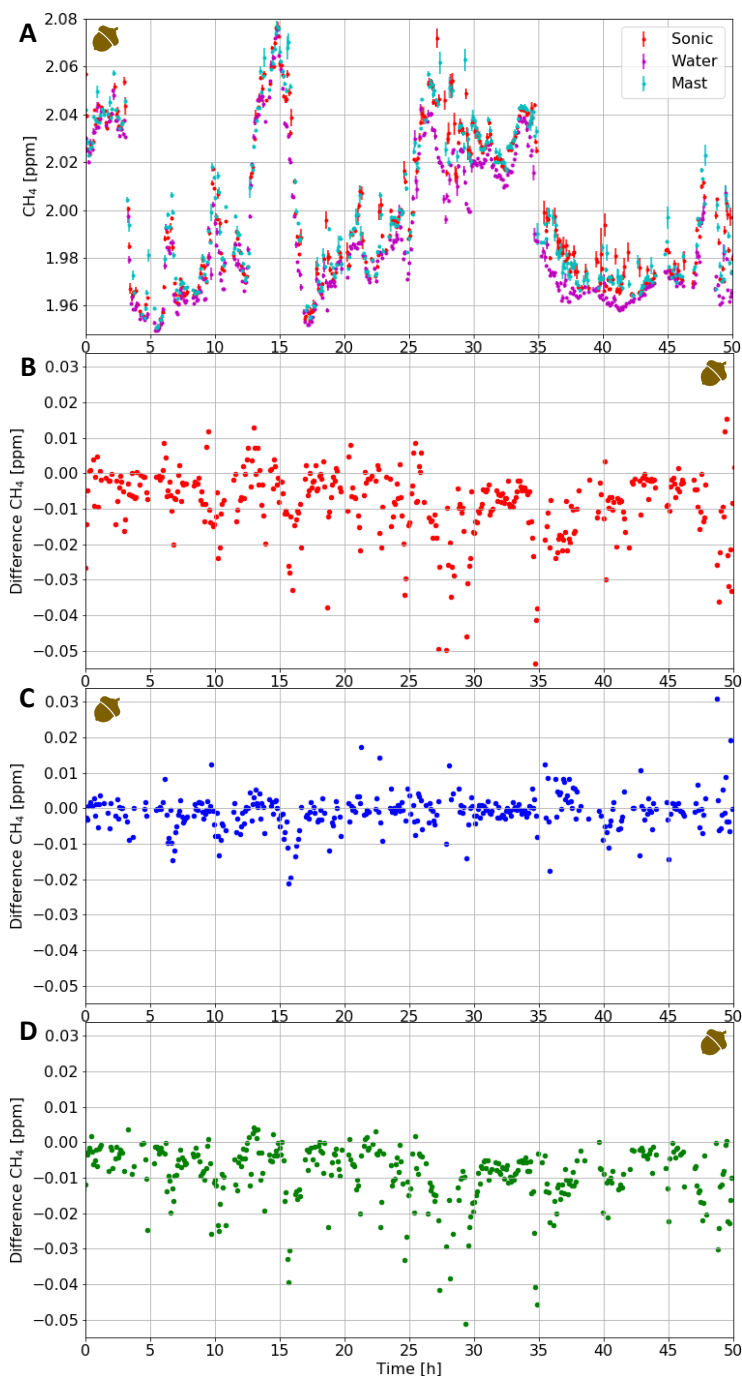
**Figure 45A:** Average  $\text{CH}_4$  mixing ratios of the different inlets. **45B:** Average  $\text{CH}_4$  mixing ratios of whole 5 minutes, the first, and the last minute of the measurement from the inlet at the level of the sonic. **45C:** Difference between the average  $\text{CH}_4$  mixing ratio just above the water and at the level of the sonic (water-sonic). **45D:** Difference between the average  $\text{CH}_4$  mixing ratio at the level of the sonic and in the mast (sonic-mast). **45E:** Difference between the average  $\text{CH}_4$  mixing ratio just above the water and in the level mast (water-mast). All are plotted against time and all are measured in summer.

Figure 45A displays the average methane mixing ratios for each inlet in summer. The average methane mixing ratio for the inlet at the level of the sonic is the average for the entire 5 minutes the air from that inlet was measured. Figure 45B also shows the averages for the first and the last minute the air from the inlet at the level of the sonic was measured. In both of the figures all averages with a standard deviation larger than 0.03 ppm were removed. A lower maximum standard deviation leads to insufficient coverage of the methane peak between 35 and 40 hours after the first CTD. Using these averages the differences between the average methane ratios of different inlets were determined and plotted in figure 45C (water-sonic), 45D (sonic-mast) and 45E (water-mast). The differences are mostly close to zero, but during the periods of higher variance the differences also vary more. Overall the  $\text{CH}_4$  mixing ratio just above the water is a little higher than the mixing ratio at the level of the sonic (about  $5 \text{ ppb} \pm 14 \text{ ppb}$  higher) and in the mast ( $14 \text{ ppb} \pm 37 \text{ ppb}$  higher), as can be seen in table 11. The methane mixing ratio at the level of the sonic is about  $8 \text{ ppb} \pm 20 \text{ ppb}$  higher than at the level of the mast. This indicates that here methane emissions from the water are measured. For both cases where methane mixing ratios at inlets were compared to either the average  $\text{CH}_4$  mixing ratio of the whole, or part of the period measured from the inlet at the level of the sonic, the difference between the methane at an inlet and the full sonic data are more negative than the difference between the  $\text{CH}_4$  at that inlet and part of the sonic data. Which means the full sonic methane mixing ratios are on average

lower than the  $\text{CH}_4$  mixing ratio measured during the first minute of measuring from the inlet at the level of the sonic and on average higher than the  $\text{CH}_4$  mixing ratio measured during the last minute of measuring from the inlet at the level of the sonic. This is especially true during periods of large variation in the methane mixing ratios. The average differences per CTD can be found in appendix 4. The average differences over the entire duration of the 48 hour station can be found in table 11.

Figure 46A displays the average methane mixing ratios for each inlet in autumn. In this figure all averages with a standard deviation larger than 0.005 were removed. This maximum standard deviation allowed the peaks that were probably caused by contamination from our own boat, or from passing boats, to be filtered out.

From figure 46B it is clear that the methane mixing ratio at the level of the sonic is higher than just above the water and from figure 46C it can be concluded that the  $\text{CH}_4$  mixing ratio in the mast is a little higher than at the level of the sonic. In line with these conclusions, figure 46D shows that the methane mixing ratios in the mast are higher than just above the water. These conclusions about the overall differences can also be seen in table 11. When the water from the Wadden Sea emits methane, the methane mixing ratio closer to the water is expected to be higher than further away from the water surface. The opposite is seen here. This indicates that methane is taken up by the Wadden Sea in autumn, which is very unlikely, because the methane concentrations in the water are higher than those in the atmosphere. It is also possible that the water and mast inlets were mixed up when the G2301 was installed, but during system checks that did not seem to be the case. The average differences per CTD can be found in appendix 4.



**Figure 46A:** Average  $\text{CH}_4$  mixing ratios of the different inlets in autumn. **46B:** Difference between the average  $\text{CH}_4$  mixing ratio just above the water and at the level of the sonic (water-sonic). **46C:** Difference between the average  $\text{CH}_4$  mixing ratio at the level of the sonic and in the mast (sonic-mast). **46D:** Difference between the average  $\text{CH}_4$  mixing ratio just above the water and in the level mast (water-mast). All are plotted against time and all are measured in autumn.

### 3.9 Sonic

Figure 47 shows the wind speed and direction in summer and autumn plotted against time. During the period of high variation in methane mixing ratio in summer (between 35 and 40 hours after the first CTD) the wind speed seems to be decreasing and no unusual patterns can be detected in the wind direction. During the period of high methane mixing ratio variation around about 25 hours after the first CTD the wind speed is increasing. During times of variability high or variable wind speeds is expected, which seems to be the case here.

**Table 11:** Average differences between the CH<sub>4</sub> mixing ratios at different inlets in ppb.

		Average	STD
Summer	Water-Sonic full	4	13
	Water-Sonic end	5	14
	Sonic full-Mast	7	17
	Sonic start-Mast	8	20
	Water-Mast	14	37
Autumn	Water-Sonic	-9	13
	Sonic-Mast	-4	14
	Water-Mast	-15	24

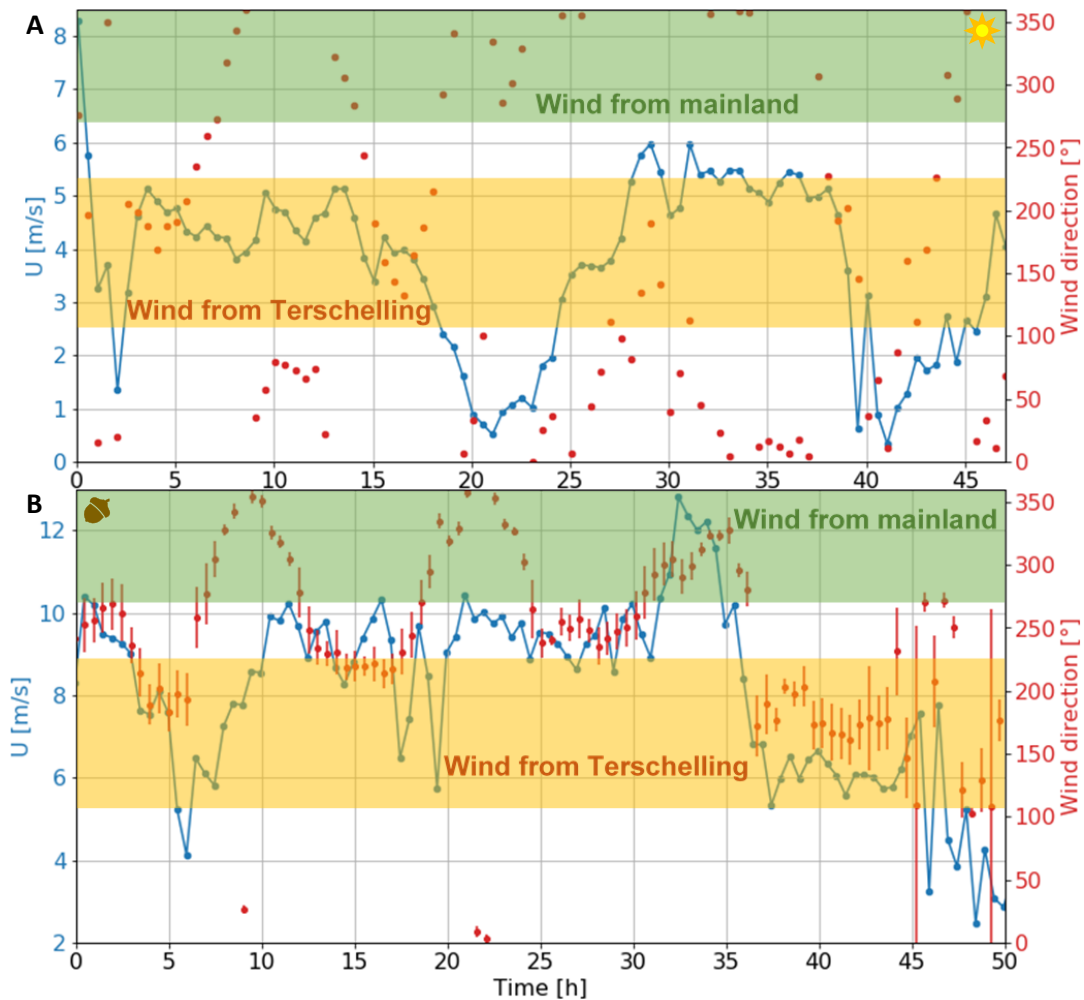


**Figure 47A:** Wind speed (blue) and direction (red) measured during the summer cruise plotted against time. **47B:** Wind speed (blue) and direction (red) measured during the autumn cruise plotted against time. In both plots the bands in which the wind blows from the mainland (green) and Terschelling (yellow) are given.

**Table 12:** Percentage of time during the 48 hour stations in summer and autumn that the wind blew from the mainland and Terschelling.

	Wind from	% times wind from here
Summer	Mainland	25.3
	Terschelling	29.5
Autumn	Mainland	34.7
	Terschelling	34.7

Figure 48A and B show that during the summer cruise the two broad methane mixing ratio peaks in the atmosphere appear at the end of the two periods with enhanced wind speeds, but no clear relation between methane mixing ratios and wind direction can be seen.

In autumn the wind speed and direction follow a similar pattern and also partly follow a similar pattern as the methane mixing ratios measured in the atmosphere (see figure 48C and D). During the first five hours after the first CTD and from about 35 hours after the first CTD onwards both the wind speed and direction seem to covary with the methane mixing ratio, but overall no relation between wind and CH<sub>4</sub> mixing ratio can be determined.

Wind from the mainland or from Terschelling, which both occurred for about 30 percent of the time in summer and autumn (see table 12), does not seem to affect the methane mixing ratio in the atmosphere.

The wind speed in autumn is higher than in summer and the wind direction varies less in autumn. Overall the sonic data

suggest that wind was not a major regulator of CH<sub>4</sub> mixing ratio in the atmosphere. This does not rule out that varying winds could have influenced plumes with higher methane mixing ratios reaching the boat, which might be the cause of the variations in methane mixing ratios in the atmosphere. Wind forcing also does not seem to influence dissolved methane concentrations, unlike what Grunwald et al. (2007 and 2009) concluded for the German Wadden Sea.

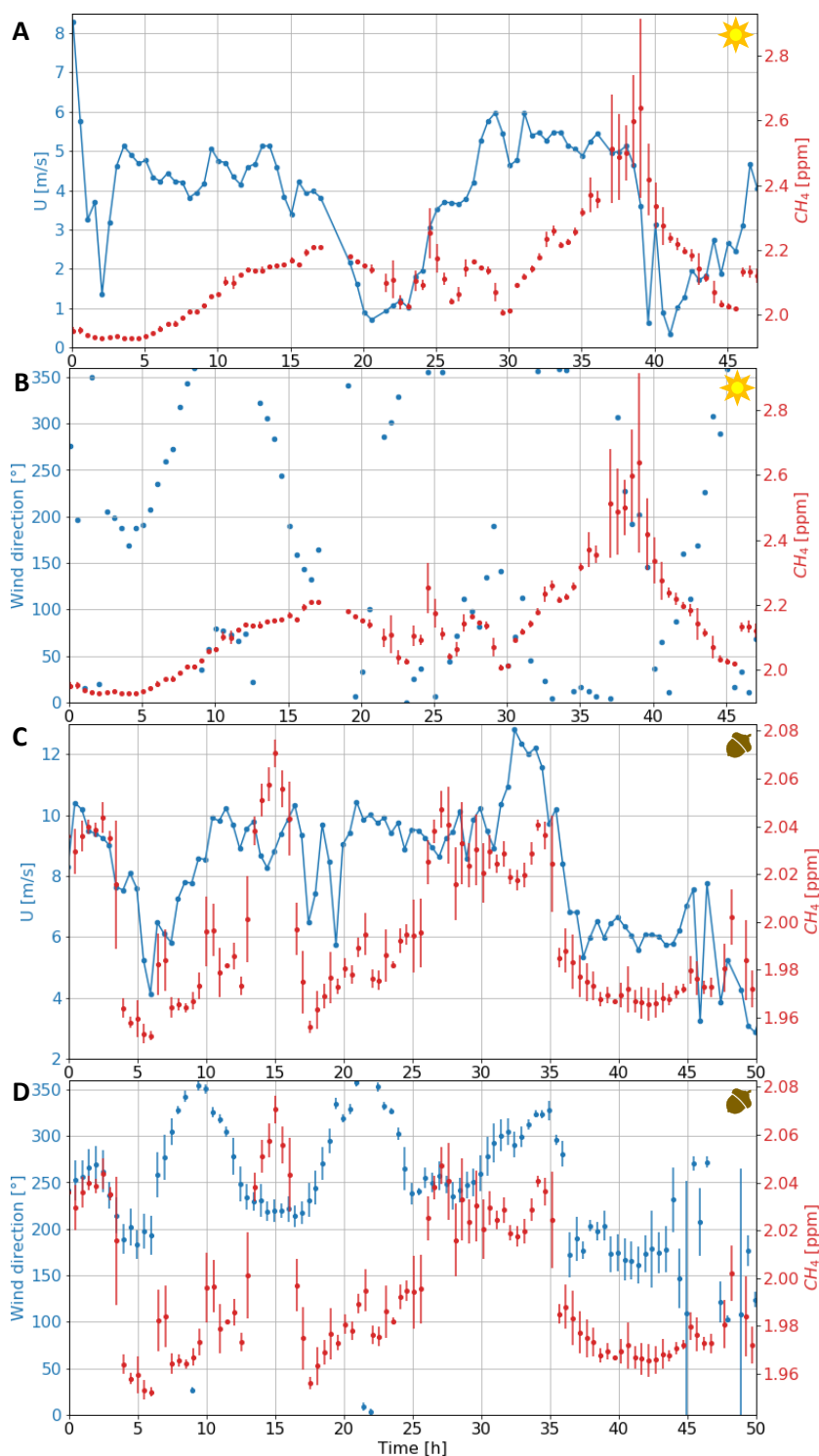


**Figure 48A:** Summer wind speed and CH<sub>4</sub> mixing ratios in the atmosphere. **48B:** Summer wind direction and CH<sub>4</sub> mixing ratios in the atmosphere. **48C:** Autumn wind speed and CH<sub>4</sub> mixing ratios in the atmosphere. **48D:** Autumn wind direction and CH<sub>4</sub> mixing ratios in the atmosphere. All of the quantities mentioned above are plotted against time.

### 3.10 Emissions

Figure 49 shows the calculated sea-air flux and the emissions (rate of CH<sub>4</sub> increase) determined with the bucket measurements. Both in summer and autumn the temporal variability of the sea-air flux and the bucket emissions are quite similar (figure 49A and C). This can also be seen in the correlations plotted in figure 49B and D. For autumn all measurements seem to lie on the same line, while for summer there may be two different populations. One very steep line consisting of measurements with a sea-air flux lower than 0.5 nmol/m<sup>2</sup>/s and one less steep line, covering the rest of the measurements. Furthermore, the sea-air flux calculated from the supersaturation of dissolved methane in the water is between about 1% and 99% lower than the measured emissions. This can also be seen in table 13 and 14. The lower value of the sea-air flux might be explained by the fact that the flux accounts for a process in which interactions with the atmosphere take place, while the emissions are measured in a bucket, closed off from the atmosphere. Wind speed, for example, influences the

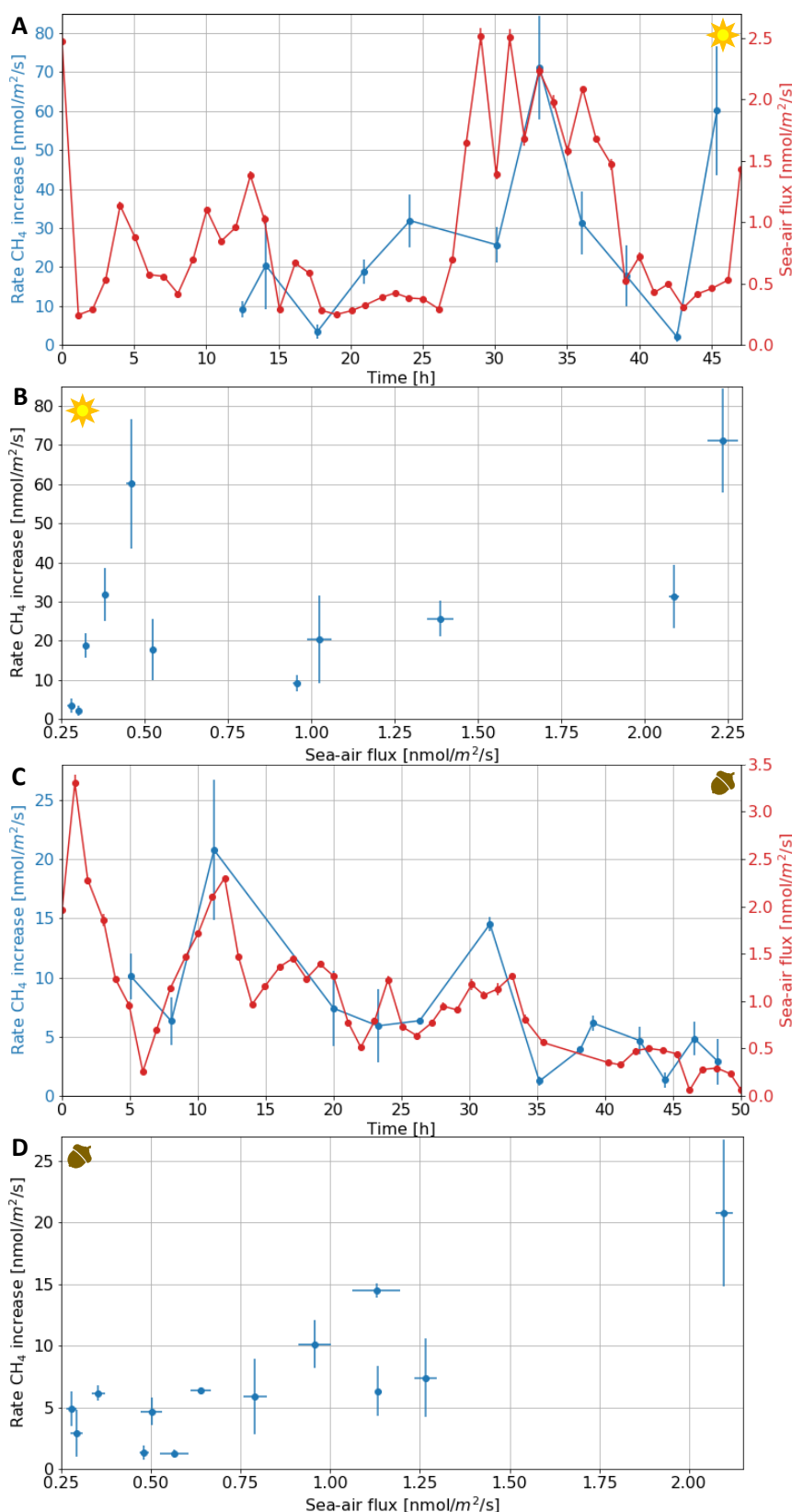


**Figure 49A:** Summer sea-air flux and rate of CH<sub>4</sub> increase determined with the bucket measurement plotted against time. **49B:** Summer rate of CH<sub>4</sub> increase plotted against sea-air flux. **49C:** Autumn sea-air flux and rate of CH<sub>4</sub> increase determined with the bucket measurement plotted against time. **49D:** Autumn rate of CH<sub>4</sub> increase plotted against sea-air flux.

the flux accounts for a process in which interactions with the atmosphere take place, while the emissions are measured in a bucket, closed off from the atmosphere. Wind speed, for example, influences the

magnitude of the sea-air flux, but it does not influence the magnitude of the bucket emissions. It suggests that bucket measurements are representative for what happens in the atmosphere, but the bucket magnifies the response.

**Table 13:** Average sea-air flux and its standard deviation and the average emissions measured with the bucket and its standard deviations for several CTD measurements during the summer cruise. All variables are in  $\text{nmol}/\text{m}^2/\text{s}$ . The last column contains the percent of the flux relative to the bucket emissions.

CTD	Flux	STD Flux	Emission	STD Emission	% Flux 
13	0.96	0.01	9.06	2.03	10.56
15	1.02	0.04	20.40	11.26	5.01
19	0.28	0.01	3.34	1.84	8.35
22	0.32	0.01	18.75	3.07	1.72
25	0.38	0.00	31.87	6.73	1.20
31	1.39	0.04	25.64	4.64	5.41
34	2.23	0.05	71.08	13.27	3.14
37	2.09	0.02	31.33	8.14	6.66
40	0.52	0.01	17.73	7.73	2.96
44	0.30	0.00	2.04	1.37	14.83
46	0.46	0.01	60.16	16.55	0.76

**Table 14:** Average sea-air flux and its standard deviation and the average emissions measured with the bucket and its standard deviations for several CTD measurements during the autumn cruise. All variables are in  $\text{nmol}/\text{m}^2/\text{s}$ . The last column contains the percent of the flux relative to the bucket emissions.

CTD	Flux	STD Flux	Emission	STD Emission	% Flux 
6	0.956476	0.044787	10.115426	1.934888794	9.455614
9	1.133654	0.003399	6.3173154	2.027676586	17.94518
12	2.098532	0.023858	20.77303	5.946149153	10.10219
21	1.264964	0.030926	7.3903373	3.170009624	17.11645
24	0.789758	0.032466	5.9110482	3.06580572	13.36072
27	0.638445	0.028925	6.3502492	0	10.05386
33	1.128253	0.067089	14.513564	0.57194042	7.773784
36	0.563831	0.039704	1.2464707	0.351303125	45.23418
37	0.35299	0.019236	6.1515268	0.615197552	5.738243
40	0.501725	0.030274	4.674687	1.146198348	10.73281
41	0.481149	0.012439	1.3312957	0.611111267	36.1414
44	0.278423	0.014425	4.8494629	1.409845566	5.741317
45	0.293477	0.01667	2.8870643	1.925863479	10.16523

## 4 Conclusion

Throughout this report three questions were attempted to be answered. Here, the results are summarized to generate the answers to each question.

### 1. Are methane emissions from the Wadden Sea measurable in the atmosphere?

The differences between the average methane mixing ratios at different heights suggest that CH<sub>4</sub> emissions might be measurable in summer. In summer the overall methane mixing ratio just above the water is a little higher than at the level of the sonic (about 5ppb ± 14ppb higher) and still higher than in the mast (14ppb ± 37ppb higher), which would indicate that just above the water methane emissions from the Wadden Sea water were measured. In autumn, however, the overall methane mixing ratio just above the water is a little lower than at the level of the sonic (9ppb ± 13ppb lower) and still lower than in the mast (15ppb ± 24ppb lower). This suggests that the Wadden Sea is taking up methane in autumn, but because the CH<sub>4</sub> concentrations in the water are higher than in the atmosphere this is unlikely.

With bucket measurements reliable emissions can be determined when the bucket remains closed for at least 20 seconds. Emissions determined with the bucket are always positive. Emissions could be negative when extended periods of methane decrease occur, but these did not occur. The source deuterium isotopic signature of the autumn air samples taken from the bucket (-226‰ ± 6‰) agrees within errors with the average deuterium isotopic signature of the water samples in autumn (-200‰ ± 33‰), confirming that the methane that accumulates in the bucket originates from the Wadden Sea water. The source <sup>13</sup>C isotopic signatures and source deuterium isotopic signatures of the air samples also suggest that the measured methane has a biogenic origin, which is expected for methane from the Wadden Sea. Finding matching deuterium isotopic signatures is therefore not surprising.

A point of concern is that the fluxes calculated from the bucket measurements are so much higher than the calculated sea-air flux based on, among others, wind speed and methane concentrations in the atmosphere and the water. The temporal variability in the sea-air flux and the bucket emissions are quite similar, especially in autumn, but the bucket emissions are consistently higher than the sea-air flux. This indicates that the bucket measurements are representative for what happens in the atmosphere, but they magnify the influence of the Wadden Sea water.

### 2. Is there a temporal cycle in the dissolved methane concentrations, oxidation rates and isotopic signatures within the water column and can this (or another) temporal cycle also be seen in the methane mixing ratios and isotopic signatures in the air above the Wadden Sea?

Dissolved methane concentrations in autumn peak just after low and high tide, when the water is relatively stagnant and methane can build up. This temporal variability is not seen in summer and not all measured dissolved methane concentrations in autumn follow the same relation to the tidal cycle. The methane concentrations in summer are on average about 4 times higher than in autumn, which could be due to the higher water temperatures in summer.

The methane oxidation increase with methane concentration in the water from concentration of about 20 nmol/L onwards. Also, the summer methane oxidation rates are on average about 8 times higher than the autumn oxidation rates, which might be due to higher summer water temperatures. The deuterium isotopic signatures in the water are more depleted for some dissolved methane concentration peaks in autumn, but no clear temporal cycle can be found in summer. The Rayleigh fractionation plot based on the isotopic signatures show that the deuterium fractionation is quite strong and negative in samples with methane concentrations lower than about 20 nmol/L, while the

overall deuterium signature seems to stay quite constant for higher concentrations.

The methane mixing ratios in the atmosphere do not follow the temporal variations in the CH<sub>4</sub> concentrations, oxidation rates, and isotopic signatures in the water over the 48 hours. However, the methane mixing ratio in summer is on average 80 ppb higher than in autumn, which is opposite to what would be expected based on methane seasonal cycles. The temporal cycles, and higher summer average methane mixing ratio are most likely caused by passing plumes with higher methane mixing ratios. This hypothesis could not be proven from the short period of data analysed here. The temporal cycle of the isotopic signatures found in the air samples does not match the temporal cycle of any of the other measured variables and is thus primarily influenced by other factors than emissions from the water.

### 3. What causes enhanced or decreased methane emissions?

For both autumn and summer the emissions determined with the bucket are related to the methane concentrations in the water, with higher emissions at higher methane concentrations. As mentioned above, the isotope data also confirm that the increase measured in the bucket originates from methane that comes out of the water.

The sea-air flux follows the same pattern as the emissions determined with the bucket, thus it can be assumed that the emissions depend on the variables that are used to calculate the sea-air flux. Partly the emissions depend on water temperature and salinity in the top 1 meter of the water. At higher water temperatures and salinities the emissions should be higher, because the solubility in the water is lower. Air temperature also influences the solubility. At higher air temperatures the emissions are higher. Apart from methane concentrations in the water, CH<sub>4</sub> mixing ratios in the atmosphere influence the methane emissions as well, with higher emissions at lower atmospheric CH<sub>4</sub> mixing ratios. Finally, higher wind speeds and higher roughness lengths also lead to higher methane emissions. Nevertheless, the dependence to these parameters in the air-sea flux calculations is rather weak.

Some other conclusions that can be drawn based on this research are:

- Methane concentrations in the sediments at different depths varied immensely in pattern with depth and in magnitude between different box cores. No reliable conclusions can be drawn from these data.
- Duplicate measurements of deuterium signatures in the Wadden Sea water are quite similar, which means the methane analysis system produces reliable results.
- For periods when the methane concentration in the water is lower than about 20 nmol/L the Rayleigh fractionation factor is about -0.10, which falls into the same range as was determined for methane-oxidizing bacteria in previous research.
- The methane concentrations in the water samples measured with a GC at the NIOZ are similar to the concentrations measured with the methane analysis system at IMAU, indicating that the methane concentrations determined with the methane analysis system are reliable.
- Variations in methane concentrations or oxidation rates in the water or in the wind speed and direction could not explain the variable noise level in the background methane mixing ratios in summer. Neither could the wind data prove the theory about plumes with higher methane mixing ratios causing the temporal variations in the measured methane mixing ratios.

## 5 Discussion

Throughout this report a number of weaknesses and uncertainties of the used setup were pointed out. Here I discuss these weaknesses and suggest possible solutions. I do not do this to poke holes in my conclusions, which are not affected by the weaknesses described below. I do this to supply a list with points to watch out for if this type of research is done again in the future. Recommendations about how to gather additional information during future cruises are also provided.

### 5.1 Measurement errors

The term “measurement error” is used for a wide range of issues that went wrong during the cruises, during the measurements in the lab or during data analysis. I discuss them successively below.

- The inlet line in the mast was not properly connected in autumn.

This allowed air from the smoking area and the outlet from the kitchen to enter the inlet line, potentially affecting the majority of the 48 hour station measurements from the mast location in autumn. It could have been prevented by checking the lines again after the mast was raised. In fact, in autumn the methane mixing ratio data contain signals that likely originate from the boat, but these peaks are also seen in the methane mixing ratio data at the level of the sonic and just above the water. This indicates that the contaminating signals represent a larger scale feature and are not only caused by the improper connection of the line to the mast. Thus, this leak did not affect the main conclusions drawn in this report.

- Methane mixing ratios at different inlets were measured for different durations in summer and autumn.

This means that average background mixing ratios are based on different amounts of measurements. This is not a major issue, but measuring each inlet for the same length of time is preferred. Based on the data analysis done in this report, measuring air from each inlet for 2 minutes is recommended.

- The bucket regularly opened up to the atmosphere and water was sucked into the lines to the G2301.

Waves and currents made it difficult to keep the bucket closed off from the atmosphere and, especially during autumn, the G2301 pump caused the bucket to sink by creating a negative pressure inside the bucket. Water splashing inside the lines frequently entered the lines and forced the measurement to stop at once. The opening of the bucket caused frequent interruptions in the increase of methane mixing ratio inside the bucket. In some cases, buckets did remain closed off for longer periods of time, but during the duration of the buckets the rates of methane increase varied. It would be interesting to measure more bucket enclosures for longer periods to investigate the variations in rates of methane increase with time. To be able to do this the bucket has to be adjusted to decrease disturbances from waves, currents and splashing inside the bucket. A solution may be attaching the bucket to a pole extending from the ship. This would allow bucket measurements to be done further away from the ship, which would already decrease the amount of disturbances caused by the bucket banging against the ship and by reflected waves. It would also allow the bucket to move more freely with the waves instead of being pulled to different sides by ropes that were now used to keep the bucket in place.

- A stone was present in the air sample pump in autumn.

This made the filling of air sample bags extremely slow and at some point impossible. Near the end of the cruise the stone was removed and samples could be taken again. Even with the stone, still quite some samples were taken without trouble and, therefore, the conclusions drawn in this report are not affected by this malfunction. Checking the air sample pump before departure could have prevented this inconvenience.

- Smaller bottles were used to take water samples to measure isotopic signatures at the end of the summer cruise.

This had to be done, because there were no more 125 ml bottles on board. By adjusting the headspace created in the smaller bottles, possible issues were bypassed. 125 ml bottles are preferred when measuring duplicates or measuring water samples with low methane concentrations.

- Different stoppers were used in summer and autumn.

Almost all summer water samples contained small air bubbles, most likely caused by the stoppers used during summer. Using the type of stoppers used in autumn is recommended.

- No  $\delta^{13}\text{C-CH}_4$  was measured in the water samples.

The  $^{13}\text{C}$  isotopic signatures in the water samples were not measured due to restricted lab access during the COVID-19 pandemic. The deuterium isotopic signatures were sufficient to draw conclusions in this report, but it would still be interesting to measure the  $^{13}\text{C}$  isotopic signatures in the water samples to see if the results support the conclusions drawn based on deuterium isotopic signatures.

- The rate coefficients for methane oxidation of the death controls were not zero.

Non-zero values found for 'blank' measurements are common for many instruments, but in this case the people at the NIOZ ensured me this was not normal. Non-zero rate coefficients for methane oxidation of the death controls indicate that not all methane oxidizing bacteria were killed by the injection of  $\text{HgCl}_2$  solution, which is unlikely, or that some radioactive water is present in the polymer mixture. The rate coefficient for the death controls was subtracted from the other rate coefficients to correct for this, which means this inconvenience did not influence the conclusions drawn in this report. The cause of these non-zero rate coefficients is, however, something that needs to be investigated further.

- The fast GHG analyser did not work in summer and in autumn the ringdown time was too low to use the measurements.

This meant no relations between eddy covariance and methane mole fractions could be drawn. Apart from the G2301 pump breaking down in autumn, the pumps also required a lot of energy from the boat, causing critical systems to falter. This is why the energy requirements of the pumps must be investigated better before joining another cruise. A fast GHG analyser can only be installed if its pump does not require too much energy in combination with the G2301 pump.

## 5.2 Uncertainties

Several of the results reported in this report have rather large uncertainties. This does not necessarily mean that something went wrong, but likely reflects a large natural variability of some parameters, which can therefore not be constrained very precisely.

- Vertical variations in the measured methane mixing ratios in the atmosphere in autumn cannot be explained.

The differences between the methane mixing ratios measured from different inlets (altitudes) in autumn point to uptake of methane, which is very unlikely. It was carefully checked that the valve sequence was correct, but since this observation contradicts the emissions recorded with the bucket, it is likely that this is an artefact of the measurement system. It could still be an unidentified mix of valve sequence, or related to possible leaks in the inlet lines. During the autumn cruise injections of pure methane were done at each inlet, but the results were only briefly studied during the cruise. Peaks showed at all inlets at which injections were done, although not all peaks were equally high. The peaks at moments of pure methane injection need to be studied in more detail to investigate the causes of the unexplained vertical variations in methane mixing ratio in autumn.

- Temporal variations in the measured methane mixing ratios in the atmosphere cannot be explained.

A higher average methane mixing ratio was found in summer than in autumn, which is opposite to what is expected based on the methane seasonal cycle in the atmosphere. The higher average methane mixing ratio in summer might be explained by plumes with higher methane mixing ratios passing over the boat. This hypothesis could not be proven in this report. A way to investigate this in future cruises would be to take samples of atmospheric air regularly. During the autumn cruise only two background air samples were taken, but they were taken very close to the water surface and not analysed separately. By taking air samples at inlets every few hours, isotopic signatures can be determined. Based on the isotopic composition of the methane in the samples conclusions about the origin of the methane in the atmosphere can be drawn.

- Temporal cycles are uncertain.

To gain more understanding of the temporal cycles found in this report, the cruises to the Wadden Sea should be repeated. Repetition of cruises, and possible longer measurement periods at the 48 hour station, would expand the amount of data and may confirm or weaken the tentative conclusions on temporal cycles found in this report.

To conclude, a number of incidents occurred to the various measurement systems used in this research project, but they did not affect the main conclusions drawn in this report. Additional information can be obtained by measuring the isotopic composition of methane in ambient air regularly (every few hours). Information on the temporal variability in the water column should be confirmed by returning to the 48 hour station in the Dutch Wadden Sea for a longer period.

## References

- Baertschi, P. (1976) Absolute  $^{18}\text{O}$  of standard mean ocean water. *Earth and Planetary Science Letters*, 31, p. 341-344.
- Bange, H.W., Bartell, U.H., Rapsomanikis, S., Andreae, M.O. (1994) Methane in the Baltic and North Seas and a reassessment of the marine emissions of methane. *Global Biogeochemical Cycles*, 8(4), p. 465-480.
- Bange, H.W. (2006) Nitrous oxide and methane in European coastal waters. *Estuarine, Coastal and Shelf Science*, 70, p. 361-374.
- Barber, T.R., Burke Jr., R.A., Sackett, W.M. (1988) Diffusive Flux of Methane from Warm Wetlands. *Global Biogeochemical Cycles*, 2(4), p. 411-425.
- Borges, A.V., Champenois, W., Gypens, N., Delille, B., Harlay, J. (2016) Massive marine methane emissions from near-shore shallow coastal areas. *Scientific Reports*, 6(27908), DOI: 10.1038/srep27908.
- Brass, M. and Röckmann, T. (2010) Continuous-flow isotope ratio mass spectrometry method for carbon and hydrogen isotope measurements on atmospheric methane. *Atmospheric Measurement Techniques*, 3, p. 1707-1721.
- Ciais, P., Sabine, C. and others (2013) Chapter 6: Carbon and Other Biogeochemical Cycles. In: *Climate Change 2013: The Physical Science Basis. Contribution of Working Group I to the Fifth Assessment Report of the Intergovernmental Panel on Climate Change / Stocker, T.F., Qin, D., Plattner, G.K., Tignor, M., Allen, S.K., Boschung, J., Nauels, A., Xia, Y., Bex, V., Midgley, P.M., United Kingdom and New York, NY, USA : Cambridge University Press*, p. 465–570.
- Cicerone, R.J. and Oremland, R.S. (1988) Biogeochemical Aspects of Atmospheric Methane. *Global Biogeochemical Cycles*, 2(4), p. 299-327.
- Crosson, E.R. (2008) A cavity ring-down analyzer for measuring atmospheric levels of methane, carbon dioxide, and water vapor. *Applied Physics B*, 92, p. 403-408.
- Dean, J.F., Middelburg, J.J., Röckmann, T., Aerts, R., Blauw, L.G., Egger, M., Jetten, M.S.M., de Jong, A.E.E., Meisel, O.H., Rasigraf, O., Slomp, C.P., in 't Zandt, M.H., Dolman, A.J. (2018) Methane Feedbacks to the Global Climate System in a Warmer World. *Review of Geophysics*, 56, [https://doi.org/ 10.1002/2017RG000559](https://doi.org/10.1002/2017RG000559).
- Dentener, F., Peters, W., Krol, M., van Weele, M., Bergamaschi, P., Lelieveld, J. (2003) Interannual variability and trend of  $\text{CH}_4$  lifetime as a measure for OH changes in the 1979 – 1993 time period. *Journal of Geophysical Research: Atmospheres*, 108 (D15).
- Derwent, R.G., Simmonds, P.G., O'Doherty, S., Stevenson, D.S., Collins, W.J., Sanderson, M.G., Johnson, C.E., Dentener, F., Cofala, J., Mechler, R., Amann, M. (2006) External influences on Europe's air quality: Baseline methane, carbon monoxide and ozone from 1990 to 2030 at Mace Head, Ireland. *Atmospheric Environment*, 40, p. 844-855.
- Duran-Matute, M., Gerkema, T., Sassi, M.G. (2016) Quantifying the residual volume transport through a multiple-inlet system in response to wind forcing: The case of the western Dutch Wadden Sea. *Journal of Geophysical Research: Oceans*, 121, p. 8888-8903.
- Egberts, L., Schroor, M., Bazelmans, J. (2018) Introduction. In, Meindert (eds), *Waddenland Outstanding: The History, Landscape and Cultural Heritage of the Wadden Sea Region*. Amsterdam: Amsterdam University Press, p. 19-28.
- Enemark, J., Fischer, L., Reise, K. (2018) Protecting the natural and cultural values of the Wadden Sea coast in the Anthropocene. In, Meindert (eds), *Waddenland Outstanding: The History, Landscape and Cultural Heritage of the Wadden Sea Region*. Amsterdam: Amsterdam University Press, p. 67-79.

- Etiope, G., Lassey, K.R., Klusman, R.W., Boschi, E. (2008) Reappraisal of the fossil methane budget and related emission from geologic sources. *Geophysical Research Letters*, 35, doi:10.1029/2008GL033623.
- Gräwe, U., Flöser, G., Gerkema, T., Duran-Matute, M., Badewien, T.H., Schulz, E., Burchard, H. (2016). A numerical model for the entire Wadden Sea: Skill assessment and analysis of hydrodynamics. *Journal of Geophysical Research: Oceans*, 121, p. 5231-5251.
- Grunwald, M., Dellwig, O., Liebezeit, G., Schnetger, B., Reuter, R., Brumsack, H. (2007) A novel time-series station in the Wadden Sea (NW Germany): First results on continuous nutrient and methane measurements. *Marine Chemistry*, 107, p. 411-421.
- Grunwald, M., Dellwig, O., Beck, M., Dippner, J.W., Freund, J.A., Kohlmeier, C., Schnetger, B., Brumsack, H. (2009) Methane in the southern North Sea: Sources, spatial distribution and budgets. *Estuarine, Coastal and Shelf Science*, 81, p. 445-456.
- Hamdan, L.J. and Wickland, K.P. (2016) Methane emissions from oceans, coasts, and freshwater habitats: New perspectives and feedbacks on climate. *Limnology and Oceanography*, 61, doi: 10.1002/lno.10449.
- Hartmann, D.L., A.M.G. Klein Tank, M. Rusticucci, L.V. Alexander, S. Brönnimann, Y. Charabi, F.J. Dentener, E.J. Dlugokencky, D.R. Easterling, A. Kaplan, B.J. Soden, P.W. Thorne, M. Wild, Zhai, P.M. (2013) Observations: Atmosphere and Surface. In: *Climate Change 2013: The Physical Science Basis. Contribution of Working Group I to the Fifth Assessment Report of the Intergovernmental Panel on Climate Change [Stocker, T.F., D. Qin, G.-K. Plattner, M. Tignor, S.K. Allen, J. Boschung, A. Nauels, Y. Xia, V. Bex and P.M. Midgley (eds.)]. Cambridge University Press, Cambridge, United Kingdom and New York, NY, USA*, p. 159-254.
- He, R., Wooller, M.J., Pohlman, J.W., Quensen, J., Tiedje, J.M., Leigh, M.B. (2012) Shifts in Identity and Activity of Methanotrophs in Arctic Lake Sediments in Response to Temperature Changes. *Applied and Environmental Microbiology*, 78(13) p. 4715-4723.
- Holmes, M.E., Sansone, F.J., Rust, T.M., Popp, B.N. (2000) Methane production, consumption, and air-sea exchange in the open ocean: An evaluation based on carbon isotopic ratios. *Global Biogeochemical Cycles*, 14(1), p. 1-10.
- Hornafius, J.S., Quigley, D., Luyendyk, B.P. (1999) The world's most spectacular marine hydrocarbon seeps (Coal Oil Point, Santa Barbara Channel, California): Quantification of emissions. *Journal of Geophysical Research*, 104(C9), p. 20703-20711.
- James, R.H., Bousquet, P., Bussmann, I., Haeckel, M., Kipfer, R., Leifer, I., Niemann, H., Ostrovsky, I., Piskozub, J., Rehder, G., Treude, T., Vielstädte, L., Griener, J. (2016) Effects of climate change on methane emissions from seafloor sediments in the Arctic Ocean: A review. *Limnology and Oceanography*, 61, p. 283-299.
- JoVE Science Education Database. (2020, May 5<sup>th</sup>) Gas Chromatography (GC) with Flame-Ionization Detection [Video file]. Retrieved from <https://www-jove-com.proxy.library.uu.nl/science-education/10187/gas-chromatography-gc-with-flame-ionization-detection>.
- Judd, A.G. (2003) The global importance and context of methane escape from the seabed. *Geo-Marine Letters*, 23, p. 147-154.
- Kamaleson, A.S., Gonsalves, M.J., Nazareth, D.R. (2019) Interactions of sulfur and methane-oxidizing bacteria in tropical estuarine sediments. *Environmental Monitoring and Assessment*, 191(496), doi:10.1007/s10661-019-7616-8.
- Keeling, C.D. (1958) The concentration and isotopic abundances of atmospheric carbon dioxide in rural areas. *Geochimica et Cosmochimica Acta*, 13, p. 322-334.

- Keppler, F., Hamilton, J.T.G., Brass, M., Röckmann, T. (2006) Methane emissions from terrestrial plants under aerobic conditions. *Nature*, 439, p. 187-191.
- Kirschke, S., Bousquet, P., Ciais, P., Saunoy, M., Canadell, J.G., Dlugokencky, E.J., Bergamaschi, P., Bergmann, D., Blake, D.R., Bruhwiler, L., Cameron-Smith, P., Castaldi, S., Chevallier, F., Feng, L., Fraser, A., Heimann, M., Hodson, E.L., Houweling, S., Josse, B., Fraser, P.J., Krummel, P.B., Lamarque, J., Langenfelds, R.L., Le Quéré, C., Naik, V., O'Doherty, S., Palmer, P.I., Pison, I., Plummer, D., Poulter, B., Prinn, R.G., Rigby, M., Ringeval, B., Santini, M., Schmidt, M., Shindell, D.T., Simpson, I.J., Spahni, R., Steele, L.P., Strode, S.A., Sudo, K., Szopa, S., van der Werf, G.R., Voulgarakis, A., van Weele, M., Weiss, R.F., Williams, J.E., Zeng, G. (2013) Three decades of global methane sources and sinks. *Nature Geoscience*, 6, p. 813-823.
- Leonte, M., Kessler, J.D., Kellermann, M.Y., Arrington, E.C., Valentine, D.L., Sylva, S.P. (2017) Rapid rates of aerobic methane oxidation at the feather edge of gas hydrate stability in the waters of Hudson Canyon, US Atlantic Margin. *Geochimica et Cosmochimica Acta*, 204, p. 375-387.
- Mahieu, K., de Visscher, A., Vanrolleghem, P.A., van Cleemput, O. (2006) Carbon and hydrogen isotope fractionation by microbial methane oxidation: Improved determination. *Waste Management*, 26, p. 389-398.
- Mau, S., Bles, J., Helmke, E., Niemann, H., Damm, E. (2013) Vertical distribution of methane oxidation and methanotrophic response to elevated methane concentrations in stratified waters of the Arctic fjord Storfjorden (Svalbard, Norway). *Biogeosciences*, 10, p. 6267-6278.
- McGinnis, D.F., Greinert, J., Artemov, Y., Beaudien, S.E., Wüest, A. (2006) Fate of rising methane bubbles in stratified waters: How much methane reaches the atmosphere? *Journal of Geophysical Research*, 111(C9), doi:10.1029/2005JC003183.
- Myhre, G., Shindell, D. and others (2013) Chapter 8: Anthropogenic and natural radiative forcing. In: *Climate Change 2013: The Physical Science Basis. Contribution of Working Group I to the Fifth Assessment Report of the Intergovernmental Panel on Climate Change / Stocker, T.F., Qin, D., Plattner, G.K, Tignor, M., Allen, S.K., Boschung, J., Nauels, A., Xia, Y., Bex, V., Midgley, P.M., United Kingdom and New York, NY, USA : Cambridge University Press*, p. 659–703.
- Navid, D. (1989) The international law of migratory species: The Ramsar convention. *Natural Resources Journal*, 29(4), p. 1001-1016.
- Nisbet, R.E.R., Fisher, R., Nimmo, R.H., Bendall, D.S., Crill, P.M., Gallego-Sala, A.V., Hornibrook, E.R.C., López-Juez, E., Lowry, D., Nisbet, P.B.R., Shuckburgh, E.F., Sriskantharajah, S., Howe, C.J., Nisbet, E.G. (2009) Emissions of methane from plants. *Proceedings of The Royal Society B*, 276, p. 1347-1354.
- Niu, M., Liang, W., Wang, F. (2018) Methane biotransformation in the ocean and its effects on climate change: A review. *Science China Earth Sciences*,
- Peltola, O., Hensen, A., Helfter, C., Belelli Marchesini, L., Bosveld, F.C., van den Bulk, W.C.M., Elbers, J.A., Haapanala, S., Holst, J., Laurila, T., Lindroth, A., Nemitz, E., Röckmann, T., Vermeulen, A.T., Mammarella, I. (2014) Evaluating the performance of commonly used gas analysers for methane eddy covariance flux measurements: the InGOS inter-comparison field experiment. *Biogeosciences*, 11, p. 3163-3186.
- Plets, R., Dix, J., Bastos, A., Best, A. (2007) Characterization of Buried Inundated Peat on Seismic (Chirp) Data, Inferred from Core Information.

- Prather, M.J., Holmes, C.D., Hsu, J. (2012) Reactive greenhouse gas scenarios: Systematic exploration of uncertainties and the role of atmospheric chemistry. *Geophysical Research Letters*, 39(9), doi:10.1029/2012GL051440.
- Reeburgh, W.S. (2007) Oceanic Methane Biogeochemistry. *Chem. Rev.*, 107(2), p. 486-513.
- Renes, H. (2018) The Wadden Sea region as a cultural landscape. In, Meindert (eds), *Waddenland Outstanding: The History, Landscape and Cultural Heritage of the Wadden Sea Region*. Amsterdam: Amsterdam University Press, p. 45-63.
- Reise, K., Baptist, M., Burbridge, P., Dankers, N., Fischer, L., Flemming, B., Oost, A.P., Smit, C., (2010) The Wadden Sea – A Universally Outstanding Tidal Wetland. *Wadden Sea Ecosystem No. 29*. Common Wadden Sea Secretariat, Wilhelmshaven, Germany, p. 7-24.
- Reuter, R., Badewien, T.H., Bartholomä, A., Braun, A., Lübben, A., Rullkötter, J. (2009) A hydrographic time series station in the Wadden Sea (southern North Sea). *Ocean Dynamics*, 59, p. 195-211.
- Rice, A.L., Gotoh, A.A., Ajie, H.O., Tyler, S.C. (2001) High-Precision Continuous-Flow Measurement of  $\delta^{13}\text{C}$  and  $\delta\text{D}$  of Atmospheric  $\text{CH}_4$ . *Analytical Chemistry*, 73, p. 4104-4110.
- Röckmann, T., Eyer, S., van der Veen, C., Popa, M.E., Tuzson, B., Monteil, G., Houweling, S., Harris, E., Brunner, D., Fischer, H., Zazzeri, G., Lowry, D., Nisbet, E.G., Brand, W.A., Necki, J.M., Emmenegger, L., Mohn, J. (2016) In situ observations of the isotopic composition of methane at the Cabauw tall tower. *Atmospheric Chemistry and Physics*, 16, p. 10469-10487.
- Rösner, H. (2018) The Wadden Sea: A natural landscape outside the dikes. . In, Meindert (eds), *Waddenland Outstanding: The History, Landscape and Cultural Heritage of the Wadden Sea Region*. Amsterdam: Amsterdam University Press, p. 81-93.
- Røy, H., Lee, J.S., Jansen, S., de Beer, D. (2008) Tide-driven deep pore-water flow in intertidal sand flats. *Limnology and Oceanography*, 53(4), p. 1521-1530.
- Saunio, M., Bousquet, P., Poulter, B., Peregón, A., Ciais, P., Canadell, J.G., Dlugokencky, E.J., Etiope, G., Bastviken, D., Houweling, S., Janssens-Maenhout, G., Tubiello, F.N., Castaldi, S., Jackson, R.B., Alexe, M., Arora, V.K., Beerling, D.J., Bergamaschi, P., Blake, D.R., Brailsford, G., Brovkin, V., Bruhwiler, L., Crevoisier, C., Crill, P., Covey, K., Curry, C., Frankenberg, C., Gedney, N., Höglund-Isaksson, L., Misalshizawa, Akihikolto, Joos, F., Kim, H., Kleinen, T., Krummel, P., Lamarque, J., Langenfelds, R., Locatelli, R., Machida, T., Maksyutov, S., McDonald, K.C., Marshall, J., Melton, J.R., Morino, I., Naik, V., O'Doherty, S., Parmentier, F.W., Patra, P.K., Peng, C., Peng, S., Peters, G.P., Pison, I., Prigent, C., Prinn, R., Ramonet, M., Riley, W.J., Saito, M., Santini, M., Schroeder, R., Simpson, I.J., Spahni, R., Steele, P., Takizawa, A., Thornton, B.F., Tian, H., Tohjima, Y., Viovy, N., Voulgarakis, A., van Weele, M., van der Werf, G.R., Weiss, R., Wiedinmyer, C., Wilton, D.J., Wiltshire, A., Worthy, D., Wunch, D., Xu, X., Yoshida, Y., Zhang, B., Zhang, A., Zhu, Q. (2016) The global methane budget 2000-2012. *Earth System Science Data*, 8, p. 697-751.
- Schroor, M. (2018) Waddenland: Concoction or reality? In, Meindert (eds), *Waddenland Outstanding: The History, Landscape and Cultural Heritage of the Wadden Sea Region*. Amsterdam: Amsterdam University Press, p. 31-44.
- Sessions, A.L., Jahnke, L.L., Schimmelmann, A., Hayes, J.M. (2002) Hydrogen isotope fractionation in lipids of the methane-oxidizing bacterium *Methylococcus capsulatus*. *Geochemica et Cosmochimica Acta*, 66(22), p. 3955-3969.
- Sheng, P., Mao, J., Li, J., Zhang, A., Sang, J., Pan, N. (2003) Atmospheric Physics. *Peking University Press*, Beijing, p. 522.

- Shipham, M.C., Bartlett, K.B., Crill, P.M., Harriss, R.C., Blaha, D. (1998) Atmospheric methane measurements in central New England: An analysis of the long-term trend and the seasonal and diurnal cycles. *Journal of Geophysical Research*, 103(D9), p 10621-10630.
- Steinle, L., Graves, C.A., Treude, T., Ferré, B., Biastoch, A., Bussmann, I., Berndt, C., Krastel, S., James, R.H., Behrens, E., Böning, C.W., Greinert, J., Sapart, C., Scheinert, M., Sommer, S., Lehmann, M.F., Niemann, H. (2015) Water column methanotrophy controlled by a rapid oceanographic switch. *Nature geoscience*, 8, p. 378-382.
- Tennekes, H. (1972) The Logarithmic Wind Profile. *Journal of the Atmospheric Sciences*, 30, p. 234-238.
- van Straaten (1954) Composition and Structure of Recent Marine Sediment in the Netherlands. *Leidse Geologische Mededelingen*, 19(1), p. 1-108.
- Weber, T., Wiseman, N.A., Kock, A. (2019) Global ocean methane emissions dominated by shallow coastal waters. *Nature Communications*, 10(4584), doi:10.1038/s41467-019-12541-7.
- Weisse, R. and Plüß, A. (2006) Storm-related sea level variations along the North Sea coast as simulated by a high-resolution model 1958-2002. *Ocean Dynamics*, 56, p. 16-25.
- Wilson, S.T., Bange, H.W., Arévalo-Martínez, D.L., Barnes, J., Borges, A.V., Brown, I., Bullister, J.L., Borgos, M., Capelle, D.W., Casso, M., de la Paz, M., Farías, L., Fenwick, L., Ferrón, S., Garcie, G., Glockzin, M., Karl, D.M., Kock, A., Laperriere, S., Law, C.S., Manning, C.C., Marriner, A., Myllykangas, J., Pohlman, J.W., Rees, A.P., Santoro, A.E., Tortell, P.D., Upstill-Goddard, R.C., Wisegarver, D.P., Zhang, G., Rehder, G. (2018) An intercomparison of oceanic methane and nitrous oxide measurements. *Biogeosciences*, 15, p. 5891-5907.
- Wu, C.S., Røy, H., de Beer, D. (2015) Methanogenesis in sediments of an intertidal sand flat in the Wadden Sea. *Estuarine, Coastal and Shelf Science*, 164, p. 39-45.
- Yamamoto, S., Alcauskas, J.B., Crozier, T.E. (1976) Solubility of Methane in Distilled Water and Seawater. *Journal of Chemical and Engineering Data*, 21(1), p. 78-80.
- Zhang, Q.L., Chang, T.L., Li, W.J. (1990) A calibrated measurement of the atomic weight of carbon. *Chinese Science Bulletin*, 35, p. 290-296.

## Appendix 1

During some bucket measurement the bucket opened frequently, allowing the methane mixing ratio within the bucket to drop. The slopes in between these moments of openings were determined.

Bucket High6, taken during the autumn cruise, is a bucket that opened often. The measurements sharing approximately the same rate of  $\text{CH}_4$  increase are depicted in figure 50A.

During other bucket measurements the bucket did not open up to the environment, but the rate of methane increase did change. In figure 50B, depicting bucket High\_up18 which was taken during the summer cruise, lines were drawn through measurements with approximately similar slopes.

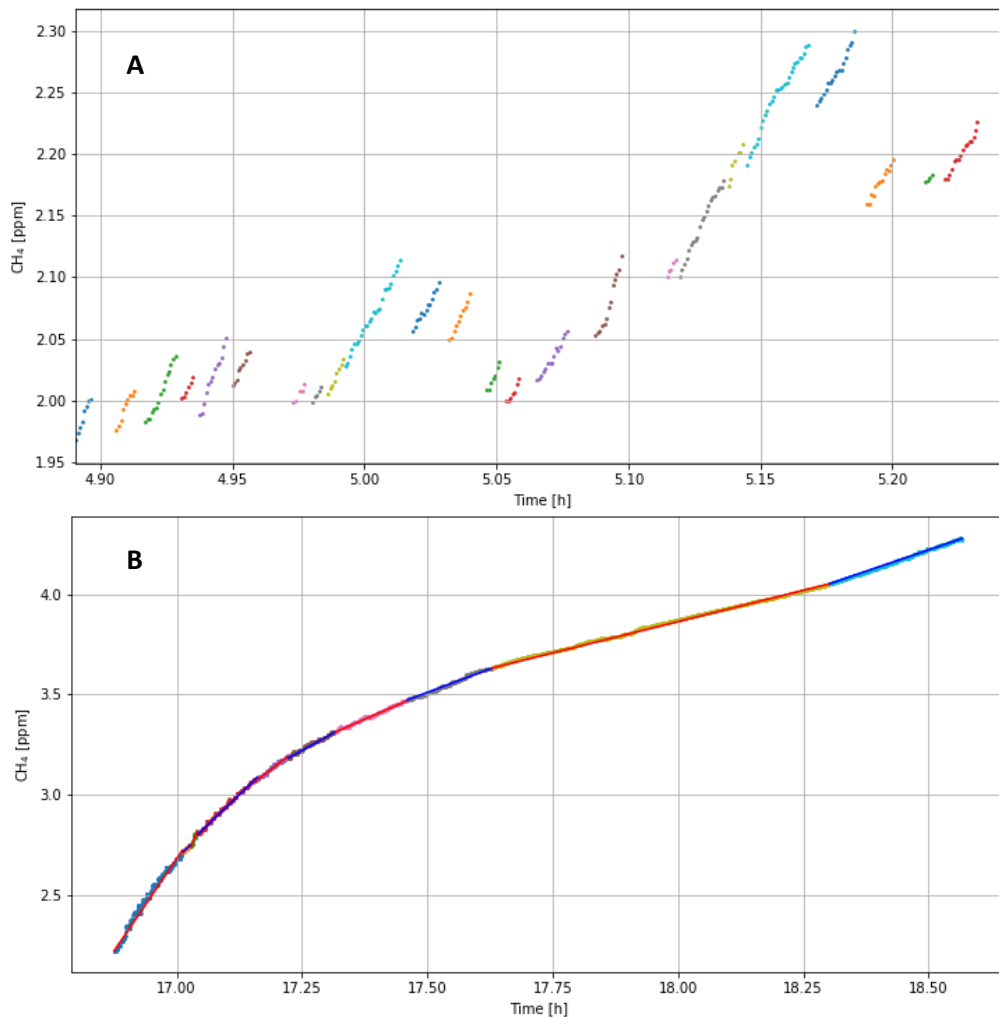


**Figure 50A:** Slopes of bucket High6, taken during the autumn cruise. **50B:** Slopes of bucket High\_up18, taken during the summer cruise.

## Appendix 2

Below the functions used to average the background G2301 data of the autumn and summer cruise are given.

### 0.0.1 Autumn

```
In [ ]: def func(t1,t2,t4,data1,data2,data4):
    # Find gaps in time to split different measured periods per value
    # At level sonic
    gapV1=[]
    for i in range(len(t1)-1):
        if t1[i+1]-t1[i]>200:
            gapV1.append(i)
    print(gapV1)

    # Split methane data and average split parts
    # Subtract 15 measurements from start to correct for switching values
    Av_V1=[]
    if gapV1[0]<=25:
        Av_V1.append(np.mean(data1[0:gapV1[0]]))
    if gapV1[0]>25:
        Av_V1.append(np.mean(data1[(0+gapV1[0]-25):gapV1[0]]))
    for i in range(len(gapV1)-1):
        Av_V1.append(np.mean(data1[(gapV1[i]+15):gapV1[i+1]]))
    if len(t1)-gapV1[-1] > 15:
        Av_V1.append(np.mean(data1[(gapV1[-1]+15):-1]))
    print(Av_V1)
    np.savetxt('Av_CTD_V1.dat', Av_V1)

    # Determine STD split parts
    STD_V1=[]
    if gapV1[0]<=25:
        STD_V1.append(np.std(data1[0:gapV1[0]]))
    if gapV1[0]>25:
        STD_V1.append(np.std(data1[(0+gapV1[0]-25):gapV1[0]]))
    for i in range(len(gapV1)-1):
        STD_V1.append(np.std(data1[(gapV1[i]+15):gapV1[i+1]]))
    if len(t1)-gapV1[-1] > 15:
        STD_V1.append(np.std(data1[(gapV1[-1]+15):-1]))
    print(STD_V1)
    np.savetxt('STD_CTD_V1.dat', STD_V1)

    # Just above water
    gapV2=[]
    for i in range(len(t2)-1):
        if t2[i+1]-t2[i]>200:
            gapV2.append(i)
    print(gapV2)
```

```

# Split methane data and average split parts
# Subtract 15 measurements from start to correct for switching valves
Av_V2=[]
if gapV2[0]<=25:
    Av_V2.append(np.mean(data2[0:gapV2[0]]))
if gapV2[0]>25:
    Av_V2.append(np.mean(data2[(0+gapV2[0]-25):gapV2[0]]))
for i in range(len(gapV2)-1):
    Av_V2.append(np.mean(data2[(gapV2[i]+15):gapV2[i+1]]))
if len(t2)-gapV2[-1] > 15:
    Av_V2.append(np.mean(data2[(gapV2[-1]+15):-1]))
print(Av_V2)
np.savetxt('Av_CTD_V2.dat', Av_V2)

# Determine STD split parts
STD_V2=[]
if gapV2[0]<=25:
    STD_V2.append(np.std(data2[0:gapV2[0]]))
if gapV2[0]>25:
    STD_V2.append(np.std(data2[(0+gapV2[0]-25):gapV2[0]]))
for i in range(len(gapV2)-1):
    STD_V2.append(np.std(data2[(gapV2[i]+15):gapV2[i+1]]))
if len(t2)-gapV2[-1] > 15:
    STD_V2.append(np.std(data2[(gapV2[-1]+15):-1]))
print(STD_V2)
np.savetxt('STD_CTD_V2.dat', STD_V2)

# In top mast
gapV4=[]
for i in range(len(t4)-1):
    if t4[i+1]-t4[i]>200:
        gapV4.append(i)
print(gapV4)

# Split methane data and average split parts
# Subtract 15 measurements from start to correct for switching valves
Av_V4=[]
if gapV4[0]<=25:
    Av_V4.append(np.mean(data4[0:gapV4[0]]))
if gapV4[0]>25:
    Av_V4.append(np.mean(data4[(0+gapV4[0]-25):gapV4[0]]))
for i in range(len(gapV4)-1):
    Av_V4.append(np.mean(data4[(gapV4[i]+15):gapV4[i+1]]))
if len(t4)-gapV4[-1] > 15:
    Av_V4.append(np.mean(data4[(gapV4[-1]+15):-1]))
print(Av_V4)
np.savetxt('Av_CTD_V4.dat', Av_V4)

```

```

# Determine STD split parts
STD_V4=[]
if gapV4[0]<=25:
    STD_V4.append(np.std(data4[0:gapV4[0]]))
if gapV4[0]>25:
    STD_V4.append(np.std(data4[(0+gapV4[0]-25):gapV4[0]]))
for i in range(len(gapV4)-1):
    STD_V4.append(np.std(data4[(gapV4[i]+15):gapV4[i+1]]))
if len(t4)-gapV4[-1] > 15:
    STD_V4.append(np.std(data4[(gapV4[-1]+15):-1]))
print(STD_V4)
np.savetxt('STD_CTD_V4.dat', STD_V4)

# Create new timeseries to match averages
# At level sonic
t_av_V1=[]
t_av_V1.append(t1[int(gapV1[0]/2)])
for i in range(len(gapV1)-1):
    t_av_V1.append(t1[gapV1[i]+20])
i=int((len(t1)-gapV1[-1])/2)
if len(t1)-gapV1[-1] > 15:
    t_av_V1.append(t1[gapV1[-1]+i])
print(t_av_V1)
np.savetxt('t_av_CTD_V1.dat', t_av_V1)

# Just above water
t_av_V2=[]
t_av_V2.append(t2[int(gapV2[0]/2)])
for i in range(len(gapV2)-1):
    t_av_V2.append(t2[gapV2[i]+20])
i=int((len(t2)-gapV2[-1])/2)
if len(t2)-gapV2[-1] > 15:
    t_av_V2.append(t2[gapV2[-1]+i])
print(t_av_V2)
np.savetxt('t_av_CTD_V2.dat', t_av_V2)

# In top mast
t_av_V4=[]
t_av_V4.append(t4[int(gapV4[0]/2)])
for i in range(len(gapV4)-1):
    t_av_V4.append(t4[gapV4[i]+20])
i=int((len(t4)-gapV4[-1])/2)
if len(t4)-gapV4[-1] > 15:
    t_av_V4.append(t4[gapV4[-1]+i])
print(t_av_V4)
np.savetxt('t_av_CTD_V4.dat', t_av_V4)

```

## 0.0.2 Summer

```
In [ ]: def func(t1,t2,t4,data1,data2,data4):
    # Find gaps in time to split different measured periods per valve
    # In top mast
    gapV1=[]
    for i in range(len(t1)-1):
        if t1[i+1]-t1[i]>200:
            gapV1.append(i)
    print(gapV1)

    # Split methane data and average split parts
    # Subtract 7 measurements form start to correct for switching values
    Av_V1=[]
    if gapV1[0]<=13:
        Av_V1.append(np.mean(data1[0:gapV1[0]]))
    if gapV1[0]>13:
        Av_V1.append(np.mean(data1[(0+gapV1[0]-13):gapV1[0]]))
    for i in range(len(gapV1)-1):
        Av_V1.append(np.mean(data1[(gapV1[i]+7):gapV1[i+1]]))
    if len(t1)-gapV1[-1] > 7:
        Av_V1.append(np.mean(data1[(gapV1[-1]+7):-1]))
    print(Av_V1)
    np.savetxt('Av_CTD_V1.dat', Av_V1)

    # Determine STD split parts
    STD_V1=[]
    if gapV1[0]<=13:
        STD_V1.append(np.std(data1[0:gapV1[0]]))
    if gapV1[0]>13:
        STD_V1.append(np.std(data1[(0+gapV1[0]-13):gapV1[0]]))
    for i in range(len(gapV1)-1):
        STD_V1.append(np.std(data1[(gapV1[i]+7):gapV1[i+1]]))
    if len(t1)-gapV1[-1] > 7:
        STD_V1.append(np.std(data1[(gapV1[-1]+7):-1]))
    print(STD_V1)
    np.savetxt('STD_CTD_V1.dat', STD_V1)

    # At level sonic
    gapV2=[]
    for i in range(len(t2)-1):
        if t2[i+1]-t2[i]>100:
            gapV2.append(i)
    print(gapV2)
```

```

# Split methane data and average split parts
# Subtract 15 measurements from start to correct for switching values
Av_V2=[]
if gapV2[0]<=85:
    Av_V2.append(np.mean(data2[0:gapV2[0]]))
if gapV2[0]>85:
    Av_V2.append(np.mean(data2[(0+gapV2[0]-85):gapV2[0]]))
for i in range(len(gapV2)-1):
    Av_V2.append(np.mean(data2[(gapV2[i]+15):gapV2[i+1]]))
if len(t2)-gapV2[-1] > 15:
    Av_V2.append(np.mean(data2[(gapV2[-1]+15):-1]))
print(Av_V2)
np.savetxt('Av_CTD_V2_full.dat', Av_V2)

# Determine STD split parts
STD_V2=[]
if gapV2[0]<=85:
    STD_V2.append(np.std(data2[0:gapV2[0]]))
if gapV2[0]>85:
    STD_V2.append(np.std(data2[(0+gapV2[0]-85):gapV2[0]]))
for i in range(len(gapV2)-1):
    STD_V2.append(np.std(data2[(gapV2[i]+15):gapV2[i+1]]))
if len(t2)-gapV2[-1] > 15:
    STD_V2.append(np.std(data2[(gapV2[-1]+15):-1]))
print(STD_V2)
np.savetxt('STD_CTD_V2_full.dat', STD_V2)

# Split methane data and average split parts
# Subtract 7 measurements from start to correct for switching values
Av_V2_s=[]
if 93>=gapV2[0]>80:
    Av_V2_s.append(np.mean(data2[0:(gapV2[0]-80)]))
if gapV2[0]>93:
    Av_V2_s.append(np.mean(data2[(0+gapV2[0]-93):(gapV2[0]-80)]))
for i in range(len(gapV2)-1):
    Av_V2_s.append(np.mean(data2[(gapV2[i]+7):(gapV2[i+1]-80)]))
if len(t2)-gapV2[-1] > 20:
    Av_V2_s.append(np.mean(data2[(gapV2[-1]+7):(gapV2[-1]+20)]))
if 20 >= (len(t2)-gapV2[-1]) > 7:
    Av_V2_s.append(np.mean(data2[(gapV2[-1]+7):-1]))
print(Av_V2_s)
np.savetxt('Av_CTD_V2_start.dat', Av_V2_s)

```

```

# Determine STD split parts
STD_V2_s=[]
if 93>=gapV2[0]>80:
    STD_V2_s.append(np.std(data2[0:(gapV2[0]-80)]))
if gapV2[0]>93:
    STD_V2_s.append(np.std(data2[(0+gapV2[0]-93):(gapV2[0]-80)]))
for i in range(len(gapV2)-1):
    STD_V2_s.append(np.std(data2[(gapV2[i]+7):(gapV2[i+1]-80)]))
if len(t2)-gapV2[-1] > 20:
    STD_V2_s.append(np.std(data2[(gapV2[-1]+7):(gapV2[-1]+20)]))
if 20 >= (len(t2)-gapV2[-1]) > 7:
    STD_V2_s.append(np.std(data2[(gapV2[-1]+7):-1]))
print(STD_V2_s)
np.savetxt('STD_CTD_V2_start.dat', STD_V2_s)

# Split methane data and average split parts
# Subtract 7 measurements from start to correct for switching valves
Av_V2_e=[]
if gapV2[0]<=13:
    Av_V2_e.append(np.mean(data2[0:gapV2[0]]))
if gapV2[0]>13:
    Av_V2_e.append(np.mean(data2[(gapV2[0]-13):gapV2[0]]))
for i in range(len(gapV2)-1):
    Av_V2_e.append(np.mean(data2[(gapV2[i+1]-13):gapV2[i+1]]))
if len(t2)-gapV2[-1] > 87:
    Av_V2_e.append(np.mean(data2[(gapV2[-1]+87):-1]))
print(Av_V2_e)
np.savetxt('Av_CTD_V2_end.dat', Av_V2_e)

# Determine STD split parts
STD_V2_e=[]
if gapV2[0]<=13:
    STD_V2_e.append(np.std(data2[0:gapV2[0]]))
if gapV2[0]>13:
    STD_V2_e.append(np.std(data2[(gapV2[0]-13):gapV2[0]]))
for i in range(len(gapV2)-1):
    STD_V2_e.append(np.std(data2[(gapV2[i+1]-13):gapV2[i+1]]))
if len(t2)-gapV2[-1] > 87:
    STD_V2_e.append(np.std(data2[(gapV2[-1]+87):-1]))
print(STD_V2_e)
np.savetxt('STD_CTD_V2_end.dat', STD_V2_e)

# Just above water
gapV4=[]
for i in range(len(t4)-1):
    if t4[i+1]-t4[i]>200:
        gapV4.append(i)
print(gapV4)

```

```

# Split methane data and average split parts
# Subtract 7 measurements from start to correct for switching valves
Av_V4=[]
if gapV4[0]<=13:
    Av_V4.append(np.mean(data4[0:gapV4[0]]))
if gapV4[0]>13:
    Av_V4.append(np.mean(data4[(0+gapV4[0]-13):gapV4[0]]))
for i in range(len(gapV4)-1):
    Av_V4.append(np.mean(data4[(gapV4[i]+7):gapV4[i+1]]))
if len(t4)-gapV4[-1] > 7:
    Av_V4.append(np.mean(data4[(gapV4[-1]+7):-1]))
print(Av_V4)
np.savetxt('Av_CTD_V4.dat', Av_V4)

# Determine STD split parts
STD_V4=[]
if gapV4[0]<=13:
    STD_V4.append(np.std(data4[0:gapV4[0]]))
if gapV4[0]>13:
    STD_V4.append(np.std(data4[(0+gapV4[0]-13):gapV4[0]]))
for i in range(len(gapV4)-1):
    STD_V4.append(np.std(data4[(gapV4[i]+7):gapV4[i+1]]))
if len(t4)-gapV4[-1] > 7:
    STD_V4.append(np.std(data4[(gapV4[-1]+7):-1]))
print(STD_V4)
np.savetxt('STD_CTD_V4.dat', STD_V4)

# Create new timeseries to match averages
# In top mast
t_av_V1=[]
t_av_V1.append(t1[int(gapV1[0]/2)])
for i in range(len(gapV1)-1):
    t_av_V1.append(t1[gapV1[i]+10])
i=int((len(t1)-gapV1[-1])/2)
if len(t1)-gapV1[-1] > 7:
    t_av_V1.append(t1[gapV1[-1]+i])
print(t_av_V1)
np.savetxt('t_av_CTD_V1.dat', t_av_V1)

# At level sonic
t_av_V2=[]
t_av_V2.append(t2[int(gapV2[0]/2)])
for i in range(len(gapV2)-1):
    t_av_V2.append(t2[gapV2[i]+50])
i=int((len(t2)-gapV2[-1])/2)
if len(t2)-gapV2[-1] > 15:
    t_av_V2.append(t2[gapV2[-1]+i])
print(t_av_V2)
np.savetxt('t_av_CTD_V2_full.dat', t_av_V2)

```

```

t_av_V2_s=[]
if 93>=gapV2[0]>80:
    t_av_V2_s.append(t2[int((gapV2[0]-80)+((gapV2[0]-80)/2))])
if gapV2[0]>93:
    t_av_V2_s.append(t2[int((gapV2[0]-80)+(((gapV2[0]-93)-(gapV2[0]-80))/2))])
for i in range(len(gapV2)-1):
    t_av_V2_s.append(t2[gapV2[i]+10])
a=int(((gapV2[-1]+20)-(gapV2[-1]+7))/2)
b=int((len(t2)-(gapV2[-1]+7))/2)
if len(t2)-gapV2[-1] > 20:
    t_av_V2_s.append(t2[gapV2[-1]+a])
if 20 >= len(t2)-gapV2[-1] > 7:
    t_av_V2_s.append(t2[gapV2[-1]+b])
print(t_av_V2_s)
np.savetxt('t_av_CTD_V2_start.dat', t_av_V2_s)

t_av_V2_e=[]
if gapV2[0]<=13:
    t_av_V2_e.append(t2[int(gapV2[0]/2)])
if gapV2[0]>13:
    t_av_V2_e.append(t2[int(gapV2[0]+((gapV2[0]-13)-gapV2[0])/2)])
for i in range(len(gapV2)-1):
    t_av_V2_e.append(t2[gapV2[i]+90])
a=int((len(t2)-(gapV2[-1]+87))/2)
if len(t2)-gapV2[-1] > 87:
    t_av_V2_e.append(t2[(gapV2[-1]+87)+a])
print(t_av_V2_e)
np.savetxt('t_av_CTD_V2_end.dat', t_av_V2_e)

# Just above water
t_av_V4=[]
t_av_V4.append(t4[int(gapV4[0]/2)])
for i in range(len(gapV4)-1):
    t_av_V4.append(t4[gapV4[i]+10])
i=int((len(t4)-gapV4[-1])/2)
if len(t4)-gapV4[-1] > 7:
    t_av_V4.append(t4[gapV4[-1]+i])
print(t_av_V4)
np.savetxt('t_av_CTD_V4.dat', t_av_V4)

```

## Appendix 3

Table 15 contains the statistical parameters of the noise levels of the methane mixing ratios in summer. The average is the average of all residuals during the hour during which the indicated CTD was taken. Because the buckets were removed from the dataset, the amount of residuals determined for each CTD vary. This is why the standard error was also determined.

**Table 15:** Average, standard deviations and standard error of the residuals determined from measurements of CH<sub>4</sub> mixing ratios measured in summer.

CTD	Average [ppb]	STD [ppb]	Standard error [ppb]
1	0.017	4.103	0.187
2	-0.009	0.826	0.038
3	-0.003	0.602	0.027
4	0.000	0.613	0.036
5	-0.001	0.519	0.024
6	0.004	0.570	0.026
7	-0.002	0.653	0.030
8	-0.012	0.857	0.039
9	0.003	0.997	0.046
10	-0.002	1.455	0.066
11	0.024	1.509	0.069
12	0.000	1.985	0.091
13	0.041	24.047	1.103
14	-0.011	2.244	0.102
15	-	-	-
16	0.003	1.465	0.067
17	-0.004	1.296	0.059
18	-	-	-
19	-	-	-
20	-0.189	1.687	0.078
21	-0.283	2.411	0.111
22	0.970	4.024	0.774
23	0.016	3.784	0.174
24	0.003	3.764	0.172
25	0.137	10.654	3.212
26	-0.070	7.078	0.324
27	-0.007	2.077	0.094
28	-0.055	1.426	0.133
29	0.004	1.535	0.070
30	-0.008	2.121	0.098
31	-	-	-
32	-0.003	1.026	0.047
33	-0.014	1.842	0.084
34	-	-	-
35	-0.041	3.374	0.153
36	-0.084	5.878	0.271
37	-	-	-
38	0.018	55.403	2.526
39	0.388	29.604	1.355
40	-	-	-
41	-0.149	12.907	0.594
42	0.004	4.690	0.215
43	-0.017	3.906	0.181
44	-0.015	10.232	0.526
45	0.012	2.425	0.112
46	0.001	2.086	0.115
47	-0.006	1.955	0.089
48	-0.063	5.752	0.262

## Appendix 4

Table 16 contains the average differences depicted in figure 45 per CTD (for summer) and table 17 contains the average differences depicted in figure 46 per CTD (for autumn).

**Table 16:** Average and standard deviation of the differences between average methane mixing ratios measured in different inlets per CTD for summer. The amount of differences that the average is based on is also given.

CTD	Water-Sonic full			Water-Sonic end			Sonic full-Mast			Sonic start-Mast			Water-Mast		
	Average	STD	Amount	Average	STD	Amount	Average	STD	Amount	Average	STD	Amount	Average	STD	Amount
1	-0.003	0.013	3	0.003	0.004	4	0.023	0.014	2	0.021	0.016	3	0.002	0.008	3
2	0.001	0.006	10	0.001	0.002	9	0.002	0.005	10	0.002	0.005	10	0.006	0.007	10
3	0.001	0.001	8	0.001	0.001	9	0.001	0.000	8	0.001	0.001	8	0.002	0.000	9
4	0.001	0.001	2	0.001	0.001	3	0.002	0.001	3	0.001	0.001	3	0.002	0.001	2
5	0.000	0.001	8	0.001	0.001	8	0.001	0.001	9	0.001	0.001	9	0.002	0.001	9
6	0.001	0.001	7	0.001	0.001	8	0.001	0.001	7	0.001	0.001	8	0.001	0.001	8
7	0.002	0.002	9	0.001	0.001	8	0.003	0.001	8	0.002	0.000	8	0.001	0.002	8
8	0.001	0.003	8	0.001	0.001	9	0.002	0.004	9	0.001	0.002	9	0.000	0.001	9
9	0.001	0.002	9	0.001	0.002	9	0.003	0.007	8	0.001	0.004	8	0.002	0.003	8
10	0.006	0.006	9	0.004	0.002	9	0.003	0.007	9	0.001	0.004	9	0.004	0.003	9
11	0.004	0.003	8	0.004	0.002	8	0.002	0.005	8	0.001	0.002	8	0.004	0.004	9
12	0.017	0.014	9	0.016	0.017	9	0.005	0.009	9	0.003	0.002	9	0.017	0.018	8
13	0.002	0.003	7	0.004	0.004	7	0.006	0.009	9	0.005	0.005	9	0.006	0.005	8
14	0.004	0.007	4	0.000	0.010	5	0.013	0.005	3	0.014	0.002	3	0.008	0.007	5
15	-0.003	0.003	6	-0.001	0.004	6	0.004	0.004	6	0.004	0.003	7	0.000	0.004	6
16	0.003	0.003	5	0.001	0.002	6	-0.003	0.011	6	0.001	0.002	6	0.001	0.001	6
17	0.003	0.003	10	0.001	0.002	9	0.004	0.003	9	0.002	0.001	9	0.001	0.002	9
18	0.000	0.003	5	0.000	0.001	6	0.004	0.003	5	0.002	0.002	6	0.004	0.002	6
19	-	-	-	-	-	-	-	-	-	-	-	-	-	-	-
20	0.000	0.003	3	-0.001	0.004	4	-0.001	0.006	4	-0.001	0.003	4	0.002	0.002	4
21	0.000	0.004	9	0.001	0.003	9	-0.001	0.003	9	-0.001	0.002	9	0.001	0.002	9
22	0.002	0.009	4	0.000	0.002	4	0.000	0.003	4	0.001	0.004	4	0.008	0.006	4
23	0.030	0.032	8	0.029	0.023	8	0.040	0.034	9	0.038	0.037	9	0.073	0.054	9
24	-0.002	0.014	8	0.001	0.005	8	0.002	0.009	7	0.004	0.005	8	0.005	0.006	8
25	0.006	0.020	6	0.007	0.008	6	0.008	0.012	7	0.010	0.018	6	0.005	0.022	6
26	0.014	0.048	4	0.037	0.030	5	0.006	0.066	4	0.015	0.017	4	-0.008	0.045	4
27	-0.004	0.023	9	0.003	0.015	10	-0.003	0.015	9	0.005	0.007	9	0.002	0.011	10
28	0.010	0.016	7	0.006	0.009	7	0.003	0.019	7	0.001	0.005	8	0.004	0.010	7
29	-0.001	0.006	4	0.002	0.001	4	0.003	0.007	5	0.003	0.004	5	0.005	0.006	5
30	-0.002	0.006	9	0.000	0.004	9	-0.002	0.005	8	0.002	0.003	9	0.009	0.008	9
31	0.001	0.003	7	0.002	0.004	7	0.002	0.007	7	0.003	0.003	6	0.004	0.004	7
32	0.005	0.001	5	0.003	0.001	5	0.005	0.002	5	0.003	0.001	5	0.001	0.001	5
33	0.004	0.003	9	0.001	0.004	9	0.006	0.002	8	0.003	0.002	9	0.002	0.002	9
34	0.006	0.007	7	0.003	0.003	7	0.006	0.010	7	0.005	0.005	7	0.006	0.003	7
35	0.005	0.003	4	0.003	0.003	5	0.010	0.002	5	0.008	0.003	5	0.010	0.003	5
36	0.008	0.005	9	0.004	0.004	8	0.014	0.005	8	0.011	0.005	8	0.013	0.004	8
37	0.016	0.023	4	0.011	0.020	6	0.043	0.016	5	0.032	0.014	6	0.029	0.028	6
38	-	-	-	-	-	-	-	-	-	-	-	-	0.205	0.000	1
39	-	-	-	0.064	0.046	4	-	-	-	0.130	0.063	2	0.225	0.068	4
40	-0.033	0.000	1	-0.025	0.053	5	0.086	0.060	2	0.088	0.053	4	0.118	0.088	4
41	0.018	0.021	3	0.016	0.024	5	0.049	0.032	4	0.071	0.039	5	0.121	0.058	5
42	0.028	0.029	9	0.029	0.022	9	0.032	0.026	9	0.035	0.021	9	0.067	0.047	9
43	0.005	0.010	8	0.008	0.003	8	0.021	0.007	8	0.020	0.005	8	0.030	0.008	8
44	0.004	0.002	4	0.007	0.002	3	0.024	0.018	4	0.036	0.026	4	0.047	0.035	4
45	-0.001	0.012	8	0.005	0.007	9	0.010	0.013	8	0.014	0.006	9	0.021	0.012	9
46	0.005	0.009	8	0.004	0.005	8	0.009	0.005	9	0.009	0.003	8	0.016	0.006	8
47	0.008	0.005	4	0.003	0.004	5	0.005	0.014	4	0.004	0.005	5	0.013	0.010	5
48	0.006	0.008	7	0.005	0.011	6	0.009	0.009	7	0.008	0.002	7	0.014	0.011	6

**Table 17:** Average and standard deviation of the differences between average methane mixing ratios measured in different inlets per CTD for autumn. The amount of differences that the average is based on is also given.

CTD	Water-Sonic			Sonic-Mast			Water-Mast		
	Average	STD	Amount	Average	STD	Amount	Average	STD	Amount
1	-0.018	0.011	3	-0.034	0.051	3	-0.068	0.078	2
2	-0.002	0.006	9	0.000	0.002	9	-0.004	0.004	10
3	-0.003	0.004	10	-0.001	0.004	10	-0.003	0.003	9
4	-0.011	0.023	11	0.005	0.021	11	-0.006	0.006	12
5	-0.007	0.006	9	-0.003	0.004	9	-0.001	0.007	9
6	-0.003	0.003	8	-0.002	0.005	7	-0.007	0.009	8
7	-0.003	0.004	6	0.000	0.001	6	-0.003	0.002	7
8	-0.004	0.008	10	-0.004	0.008	10	-0.010	0.006	10
9	-0.003	0.003	9	-0.003	0.002	10	-0.006	0.002	9
10	-0.003	0.002	8	0.001	0.001	7	-0.005	0.003	8
11	-0.007	0.009	10	0.000	0.005	10	-0.009	0.008	9
12	-0.013	0.006	8	-0.005	0.007	9	-0.016	0.006	9
13	-0.006	0.006	5	0.000	0.005	5	-0.006	0.010	5
14	-0.001	0.005	10	0.000	0.006	10	-0.001	0.009	10
15	-0.002	0.010	10	0.000	0.004	11	-0.001	0.013	10
16	0.000	0.003	7	0.001	0.001	7	0.000	0.004	8
17	-0.012	0.009	10	-0.009	0.008	11	-0.023	0.017	11
18	-0.025	0.019	9	-0.006	0.018	8	-0.030	0.020	8
19	-0.002	0.003	10	-0.002	0.004	10	-0.004	0.004	10
20	-0.008	0.012	10	-0.007	0.016	10	-0.015	0.022	10
21	-0.003	0.003	9	-0.005	0.008	9	-0.008	0.010	9
22	-0.006	0.009	8	0.001	0.004	7	-0.004	0.006	8
23	-0.011	0.009	9	-0.008	0.041	9	-0.019	0.039	9
24	-0.005	0.009	7	0.002	0.006	6	-0.006	0.009	8
25	-0.008	0.006	6	-0.001	0.005	5	-0.008	0.003	6
26	-0.014	0.012	10	-0.001	0.008	11	-0.013	0.011	10
27	-0.003	0.008	11	-0.001	0.005	10	-0.010	0.009	10
28	-0.014	0.003	8	-0.002	0.003	8	-0.013	0.006	9
29	-0.047	0.024	9	-0.006	0.015	9	-0.048	0.025	9
30	-0.016	0.019	8	0.000	0.008	9	-0.018	0.025	9
31	-0.020	0.012	11	-0.001	0.007	11	-0.022	0.013	11
32	-0.010	0.004	9	-0.001	0.002	9	-0.009	0.003	8
33	-0.007	0.003	8	0.000	0.002	8	-0.006	0.004	10
34	-0.007	0.002	11	-0.002	0.001	10	-0.010	0.006	11
35	-0.005	0.002	9	0.000	0.001	10	-0.017	0.006	9
36	-0.020	0.017	11	-0.001	0.004	10	0.007	0.016	12
37	-0.010	0.006	11	-0.003	0.010	10	-0.021	0.025	10
38	-0.010	0.009	9	-0.011	0.017	9	-0.017	0.014	9
39	-0.014	0.006	11	-0.012	0.027	9	-0.019	0.028	10
40	-0.004	0.004	5	0.000	0.010	4	-0.007	0.005	6
41	-0.002	0.002	10	-0.011	0.025	11	-0.019	0.027	9
42	-0.007	0.003	3	-0.001	0.002	3	-0.014	0.009	5
43	-0.004	0.003	9	-0.004	0.007	10	-0.003	0.007	9
44	-0.002	0.001	3	-0.002	0.001	3	-0.013	0.010	5
45	-0.008	0.005	10	0.000	0.004	9	-0.032	0.010	6
46	-0.031	0.007	2	0.009	0.019	3	0.010	0.016	5
47	-0.010	0.017	8	0.000	0.005	7	-0.018	0.020	7